The Dissertation Committee for Mary Elizabeth Miller Certifies that this is the approved version of the following dissertation:

Sphingomyelinases and Lysosomal Trafficking in *Ebolavirus* Entry

Committee:

Robert A. Davey, Ph.D., Supervisor

Clarence J. Peters, M.D.

Thomas G. Ksiazek, D.V.M., Ph.D.

Mark R. Hellmich, Ph.D.

Christopher F. Basler, Ph.D.

Dean, Graduate School

Sphingomyelinases and Lysosomal Trafficking in *Ebolavirus* Entry

by

Mary Elizabeth Miller, B.S., M.A.

Dissertation

Presented to the Faculty of the Graduate School of

The University of Texas Medical Branch

in Partial Fulfillment

of the Requirements

for the Degree of

Doctor of Philosophy

The University of Texas Medical Branch

August, 2011

Dedication

To my loving family.

Acknowledgements

I would like to express my profound appreciation to my mentor, Dr. Robert Davey, for his limitless patience and support while allowing me the freedom to explore my own ideas, learn from my mistakes, and become a better scientist. To my committee members, Dr. Clarence Peters, Dr. Thomas Ksiazek, Dr. Christopher Basler, and Dr. Mark Hellmich, I am incredibly honored and humbled to have been guided by your expertise, and am sincerely grateful for your critical, honest feedback. Special thanks are given to Dr. Andrey Kolokoltsov, Dr. Mohammad Saeed, Dr. Olena Shtanko, Dr. Zeming Chen, Shramika Adhikary, Jia Wang, and Alex McAuley for their mentorship, technical guidance, support, and friendship. To Colonel (Ret.) Daniel Strickman, Colonel Robert Bowden, and Dr. Eric Gaidos, I give my deepest gratitude for inspiring and encouraging me to pursue my scientific career. I would also like to express my sincere gratitude to the U.S. Army for affording me the opportunity to earn my doctoral degree, as well as General David Petreus, General Ray Odierno, General Benjamin Mixon, Colonel Walter Piatt, and Lieutenant Colonel Thomas Rogers for releasing me from Iraq in order to start my degree program on time. Lastly, but most importantly, I would like to thank my family for their fathomless optimism, encouragement, and support.

Sphingomyelinases and Lysosomal Trafficking in *Ebolavirus* Entry

Publication No._____

Mary Elizabeth Miller, Ph.D.

The University of Texas Medical Branch, 2011

Supervisor: Robert A. Davey

Ebolavirus (EBOV) is a negative sensed, single-strand filovirus which causes up to 90% mortality. Despite increasing outbreaks over the past decade, no approved vaccines or therapies exist. One drug treatment strategy is to target virus entry mechanisms. EBOV enters the cell using a macropinocytosis-like mechanism, which requires actin, microtubules, and phosphatidylinositol 3-kinase (PI3K). Additionally, pH-dependent lysosomal enzymes, cathepsins B and L, are needed to proteolytically cleave the virus surface glycoprotein. This action facilitates fusion between the virus and cell membranes prior to infection. However, it is unclear where fusion occurs in the cell. Furthermore, although EBOV colocalizes with early endosomes and late endosomes, the role of lysosomes has yet to be elucidated.

To determine whether EBOV colocalizes with lysosomes during entry, fluorescently-tagged virus-like particles (VLPs) were generated by overexpressing EBOV glycoprotein and virus protein 40 (VP40-GFP) in 293FT cells. EBOVLP colocalization with lysosomal marker, Lamp1, was visualized using an immunofluorescence assay. Interestingly, colocalization occurred in non-permeabilized cells, suggesting an interaction with EBOVLPs and lysosomes at the cell surface. By applying chemical and genetic inhibitors of lysosomal exocytosis to cells inoculated with replication-competent EBOV, it appeared that this vesicle trafficking pathway was required for infection. During lysosomal exocytosis, pH-dependent acid sphingomyelinase (ASM) is released to the plasma membrane's outer leaflet, resulting in ASM-dependent macropinosome formation. Because EBOV enters via a macropinocytosis-like mechanism, the role of ASM in infection was assessed. Specific ASM chemical inhibitors and RNA interference (RNAi) were used to show that ASM was important for EBOV-GFP infection. A mechanistic approach was then employed to isolate which step of viral entry – binding, internalization, trafficking, or fusion – was being blocked by ASM inhibition. Using a mixing contents assay, it was determined that ASM inhibitors target a fusion or pre-fusion step. It was also found that ASM colocalized with EBOVLPs at the plasma membrane shortly after binding, similar to Lamp1. Finally, pseudotyped viruses containing a common core virus encoated with either

EBOV, Lassa virus (LASV), or Venezuelan Equine Encephalitis virus (VEEV) surface glycoproteins were incubated with cells treated with ASM inhibitors. EBOV GP pseudotyped viruses were more sensitive to ASM inhibition, suggesting a GP-specific role for ASM in entry. Next, because ASM was found to be important, the role of other sphingomyelinases in EBOV infection was assessed. A role for neutral sphingomyelinase 2 activation was also tested by applying the same assays as for ASM. It was determined that NSM inhibitors also block EBOV infection at a fusion or pre-fusion step of EBOV entry.

Taken together, these findings suggest that EBOV binding stimulates lysosomal exocytosis, resulting in sphingomyelinase-dependent infection of cells. In conclusion, inhibitors of lysosomal exocytosis and sphingomyelinases may be useful as potential drug therapies to prevent EBOV infection.

Table of Contents

LIST OF TABLES

LIST OF FIGURES

CHAPTER 1: INTRODUCTION

FILOVIRUSES

EPIDEMIOLOGY

Filoviruses generate up to 90 percent mortality in humans, yet relatively little is known of how these viruses are maintained or transmitted in nature. Furthermore, because natural infection often occurs in remote areas of Africa, understanding human disease sufficiently to develop effective treatments and vaccines has been difficult. Filoviruses belong to the order *Mononegavirales,* which includes other negative sense, single-stranded enveloped viruses such as Paramyxoviruses, Rhabdoviruses, and Bornaviruses. Due to their thread-like structure, filoviruses are further assigned to the family, *Filoviridae,* which has two genera - *Marburgvirus* and *Ebolavirus*.

Ebolavirus has five species: *Zaire Ebolavirus*, *Sudan Ebolavirus*, *Tai Forest Ebolavirus*, *Bundibugyo Ebolavirus*, and *Reston Ebolavirus*. Ebolavirus first came to light in 1976 during an outbreak in Yambuku, Zaire (Pattyn et al., 1977). Of the 318 cases, 88 percent died. The same year, another outbreak occurred in Sudan with 284 cases (Bowen et al., 1977). In this case, the mortality was only 53 percent. Although not identified until years later, *Zaire Ebolavirus* caused the Zaire outbreak, while *Sudan Ebolavirus* was responsible for the outbreak in Sudan (Cox et al., 1983). In 1977, a patient died of *Zaire Ebolavirus* in Zaire (Heymann et al., 1980). Two years later in Sudan, 34 people became infected with *Sudan Ebolavirus*, with 65 percent being fatal (Baron et al., 1983; Bowen et al., 1980). In 1989 and 1990, the first four instances of *Reston Ebolavirus* were identified in quarantine facilities in Virginia, Texas, and Pennsylvania, which had all received infected monkeys from the same source in the Philippines (1992; Jahrling

et al., 1990). Facilities in Italy and Texas received additional shipments of infected monkeys from the Philippines in 1992 and 1996, respectively (Johansen et al., 1996). Although this virus was fatal in monkeys, none of the 5 animal handlers developed febrile illness despite 3 of 5 handlers having sero-converted, and a fourth having both IgM and IgG filovirus-specific antibodies. From 1994 to 1996, a series of *Zaire Ebolavirus* outbreaks occurred in Gabon and Zaire (Georges-Courbot et al., 1997a; Georges-Courbot et al., 1997b; Khan et al., 1999), which were possibly sustained through continued passage among animal hosts. The first event presented in Gabon, generating 49 cases with 65 percent mortality. In 1995, 315 people were infected in Zaire, with mortality as high as 88 percent. In 1996, the virus reappeared in Gabon, with 37 cases in the early in the year, and 60 cases occurring later the same year. Case fatality was 57 and 75 percent, respectively. Within the timeframe of the Gabon-Zaire outbreaks, *Tai Forest Ebolavirus* appeared in two isolated events (Le Guenno et al., 1995). In 1994, a primatologist became infected while performing a necropsy on an infected chimpanzee, but survived. A year later, a refugee in Liberia showed symptoms of the illness, but also survived. From 2000 to 2002, two large outbreaks of *Sudan Ebolavirus* and *Zaire Ebolavirus* occurred simultaneously. In Uganda, 53 percent of the 425 infected died. In Gabon and Republic of Congo (RC), 79 percent of 123 infected died. This lingering sequence of outbreaks continued into 2003, with 143 cases in RC early in the year, and 35 cases several months later. Case fatality was 90 and 83 percent, respectively. A year later, 17 cases of *Sudan Ebolavirus* presented in Sudan (Onyango et al., 2007). In 2005, another 12 cases of *Zaire Ebolavirus* appeared in RC with 75 percent mortality. 2007 was highlighted with the first cases of *Bundibugyo Ebolavirus,* which occurred during an outbreak in Uganda that continued into 2008

(Towner et al., 2008). Of the 102 cases, 42 percent died. The same year, the World Health Organization reported an outbreak of *Zaire Ebolavirus* in Democratic Republic of Congo (DRC, formerly Zaire) which resulted in 15 deaths of 32 suspected cases (2007a; 2007b). In 2008, domestic pigs infected with *Reston Ebolavirus* provided the first evidence of sustained virus transmission in the Philippines (Barrette et al., 2009). Again, there were no signs of illness in humans who handled the pigs; however, antibodies were present in 6 cases. With a noticeable escalation of outbreaks over the past decade, the discovery of a new species in 2007, the suggestion of prolonged transmission in the Philippines, and the lack of effective treatments or vaccines, Ebolavirus has become a serious public health threat.

Little is known of how *Ebolavirus* is maintained in nature. It is thought that bat species, such as *Hypsignathus monstrosus*, *Epomops franqueti*, *Myonycteris torquata*, and others are possible reservoirs; however, direct transmission of virus to humans has not been documented. The reservoir may spread virus by contaminating a common food source, such as fruit or vegetation, with its saliva or feces (Hayman et al., 2010; Leroy et al., 2005; Pourrut et al., 2009). Or perhaps environmental changes cause the reservoir to alter its prey selection or foraging behavior, forcing it to come in contact with susceptible hosts, such as primates, bush pigs, and duikers. Once these animals become infected, they can transmit high titers of virus to other susceptible hosts through contact with bodily fluids such as semen, tears, breast milk, saliva, and blood (Bausch et al., 2007; Dowell et al., 1999). The most common source of human infection is contact with other infected humans (Groseth et al., 2007).

PATHOLOGY

Filoviruses are introduced through breaks in the skin, or mucosal surfaces such as the eyes, nose, and mouth. After a 4 to 10 day incubation, symptoms present suddenly. Patients experience fever, chills, headache, malaise, and muscle aches, followed by abdominal pain, nausea, vomiting, sore throat, and dry cough. Between days 5 and 7, a characteristic maculopapular rash appears on the torso. As the disease progresses, systemic manifestations appear including gastrointestinal, neurologic, respiratory, and vascular involvement. The immune response becomes deregulated, resulting in widespread inflammation, excessive T cell apoptosis, and little to no specific antibody production. Necrosis becomes evident in the liver, spleen, and kidneys. In severe cases, hemorrhaging occurs in the gastrointestinal and urogenital tracts, eyes, nose, and mouth. Sustained inflammation, extensive coagulation disruption, and vascular leakage eventually lead to multiple organ failure and death between days 7 and 16. (Bwaka et al., 1999; Kalongi et al., 1999; Nikiforov et al., 1994; Nkoghe et al., 2005; Okome-Nkoumou and Kombila, 1999; Teepe et al., 1983)

Macrophages, monocytes, and dendritic cells are early targets of infection. They provide a safe site for virus replication, a means to distribute virus to other susceptible cells, and also deregulate the host immune response by overexpressing inflammatory cytokines. This, in turn, makes other tissues and organs more susceptible to virus infection, providing more sites for virus replication. The sustained and inappropriate overexpression of inflammatory cytokines, results in tissue damage, large scale T cell apoptosis, natural killer (NK) cell death, and the inability of B cells to produce specific antibodies. Compared to fatal cases, survivors have abnormally high T cell counts, lower virus burden, lower nitric oxide (NO), substantially more CD8+ cell activation, and detectable antibodies circulating in the blood upon presentation of symptoms.

(Bosio et al., 2003; Bray and Geisbert, 2005; Feldmann and Geisbert, 2010; Geisbert et al., 2003b; Geisbert et al., 2003c; Hartman et al., 2010; Stroher et al., 2001; Zampieri et al., 2007)

THERAPIES AND VACCINES

Development of effective treatments and vaccines against filoviruses has been challenging for many reasons. First, early events of human disease pathology are not as well understood because initial symptoms are non-specific, and disease progression is fairly rapid, with patients either recovering or dying within 2 to 3 weeks of onset. Second, few animal models exist for filovirus infection. Non-human primate disease most closely mimics human disease; however, primate research is extremely expensive, and bears a high moral burden. Although not naturally prone to filovirus infection, mice and guinea pigs can serve as useful models for initial vaccine trials. After serial passage, the virus adapts to the host animal and produces lethal infection. However, there are less similarities to human infection in these models compare to the non-human primate model (Hoenen et al., 2006; Ryabchikova et al., 1999). Finally, because filoviruses are so lethal and infectious, studying live virus is restricted to Biosafety Level 4 (BSL4).

Because rodent models do not mimic human disease, treatments that offer protection in mice or guinea pigs often prove ineffective in non-human primates. Despite this, there are some promising candidates, such as the employment of small interfering RNA (siRNAs) or other antisense oligonucleotides. However, oligonucleotide based therapies can be easily overcome by generation of point mutations at the site of oligo interaction. Questions about dosage required and cost effectiveness of the delivery vehicle also make oligonucleotide therapies difficult to execute in the field (Gitlin et al., 2005). Although not tested in rodents, several coagulation

modulation strategies have shown to be effective in humans and non-human primates. Heparin sulfate has been useful as a therapeutic treatment in humans (Gear et al., 1975). In non-human primates, activated protein C, and inhibitors of the tissue factor pathway provide some protection against lethal infection (Gear et al., 1975; Geisbert et al., 2003a).

Vaccine development has made great strides, with several candidates successfully completing trials in non-human primates. An adenovirus type 5 vaccine in already in clinical trials, but it requires a high dose and may not work on those with pre-existing immunity to the adenovirus vector (Ledgerwood et al., 2010). Another candidate, which uses human parainfluenza virus type 3, requires two doses in non-human primates. Because this vaccine employs a replication-competent virus for delivery, there are substantial safety concerns (Bukreyev et al., 2010). Yet another strategy uses a replication-competent vesicular stomatitis virus (VSV) to induce protective immunity both pre- and post-exposure with only one dose. By applying virus-like particles as a vaccine, one is exposed to a majority of the filovirus proteins, without risk of infection. Three doses are required in non-human primates (Jones et al., 2005). Although there are many promising vaccine candidates, none have been proven effective in humans thus far.

DRUG TREATMENTS

Identifying drugs which inhibit filovirus infection has been equally elusive. Ribavirin, an effective antiviral drug used to treat other types of hemorrhagic fever virus infections by inducing lethal mutations, is not effective against filoviruses (Andrei and De Clercq, 1993; Cameron and Castro, 2001; Canonico et al., 1984; Crotty and Andino, 2002; Sidwell et al., 1972; Vignuzzi et al., 2005). Additionally, many entry and fusion inhibitors which have been useful

against HIV, RSV, and influenza virus infections have not yet been tested against EBOV (Gene et al., 2009; Teissier et al., 2011). More recently, LJ001, an antiviral targeting entry of enveloped viruses into host cells, was identified. However, the application of such a drug *in vivo* is questionable since it would likely disrupt host cellular membranes just as it does viral membranes (Wolf et al., 2010).

EBOLAVIRUS STRUCTURE, GENOME ORGANIZATION & PROTEIN FUNCTION

Ebolaviruses have varying morphology due to their thread-like structure. Although they have a uniform diameter of 80 nanometers (nm), their length can be as long as 14,000 nm. Additionally, they can form circles, T-shapes, and "6's" which alter their overall size. Their large size may be an important feature in virus entry, with the optimum size for infection being 970 nm (Kiley et al., 1982).

Ebolavirus is a non-segmented enveloped virus with negative sense, single-stranded RNA (Figure. 1). Its 19 kilobase genome contains seven genes in the following order: nucleoprotein (NP), virus protein (VP) 35, VP40, glycoprotein (GP), VP30, VP24, and polymerase (L). L is an RNA-dependent RNA polymerase that works in concert with its co-factor, VP35, to transcribe the viral genome. VP35 also inhibits host type I interferon signaling. VP30 is a minor nucleoprotein that triggers transcription by binding RNA. The major nucleoprotein, NP, surrounds the polymerase/genome complex, forming the nucleocapsid. Surrounding the nucleocapsid, is the matrix. VP40 is a major matrix protein which is essential for virus assembly and budding. VP40 alone can form virus like particles with the same morphology as infectious virus particles (Jasenosky et al., 2001). VP24 is a minor matrix protein that aids in virus assembly, and also inhibits interferon signaling (Johnson et al., 2006; Leroy et al., 2002; Noda et

al., 2002; Ruigrok et al., 2000). The GP gene is polycistronic, generating both secreted and structural, or surface, GP (Hood et al., 2010). The secreted form is unique to *Ebolavirus*, and is secreted from host cells during early infection; however, its exact function is unknown (Falzarano et al., 2006). The structural GP starts as a single protein, but is later cut at a furin cleavage site, forming a GP1-GP2 heterodimer. The GP1-GP2 heterodimers trimerize, making the GP spikes on the virion. Because the matrix is enveloped by host-derived lipids, structural GPs are the first virus proteins to interact with host cells upon entry. The structural GPs are important in viral entry due to their access to host cell receptors, and their ability to undergo fusion with host cell membranes (Brindley et al., 2007; Hood et al., 2010).

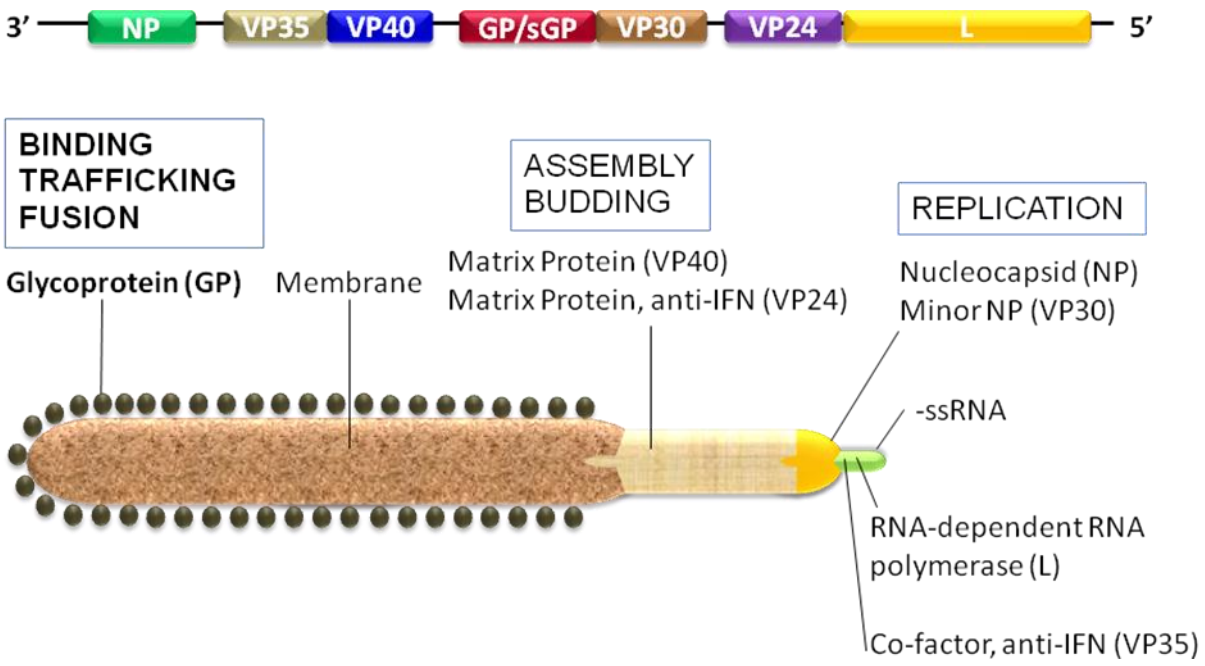

Figure 1. EBOV genome and virus particle structure. The surface glycoprotein is important in virus binding, trafficking, and fusion. The envelope is composed of cell membrane lipids which are incorporated into the virus particle during budding. The matrix proteins, VP40 and VP24, are required for virus assembly and budding. As the major matrix protein, VP40 can form filamentous virus-like particles by itself. VP24 also functions to interfere with host interferon

(IFN) signaling. The nucleocapsid proteins bind RNA and trigger transcription. RNA-dependent RNA polymerase, L, and its co-factor, VP35, transcribe the viral genome. Additionally, VP35, like VP24, interferes with host IFN signaling.

VIRUS-LIKE PARTICLES (VLPS)

Because of the unique self-assembling properties of VP40 matrix protein, 293FT cells transfected with VP40-expressing plasmids can generate virus-like particles bearing the same morphology as wild type virus (Jasenosky et al., 2001; Johnson et al., 2006). Additionally, when cells are dually transfected with EBOV GP- and VP40-expressing plasmids, virus-like particles produced mimic the wild type virus not only in morphology, but also in GP-mediated binding and cell signal activation (Bosio et al., 2004; Martinez et al., 2007). Because VLPs lack the viral genome, they are replication incompetent and non-infectious. Therefore, they can safely be used in BSL2, providing a valuable tool for entry research.

EBOV GP PSEUDOTYPED VIRUSES

Additionally, other tools for EBOV entry have been developed to overcome the limitations associated with studying a BSL4 agent. Pseudotyped viruses allow researchers to investigate EBOV entry in BSL2 by isolating the role of the EBOV GP in binding, internalization, trafficking, and fusion. This is because pseudotyped viruses are composed of a non-lethal core virus, such as lentivirus, murine leukemia virus (MLV), or vesicular stomatitis virus (VSV), which contains a reporter gene (GFP, Luciferase) in the virus genome. In some cases, the envelope protein open reading frame (ORF) is deleted to make the pseudotyped virus replication incompetent. The core virus is then encoated with EBOV GP. Therefore, the pseudotyped virus's morphology mimics that of the core virus, not that of EBOV. For this reason, studies which use pseudotyped viruses should always be verified with wild type EBOV

to ensure that morphology is not a factor which effects virus entry. Additionally, because the pseudotyped virus genome is that of the core virus, lentivirus and retrovirus-based systems require 48 hours for reporter expression; whereas VSV-based systems require only about 8 hours for reporter expression (Kolokoltsov and Davey, 2004; Kolokoltsov et al., 2006a; Kolokoltsov et al., 2006b; Kolokoltsov et al., 2005; Saeed et al., 2006). Because pseudotyped viruses assume the morphology of the core virus, they may enter the cell using different mechanisms than the wild type virus. Therefore, all pseudotyped virus studies should be confirmed with wild type EBOV.

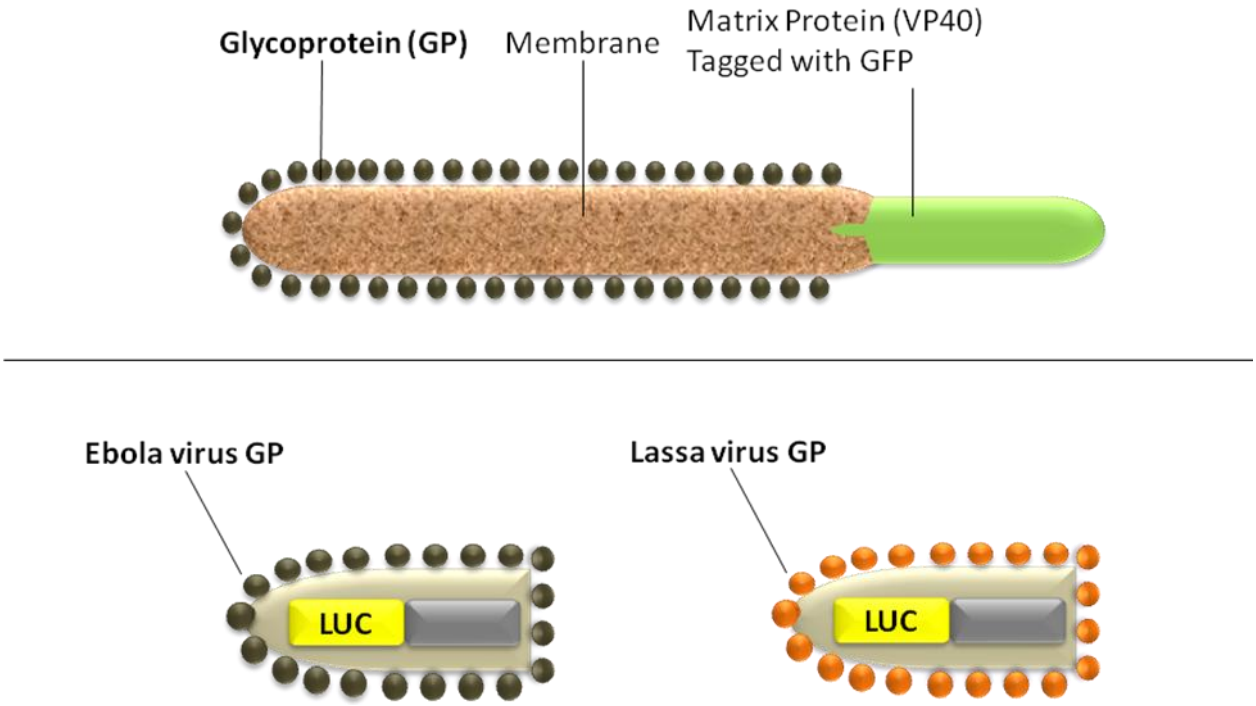

Figure 2. EBO-virus like particles and EBOV GP pseudotyped virus particles. (Top) By dual transfecting 293HEK cells with GFP-tagged VP40 matrix protein and EBOV GP, non-infectious, replication incompetent fluorescent virus particles are generated which can be used for visualizing virus entry pathways in BSL2. These particles have the same size and morphology as the wildtype virus. (Bottom) Pseudotyped virus particles containing a common, non-infectious, replication-incompetent core virus such as Vesicular Stomatitis Virus (VSV) are encoated with different virus glycoproteins. These viruses can be used in BSL2 to determine the specificity of a treatment to the virus GP. However, because these virus particles assume the shape and size of

the core virus (in this case, VSV), experiments using these particles should be verified using wildtype virus. (See Methods).

ENTRY MECHANISMS INTO MAMMALIAN CELLS

Endocytosis is a cellular process that facilitates redistribution of membrane proteins and lipids while internalizing nutrients and other cargo. Many uptake mechanisms exist (Figure 2). These mechanisms can be distinguished by the size of their cargo, and what proteins are associated with internalization (Kumari et al., 2010).

Clathrin-mediated endocytosis (CME) internalizes cargo up to 100 to 200 nm in diameter. Clathrin heavy and light chains assemble into heterodimers under the cell membrane. These heterodimers then trimerize into the clathrin triskelion, and form higher order structures that drive formation of coated pits on the plasma membrane. Most often interaction of cellular receptors with ligand initiates a signaling cascade which triggers actin and microtubule rearrangement. (Kumari et al., 2010; Mercer and Helenius, 2009).

Caveolae-mediated endocytosis handles cargo around 100 nm in diameter. Instead of clathrin, caveolae are formed by caveolin-1, an integral membrane protein that binds cholesterol to form cave-like invaginations on the cell surface. Like CME, this mechanism requires rearrangement of actin and microtubules to internalize cargo. (Mercer and Helenius, 2009) (Kumari et al., 2010).

Larger cargo, with a diameter of 500 nm or more, is internalized by either phagocytosis or macropinocytosis. Phagocytosis is limited to specialized cells, such as immune cells, which selectively take up large particles, microbes, dying cells, and other cell debris. The process begins with cargo recognition and receptor binding, followed by actin rearrangement, and formation of a cup-like membrane protrusion around the cargo. This process is heavily

dependent on actin, microtubules, and myosin to form the membrane extensions (Kumari et al., 2010; Mercer and Helenius, 2009).

Macropinocytosis facilitates large scale fluid phase uptake by forming blebs that extend out from the cell surface and encapsulate the cargo. Formation of these blebs requires actin, microtubules, and myosins. As the cargo is drawn into the cell, macropinosomes form, ranging from 200 nm to 10μm in diameter. Macropinocytosis is regulated by tyrosine kinases, and PI3K, among others (Kumari et al., 2010; Mercer and Helenius, 2009). The blebs formed during macropinocytosis rapidly fill with actin and actin-associated proteins before being drawn back into the cell (Mercer and Helenius, 2009).

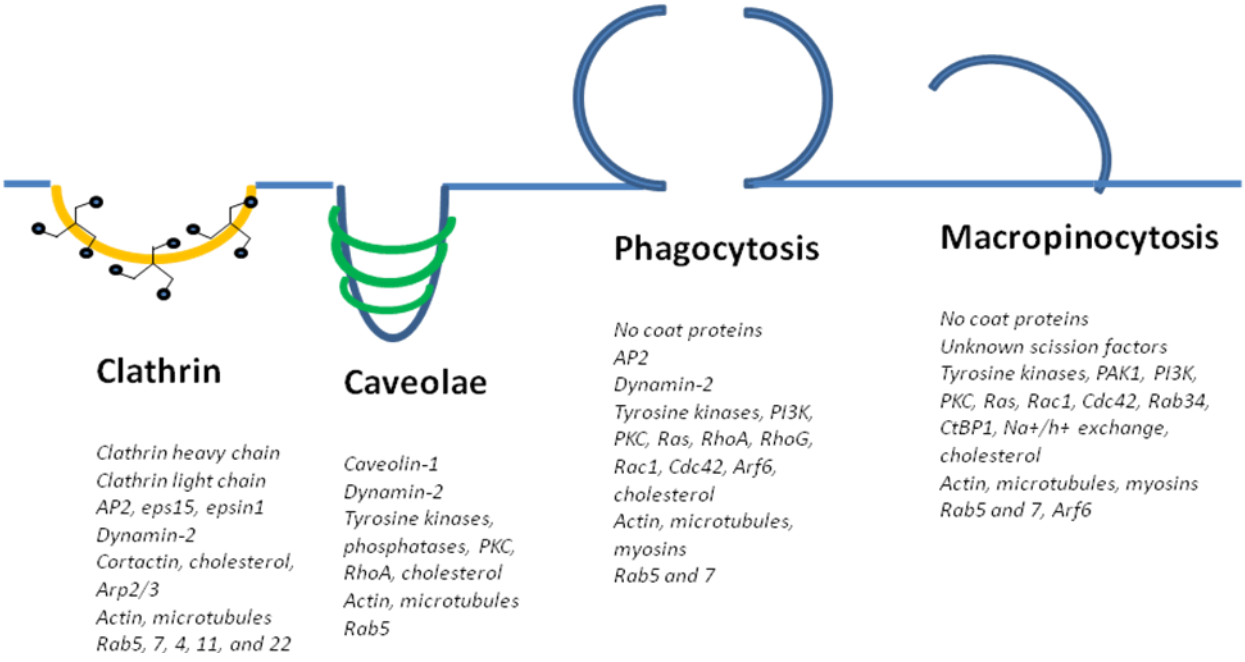

Figure 3. Major mechanisms of entry in mammalian cells. Clathrin-mediated entry requires clathrin heavy and light chains, and internalizes cargo between 100 to 200 nm. Caveolae, composed of caveolin-1, are restricted to cargo of 100 nm or smaller. Phagocytosis can take up cargo as large as 500 nm, and does not require coat proteins such as clathrin or caveolin. Finally,

macropinocytosis is a process used by non-phagocytic cells to take up both large amounts of cargo, varying greatly in size (Mercer and Helenius, 2009; Mercer et al., 2010).

EBOV REPLICATION CYCLE

EBOV replication involves several steps (Figure 4). During entry, the virus is thought to interact with unknown cellular receptors, triggering signaling events which facilitate actin- and tubulin-dependent endocytic uptake (Yonezawa et al., 2005). Next, it was proposed that viral surface glycoprotein (GP) was proteolytically cut at a furin cleavage site by pH-dependent cellular enzymes, cathepsin B and L. However, it was later discovered that cathepsin L is not required for cleavage of GP in human dendritic cells, which are early targets of EBOV infection (Chandran et al., 2005; Kaletsky et al., 2007; Martinez et al., 2010; Schornberg et al., 2006). The importance of pH-dependent cellular enzymes in EBOV entry was further suggested since reduced pH alone does not trigger GP_0 to undergo fusion. However, lysosomotropic agents, which increase endosomal pH, inhibit EBOV fusion with cellular membranes (Chandran et al., 2005; Ito et al., 1999; Takada et al., 1997). Once fusion is complete, the uncoated nucleocapsid is released into the cytosol, where the viral polymerase, L, transcribes the negative sense virus RNA into positive sense vRNA. Then, the cell translates the positive sense vRNA into viral proteins. After replication, VP40 matrix proteins and GPs are transported to lipid rafts in the plasma membrane. The nucleocapsid components assemble outside the nucleus, and are routed to the plasma membrane. VP40 and GP coat the nucleocapsids as they bud from the membrane, resulting in fully formed, infectious viral particles (Dolnik et al., 2008).

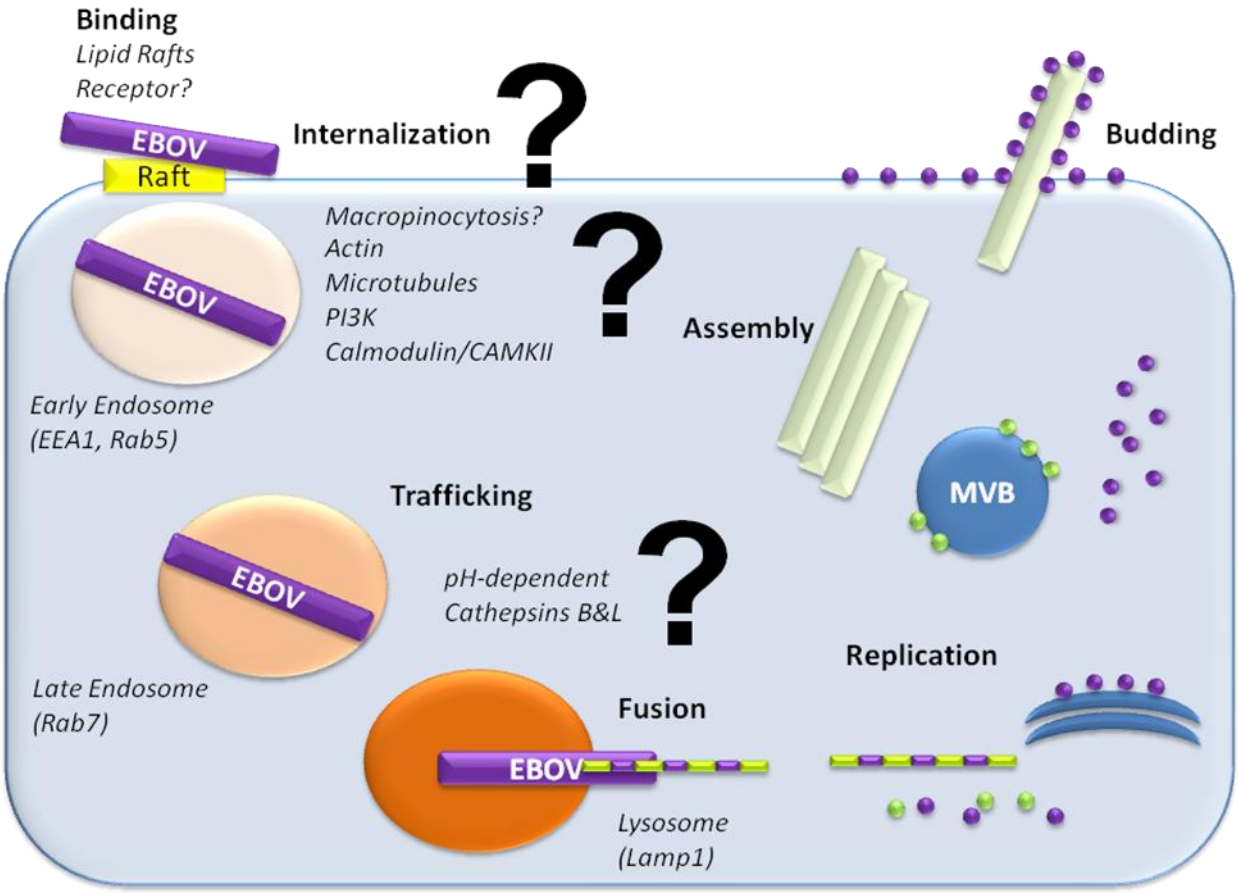

Figure 4. The EBOV replication cycle. The virus binds cholesterol-rich lipid rafts at the cell surface, and triggers internalization through an unknown receptor. Previously, it was proposed that EBOV entry was either clathrin- and caveolin-dependent. However more recent work suggests that a macropinocytosis-like mechanism is required which is independent on clathrin or caveolin. Additionally, PI3K, actin, microtubules, calmodulin, and calmodulin kinase II are required for entry. EBOV trafficking is known to involve early and late endosomes, but it is unknown where fusion occurs, or if lysosomes are involved in entry. During fusion, the glycoproteins are proteolytically modified by lysosomal pH-dependent cathepsins. The nucleocapsid and genome are released into the cytosol, where replication occurs. Glycoproteins and matrix proteins are routed to the plasma membrane, where they encapsulate the nucleocapsid and genome during budding. There are still many unknowns regarding what type of lipid rafts are bound during entry, what triggers macropinocytosis, where fusion occurs, and what role lysosomes play in entry.

EBOV RECEPTOR CANDIDATES

Since its discovery over 30 years ago, relatively little is known of how EBOV enters mammalian cells. Initially, it was thought that EBOV bound asialoglycoprotein receptors like MARV; however, EBOV was still able to infect hepatocytes despite having sialylated glycans on its GPs (Becker et al., 1995). Wool-Lewis et al. suggested that B and T lymphocyte cell lines were resistant to infection by EBOV GP-encoated MLV particles because they lacked the receptor required for EBOV entry (Wool-Lewis and Bates, 1998). However, it was recently shown that EBOV can enter adherent T and B cells (Dube et al., 2010). Takada et al. found that β_1-integrins were down-regulated during EBOV infection, and proposed a role for these proteins in viral entry (Takada et al., 2000). Several years later, Schornberg et al. discovered that $\alpha_5\beta_1$-integrins are not directly involved in virus binding or internalization, but rather control the availability of endosomal cathepsins for proteolytic cleavage of viral GPs during entry (Schornberg et al., 2009). Chan et al. suggested that folate receptor α was an important co-factor for EBOV entry since overexpression of the receptor in Jurkat T cells – a cell line which normally resists infection at an MOI of 10 - resulted in infection (Chan et al., 2001). Empig et al. also proposed that caveolin-1 was required for virus entry, since infection with pseudotype virus was inhibited by cholesterol-sequestering drugs known to disrupt caveolae. Additionally, immunofluorescence microscopy suggested virus co-localization with caveolin-positive lipid rafts (Empig and Goldsmith, 2002). Next, Alvarez et al. used lentiviral pseudotyped viruses to show that C-type lectins, DC-SIGN and L-SIGN, were potential co-factors for entry (Alvarez et al., 2002). Additionally, Simmons et al. further suggested the importance of DC-SIGN in facilitating EBOV's broad tropism, and infection of early targets, such as macrophages

(Simmons et al., 2003a). However, contrary to what had previously been described, Simmons et al. showed that caveolae and folate receptor α were not required for EBOV entry for several reasons. First, macrophages are early and susceptible targets of virus infection, yet do not express detectable levels of folate receptor α. Second, T cells, which normally lack caveolae and folate receptor α, are not infected by EBOV. Finally, overexpression of caveolin-1 and folate receptor α in T cells did not result in infection (Simmons et al., 2003b). The role of DC-SIGN as a major receptor was disputed by Marzi et al.., where it was shown to improve virus attachment and allow for a slight increase in infectivity of normally infection-resistant B cells (Marzi et al., 2007). Other co-factors have also been indicated as important for virus infection. Bavari et al. showed that EBOV entry also requires cholesterol-enriched lipid rafts since pre-treatment of cells with methyl-β-cyclodextrin (MβCD), a cholesterol depleting drug, greatly reduced infection (Bavari et al., 2002; Saeed et al., 2010). However, lipid rafts are composed of a mixture of lipids, predominantly sphingomyelin. The selectivity of this agent has been questioned since MβCD also depletes sphingomyelin (Giocondi et al., 2004) as well as being highly cytotoxic. Therefore, although many receptor candidates exist, to date, no single cell molecule appears critical for mediating virus binding and entry into cells. Also, many of the receptor candidates have been refuted, although the differences in tests performed and cells used vary widely. Dependence on pseudotyped virus particles may have contributed to much of this confusion, and emphasizes the need to perform supporting work with wild type virus particles. In summary, the identity of the EBOV receptor appears elusive at the moment.

EBOV ENDOCYTOSIS AND TRAFFICKING

Understanding the endocytic mechanism that internalizes EBOV has been equally challenging. As discussed previously, caveolae are not required for virus entry because cells lacking caveolin-1 can become infected, and cells that are resistant to infection do not become more susceptible to infection when caveolin-1 is overexpressed (Simmons et al., 2003b). Using a variety of chemical inhibitors, Sanchez suggested that EBOV entry occurred via a clathrin- or caveolin-mediated endocytic pathway, requiring cellular receptors, actin filaments, and microtubules. First, many drugs are known to have pleiotropic effects – some of which have been well-characterized, some of which have not. Chlorpromazine, for example, is classically used to identify clathrin-mediated entry, yet it is also a calmodulin antagonist and acid sphingomyelinase inhibitor (Masson et al., 1992). The impact of this drug was studied with wild type EBOV, but readout of the assay was based on visualizing the approximate percentage of uninfected detached cells after 72 hours of drug treatment. Chemical toxicity can cause cell detachment without virus being present, so by using this analytical method, it is unclear as to whether the cells had detached due to drug toxicity or some other factor (Sanchez, 2007). Using pseudotyped virus, Bhattacharyya et al. recently suggested that EBOV enters via clathrin-mediated endocytosis since infection was blocked with either sucrose, chlorpromazine, a dominant-negative for Eps 15, or siRNA against the clathrin heavy chain (Bhattacharyya et al., 2010). There are concerns here as well. First, Ivanov discussed that sucrose is an inappropriate tool for identifying clathrin-mediated endocytosis as a mechanism of entry since the treatment generates considerable osmotic stress to the cell, which likely alters and stimulates signaling pathways that would not be activated under normal conditions (Ivanov, 2008). Second, as previously mentioned, chlorpromazine has other effects. Third, this did not rule out other

endocytic pathways, such as macropinocytosis. Macropinocytosis is a carefully regulated process involving coordinated endo- and exocytosis to balance cell volume (Falcone et al., 2006). The increased osmotic stress suggests that fluid-phase uptake may be altered or blocked, in addition to other uptake mechanisms. Fourth, HIV pseudotypes were used, which means the size and shape of the viral particle was that of HIV, not the long filamentous EBOV particle. Because pseudotyped virus particles may be selectively internalized based on size, this assay system may not accurately reflect how wild type EBOV enters the cell. In 2008, Saeed et al. showed that phosphoinositide-3 kinase (PI3K)-Akt pathway was important for EBOV entry, using γ-irradiated wildtype EBOV, or lentiviruses coated with EBOV GP, demonstrating that GP can stimulate PI3K in both systems (Saeed et al., 2008). Later, in 2009, work by Kolokoltsov et al. showed that EBOV entry is inhibited by specific genetic and chemical inhibitors of calmodulin and calmodulin-kinase II (Kolokoltsov et al., 2009). In 2010, two independent groups suggested that EBOV enters the cell via macropinocytosis. Nanbo et al. used EBOV GP encoated VSV particles, EBO virus-like particles (EBOVLPs), and biologically contained EBOV to show that EBOV GP activates actin cytoskeleton rearrangement, membrane ruffling, and macropinocytosis via a PI3K/PAK1-dependent pathway (Nanbo et al., 2010). Saeed et al. used wild type virus to show EBOV entry does not require clathrin, caveolae, or dynamin, but is dependent on macropinocytic proteins, Pak1 and Ctbp1/BARS (Saeed et al., 2010).

In summary, EBOV binds to lipid rafts, and is internalized via a macropinocytosis-like mechanism. This process is independent of clathrin and caveolin, but requires calmodulin, calmodulin kinase II (CAMKII), PI3K, microtubules, and actin. Once inside the cell, EBOV

moves from the early to late endosomes. However, it is unknown what triggers this macropinocytosis-like entry mechanism.

SPHINGOMYELIN/CERAMIDE PATHWAY

SPHINGOMYELIN: A MAJOR MAMMALIAN SPHINGOLIPID IMPORTANT IN MEMBRANE FUNCTION

Cell membranes are composed of lipids and proteins. Sphingomyelin (N-acyl-sphingosyl-1-phosphocholine) is one of the most predominant lipids in mammalian plasma and organelle membranes (Ishitsuka and Kobayashi, 2004; Shakor et al., 2003; Shogomori and Kobayashi, 2008; Yamaji et al., 1998). Sphingomyelin is a sphingophospholipid with two long hydrophobic hydrocarbon chains attached to a bulky, highly charged phosphocholine headgroup. Due to its zwitterionic properties, the overall charge is neutral. In contrast, cholesterol (cholest-5-*en*-3-β-ol) is a neutral sterol, consisting of a small polar headgroup attached to a large hydrophobic region with several fused steroid rings and a tail. Cholesterol preferentially associates with sphingomyelin to form distinct detergent-resistant microdomains (DRMs), or lipid rafts, with sphingomyelin concentrated on the membrane's outer leaflet. The physical and chemical properties of cholesterol and sphingomyelin cluster receptor proteins within rafts, creating signaling platforms for endocytosis, exocytosis, and other cell functions (Barenholz, 2004). Work by Rogasevskaia et al. suggested that the role of sphingomyelin in DRMs is more specific. Although cholesterol contributes to membrane elasticity, vesicle fusion, and fusion efficiency, sphingomyelin can act as an environmental sensor, responding to calcium concentration to trigger membrane fusion (Rogasevskaia and Coorssen, 2006). Another critical role of sphingomyelin is seen when it is hydrolyzed by sphingomyelinases. Sphingomyelinases

cleave off the bulky phosphocholine headgroup, leaving behind the lipid, ceramide (Figure 5). Ceramide can exclude cholesterol from the raft, but retains cholesterol's ability to fuse membranes. The wedge-shaped structure of ceramide causes negative membrane curvature and invagination. (Rogasevskaia and Coorssen, 2006). Additionally, ceramide and its metabolites – sphingosine, ceramide-1-phosphate, and sphingosine-1-phosphate are responsible for activation of signaling pathways for apoptosis, inflammation, cell cycle arrest, proliferation, and differentiation (Bartke and Hannun, 2009; Cremesti et al., 2002; Ohanian and Ohanian, 2001; Smith and Schuchman, 2008; Wymann and Schneiter, 2008). Therefore, sphingomyelin and its products play important roles in many cellular membrane-related processes.

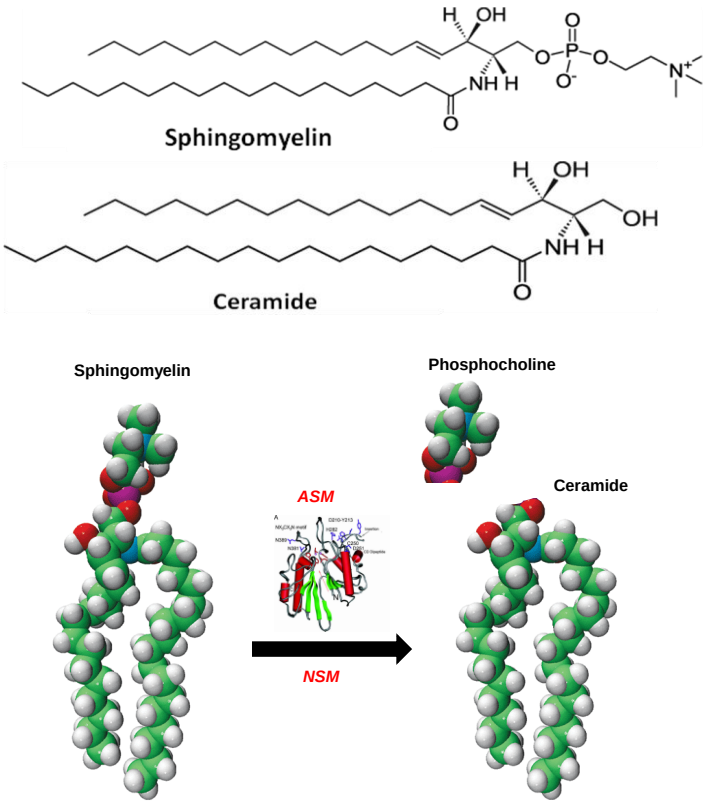

Figure 5. Sphingomyelin hydrolysis to ceramide by acid or neutral sphingomyelinases (ASM, NSM). (Top) Lipids represented as space filling models. The structure of ASM as determined by x-ray crystallography is shown in the center (Seto et al., 2004)(Bottom) Schematic of how

sphingomyelinases cleave the bulky phosphocholine headgroup from sphingomyelin to form ceramide.

SPHINGOMYELINASES: ENZYMES THAT HYDROLYZE SPHINGOMYELIN TO FORM CERAMIDE

Sphingomyelinases are enzymes which hydrolytically cleave the phosphocholine headgroup from sphingomyelin to form ceramide (Figure 5). Sphingomyelinase-induced ceramide signaling has been shown to sequentially activate tyrosine kinase, p21-activated kinase (PAK1), and PI3K, resulting in cell proliferation (Hanna et al., 1999). Sphingomyelinases are characterized by their subcellular location, pH optima, and associated cofactors.

ACID SPHINGOMYELINASES

Acid sphingomyelinases consist of two isoforms derived from the same gene, *SMPD1* (sphingomyelin phosphodiesterase 1) (Ferlinz et al., 1994). During transcription, three mRNA splice variants are produced, with only one being translated into an active enzyme. Glycosylation and peptide processing begin in the endoplasmic reticulum (ER) and terminate in the Golgi apparatus. A mannose-6-phosphate residue is added to the pro-lysosomal form, targeting the pro-enzyme to lysosomes (Claus et al., 2009; Zeidan and Hannun, 2010). Once the 72 to 75 kDa pro-acid sphingomyelinase enters the lysosome, a thiol-sensitive protease removes the C-terminus cysteine residue. This modification activates the enzyme, and is thought to facilitate interaction with lysosomal zinc. Active lysosomal acid sphingomyelinase (L-SMase) is 65kDa, lacks an intact C-terminus, is zinc-independent, and is degraded by a leupeptin-sensitive protease, which reduces the enzyme to a 52 kDa inactive form. L-SMase attaches to the inner leaflet of the vesicle via electrostatic forces, is most active at pH 5, and is sensitive to the drug desipramine. Pro-acid sphingomyelinase that leaves the Golgi without a mannose-6-phosphate

residue is released extracellularly via the Golgi secretory pathway. Unlike the lysosomal isoform, secretory sphingomyelinase (S-SMase) is 75 to 80 kDa, is zinc-dependent, has an unmodified C-terminus, is extracellular, and is insensitive to desipramine (Jenkins et al., 2011). S-SMase is active in a pH range from 5 to 7, allowing it to hydrolyze sphingomyelin on the outer leaflet of cell membranes, and even sphingomyelin-encoated low density lipoprotein (LDL) circulating in the bloodstream (Zeidan and Hannun, 2010).

L-SMase is distributed throughout all tissues, and both isoforms are found in serum, urine, saliva, synovial fluid, and in especially high concentrations in tears (Schissel et al., 1996; Takahashi et al., 2000). S-SMase is secreted by human monocyte-derived macrophages, human skin fibroblasts, and microglial cells, with human vascular endothelial cells being the most abundant source of the enzyme. Also, during monocyte differentiation to macrophages, S-SMase is notably upregulated (Marathe et al., 1998; Schissel et al., 1998; Schissel et al., 1996).

Acid Sphingomyelinase Activation and Regulation

Acid sphingomyelinases are activated by numerous agonists, such as cellular receptors, cytotoxic agents, oxidative stress, and certain pathogens. Enzymatic activation through ligand-receptor interactions includes ligands TNF-α, TRAIL, CD95, CD40, and IL-1 (Zeidan and Hannun, 2010). The cytotoxic agents, cisplatin, PMA, and doxorubicin, also trigger acid sphingomyelinase activity. In fact, UV light and LPS can initiate enzymatic activation. Finally, several bacteria and viruses have been shown to stimulate acid sphingomyelinase while entering mammalian cells (Zeidan and Hannun, 2010).

Regulation of acid sphingomyelinases occurs through several mechanisms. First, certain agonists selectively activate the secretory isoform. Recent work by Jenkins et al. suggests that

inflammatory cytokines (e.g. TNF-α and IL-1β) preferentially upregulate S-SMase, without effecting L-SMase. Treatments with certain chemicals, such as PMA, increased S-SMase activity ten-fold, while decreasing L-SMase by half in treated cells. Similarly, NH_4Cl simultaneously increased S-SMase activity while reducing L-SMase activity. This likely increases ceramide formation on the outer leaflet of cell membranes. Second, extreme differences in isoform half lives may play a role in regulation. L-SMase has a relatively high turnover ($t_{1/2}$ = ~5h) compared to the extremely stable S-SMase ($t_{1/2}$ = ~48h). Because of this, small increases in S-SMase concentration and activity may become greatly exaggerated over time. Third, regulation may occur through a key phosphorylation site. Jenkins et al. replaced serine 508 (S508) with alanine to generate an acid sphingomyelinase mutant which retains approximately 30 to 70 percent L-SMase activity, while abolishing its secretory function. The phosphorylation site at S508 is thought to be another form of regulation for this enzyme (Jenkins et al., 2010).

ASM –Dependent Endocytosis

Lysosomal ASM plays an important role in endocytosis. Zha et al. found that when macrophages and fibroblasts were treated with sphingomyelinase, numerous uncoated vesicles - approximately 400 nm in diameter - would pinch off from the plasma membrane, and internalize within ten minutes of treatment. During this large scale endocytic event, 15 to 30% of the plasma membrane was internalized. These large sphingomyelinase-induced vesicles transported fluid phase markers, suggesting they were macropinosomes. This process was also found to be independent of clathrin and caveolin. Furthermore, Zeidan et al. showed that ASM-induced

ceramide triggers actin rearrangement, cytoskeleton remodeling, and retraction of filopodia (Zeidan et al., 2008).

More recently, Tam et al. proposed that ASM-dependent endocytosis required lysosomal ASM to translocate to the outer leaflet of the plasma membrane via lysosmal exocytosis. There, ASM is likely retained within a temporary acidic pocket al.ong the membrane surface. ASM then hydrolyzes the sphingomyelin to ceramide, leading to ceramide macrodomain formation, membrane invagination, and endocytosis of the membrane. In this way, cells use lysosomal exocytosis to trigger ASM-dependent endocytosis (Tam et al., 2010) (Figure 6).

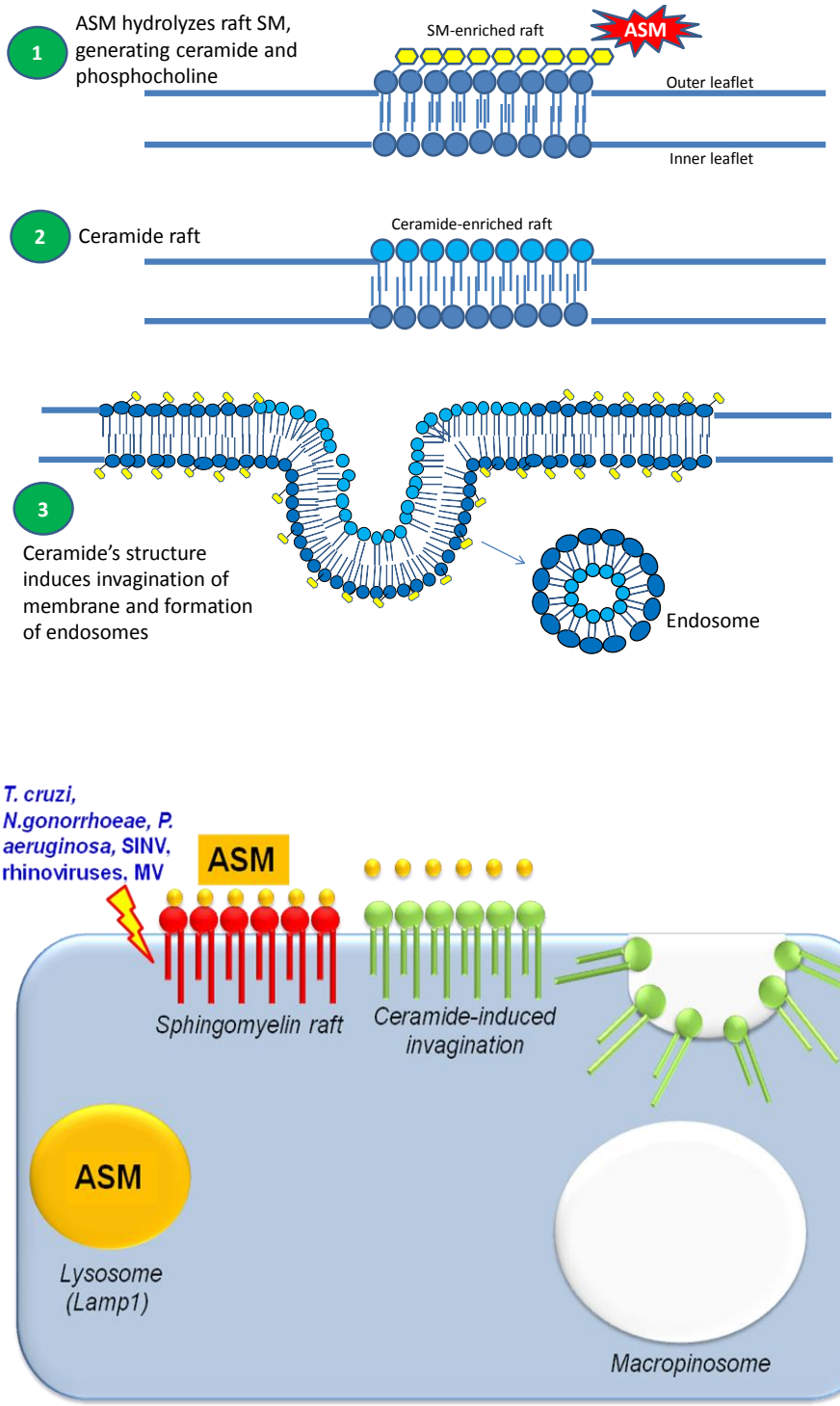

Figure 6. ASM activation results in formation of endocytic vesicles, or macropinosomes. (Top) ASM cleaves phosphocholine from sphingomyelin on the outer leaflet of the plasma membrane to form ceramide. This forces the membrane to pinch inward. (Bottom) When activated by

certain stimuli, lysosomal ASM translocates to the outer leaflet via lysosomal exocytosis. There, it converts sphingomyelin to ceramide. As the membrane invaginates, a macropinosome forms.

Mechanism of Action for ASM Inhibitors

Sphingomyelinase-generated ceramide has attracted much attention recently due to its increasing role in many human diseases. As a result several specific sphingomyelinase inhibitors have been discovered – many of which are already FDA-approved, and currently being used to treat other diseases. There are many different mechanisms of action that have been described for acid sphingomyelinase inhibitors.

First, functional inhibitors, such as imipramine, desipramine, amitriptyline, chloroquine, and chlorpromazine, are thought to act as weak bases. Because lysosomal membranes are less permeable to protonated bases, the drugs accumulate in the lysosomes. The electrostatic forces that attach acid sphingomyelinase to the inner leaflet of the lysosomal membrane become disrupted by the buildup of weak bases. As a result, the enzyme detaches from the membrane, and is targeted for proteolytic degradation. However, not all lipophilic weak bases inhibit acid sphingomyelinase activity (Hurwitz et al., 1994; Kornhuber et al., 2010; Kornhuber et al., 2008; Yoshida et al., 1985). Interestingly, functional acid sphingomyelinase inhibitors are found across many drug classes, but their distribution is largely concentrated within two classes: antihistamines for systemic use (ATC drug class R06), and psychoanaleptics (ATC drug class N06) (Kornhuber et al., 2010). By inhibiting V-ATPase function, Bafilomycin A increases lysosomal pH, and effects ASM activity in a similar manner.

Second, a few direct inhibitors exist, such as phosphatidyl-myo-inositol-3,4,5 triphosphate, phosphoinositide analogues, SMA-7, AD2765, biphosphonates, and plant-derived

α-mangostin. Biphosphonates, which are used to treat osteoporosis, are some of the most potent inhibitors to date. But due to their rapid absorption from the blood to bone, their efficacy as *in vivo* inhibitors is questionable (Arenz, 2010; Kornhuber et al., 2010).

Third, acid sphingomyelinase inhibitors characterized as tricyclic anti-depressants (e.g., desipramine, imipramine) are thought to destabilize detergent-resistant membranes, or lipid rafts. Klingenstein et al. found that desipramine treatment disrupted membrane raft integrity, and redistributed cholesterol from the plasma membrane to intracellular compartments (Klingenstein et al., 2006) (Figure 7). Later work by Pakkanen et al. suggested that parvovirus trafficking was inhibited by desipramine's disordering of lipid rafts in endosomal compartments. Because no virus was left bound to the outside of the cell, it was suggested that the drug worked on intracellular compartments, possibly blocking viral uncoating (Pakkanen et al., 2009a; Pakkanen et al., 2009b).

A fourth mechanism of action is that the inhibitors may act as a non-specific detergent, much like CHAPS. It was further suggested that the amphiphilic properties of desipramine alone are not sufficient to detach the enzyme from the lysosomal membrane (Kolzer et al., 2004).

As a fifth mechanism, some acid sphingomyelinase inhibitors may work indirectly by blocking other proteins required for normal enzyme function. Masson et al. inhibited acid sphingomyelinase with W-7, a potent calmodulin kinase inhibitor, suggesting that acid sphingomyelinase activity is calmodulin kinase-dependent. It was further suggested that anti-depressants such as desipramine; and phenothiazines, such as chlorpromazine; may also inhibit acid sphingomyelinase through calmodulin antagonism, but to a lesser extent (Masson et al., 1989; Masson et al., 1992).

Finally, the most commonly used acid sphingomyelinase inhibitors – desipramine, imipramine, and amitriptyline – are non-toxic in cell culture at or below 25 μM, and do not inhibit other known lysosomal enzymes, or neutral sphingomyelinases (Hurwitz et al., 1994; Kornhuber et al., 2010; Kornhuber et al., 2008). Furthermore, recent work by Jenkins et al. shows that desipramine inhibits only the lysosomal form, not the secretory form, of acid sphingomyelinase (Jenkins et al., 2011). This difference allows for further dissection of the role of each sphingomyelinase isoform in disease.

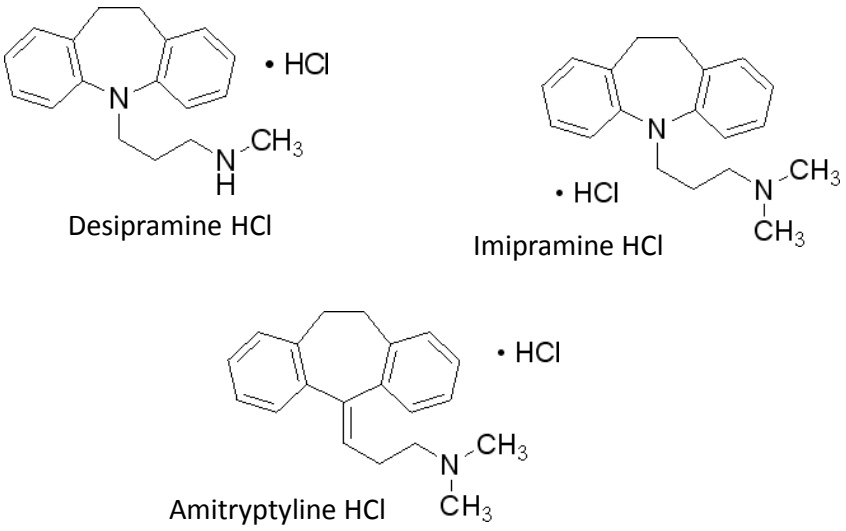

Figure 7. ASM inhibitors. Desipramine, imipramine, and amitriptyline are class II amphiphiles and tricyclic anti-depressants, which have been shown to inhibit ASM activity with equal efficacy.

NEUTRAL SPHINGOMYELINASES:

Neutral sphingomyelinases (NSMs) hydrolyze sphingomyelin to form ceramide with optimum activity at neutral pH. There are several NSM isoforms, but, unlike ASM, each is encoded by a different gene. *SMPD2* generates NSM1, which is composed of 423 amino acids, and found mostly in the ER. NSM2 is the product of *SMPD3*, is 655 amino acids long, and is concentrated along the inner leaflet of the plasma membrane, and the cytosolic leaflet of multivesicular bodies (Claus et al., 2009; Marsh and van Meer, 2008; Tani and Hannun, 2007; Wu et al., 2010). Lastly, NSM3 is generated by *SMPD4*, contains 866 amino acids, and is predominantly localized to the ER, Golgi, and trans-Golgi network (Claus et al., 2009; Wu et al., 2010). NSMs1 and 3 have transmembrane domains and require a zinc co-factor, but NSM2 does not. However, NSM2 has a collagen-like domain, which the other two isoforms lack. Surprisingly, sequence homology among the three NSMs is quite low despite their similar function (Wu et al., 2010).

Neutral Sphingomyelinase Activation and Regulation:

Although more NSMs have been discovered, relatively little is known about their activation and regulation compared to ASMs. Because the neutral sphingomyelinase isoforms were once thought to be the same enzyme, most work to date discusses NSMs in more general terms. Like ASMs, NSMs are activated by TNF-α, IL-1β, UV light, LPS, and cytotoxic drugs. However, they can also be stimulated by amyloid-β peptides and mechanical stress (Clarke and Hannun, 2006; Czarny et al., 2003; Wu et al., 2010). NSM activation plays a role in multiple cellular pathways, including cell growth, cell cycle arrest, apoptosis, cancer pathogenesis, neurodegenerative disorders, and inflammation (Clarke and Hannun, 2006; Wu et al., 2010).

Regulators of NSM include RACK1, FAN, PKC, caveolin-1, glutathione, oxidative stress, and proteases (Clarke and Hannun, 2006; Veldman et al., 2001).

Because NSM2 is localized to the cytosolic side of the plasma membrane, much attention has been focused on this enzyme. Kim et al. showed that NSM2 activation is calcium-dependent (Kim et al., 2010). Filosto et al. further suggested that calcineurin, a calcium/calmodulin-dependent phosphatase, was directly bound to NSM2, and directly regulated the enzyme much like an "on/off switch" (Filosto et al., 2010).

NSM2, Blebbing, and Exosome Formation

NSM 2 has two known functions in cells – bleb formation and exosome formation. Work by Trajkovic et al. showed that treatment of cells with NSM 2-targeting siRNA, or GW4869, a specific NSM inhibitor, decreased formation of ceramide-rich exosomes from multivesicular bodies, which subsequently reduced the number of exosomes secreted from the plasma membrane (Marsh and van Meer, 2008; Trajkovic et al., 2008). Pro-apoptotic stimuli can also cause sphingomyelin on the outer leaflet of the plasma membrane to flip to the inner leaflet. There, cytosolic NSM 2 converts sphingomyelin to ceramide. Due to ceramide's structure, it no longer forms a tight junction with cholesterol. As a result, membrane disruption occurs, leading to membrane shedding and blebbing. (Ohanian and Ohanian, 2001; Tepper et al., 2000; van Blitterswijk et al., 2003) (Figure 8).

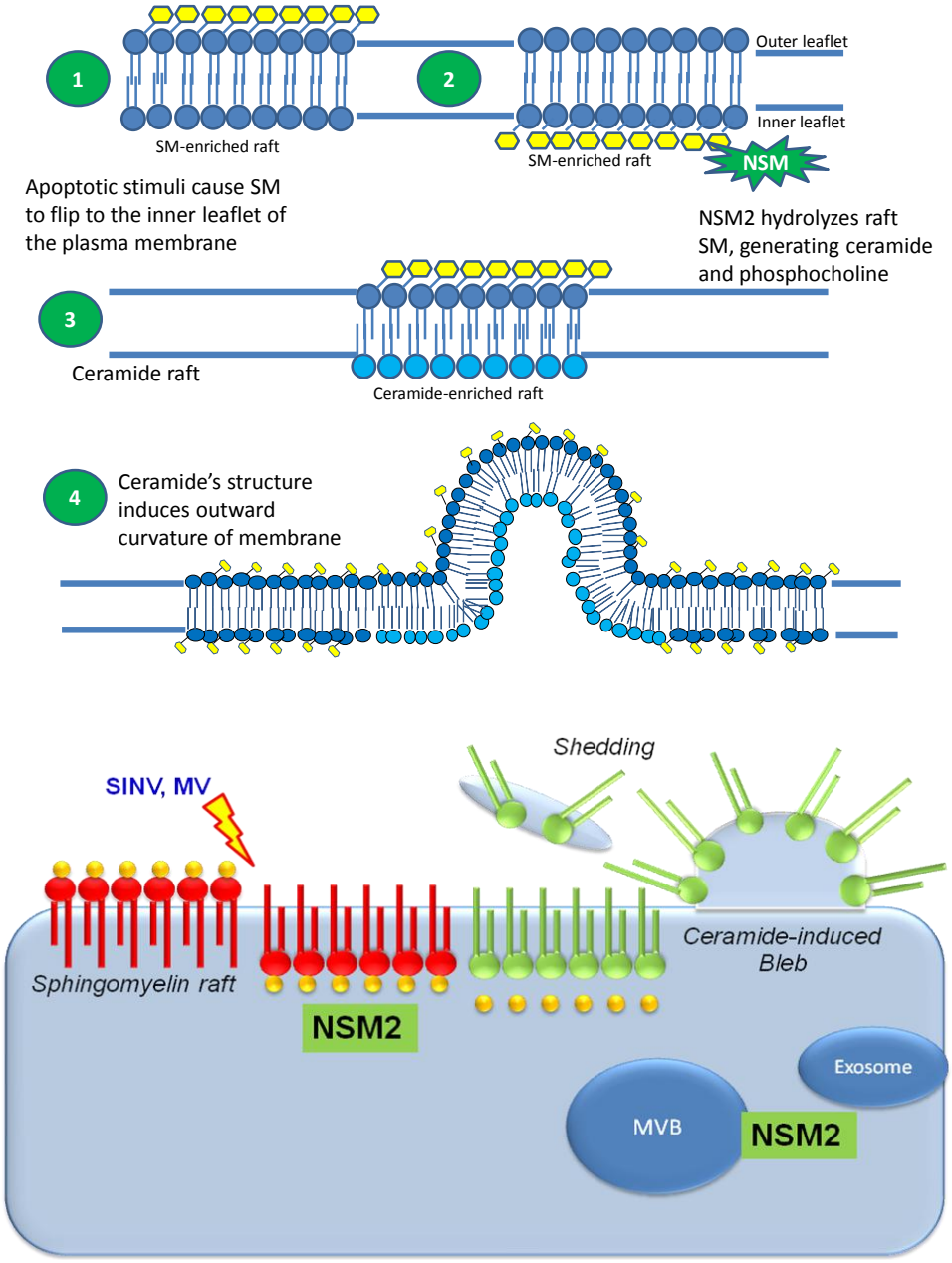

Figure 8. NSM2 activation results in formation of blebs and exosomes. (Top) Pro-apoptotic stimuli cause sphingomyelin to flip to the inner leaflet where NSM2 converts it to ceramide. This forces the membrane to pinch outward. (Bottom) When NSM2 forms ceramide on the inner leaflet of the plasma membrane, blebs form. However, NSM2-induced ceramide formation on multi-vesicular bodies results in exosome formation.

Mechanism of Action for NSM Inhibitors

Several neutral sphingomyelinase inhibitors have been developed to counter the effects generated by activation of the sphingomyelinase/ceramide pathway (Figure 9). Scyphostatin, a purified by-product of the fungus *Trichopeziza mollissima*, is a specific inhibitor of mammalian neutral sphingomyelinase. At 1 μM, it inhibits enzyme activity by 50 percent (Nara et al., 1999a; Nara et al., 1999b). Due to scyphostatin's specificity and potency, analogues such as manumycin A and spiroepoxide were developed. Both analogues, of course, act as potent, irreversible, and competitive inhibitors of sphingomyelin. However, manumycin A is a more potent inhibitor than spiroepoxide (Arenz et al., 2001; Wascholowski and Giannis, 2006) (Figure 8). Next, non-epoxy sphingolactones were developed. They bind neutral sphingomyelinase's active site, acting as specific, competitive, and irreversible inhibitors of the enzyme. Of the sphingolactones, sphingolactone-24 is the most potent (Wascholowski and Giannis, 2006). Lastly, GW4869 is a specific, potent, and non-competitive inhibitor of neutral sphingomyelinase, with 1 μM inhibiting enzyme activity by 50 percent. In characterizing the effects of GW4869 on TNF-α-induced apoptosis, Luberto et al. found that 20 μM GW4869 provided cells with complete protection, whereas 10 μM offered only partial protection. Of the various signs of apoptosis observed – chromatin condensation, mitochondrial swelling, and membrane blebbing – GW4869 had the most pronounced effect in reducing blebbing (Luberto et al., 2002; Marchesini et al., 2003).

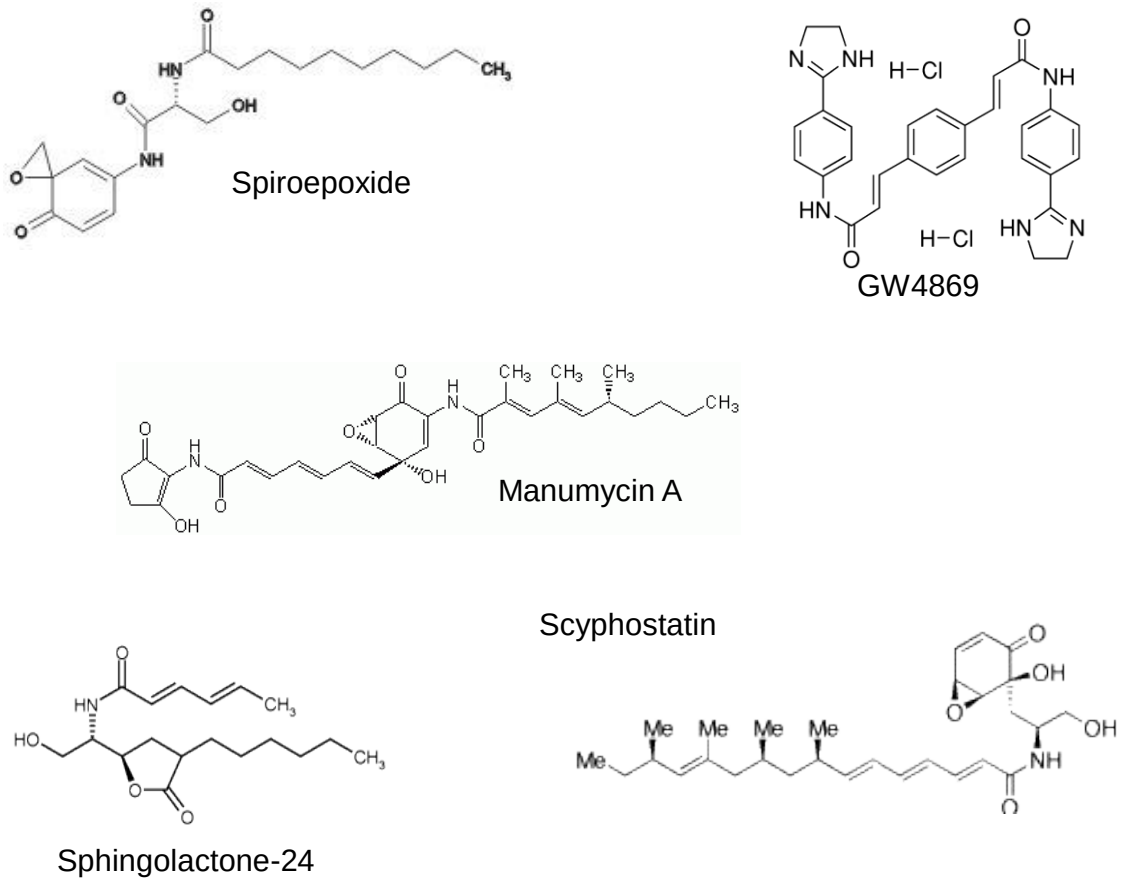

Figure 9. NSM inhibitors. Spiroepoxide and manumycin A are analogues of scyphostatin, and all act as specific, competitive, irreversible inhibitors of NSM. Sphingolactone-24 is the most potent inhibitor because it binds the enzyme's active site. GW4869 is a specific, potent, non-competitive inhibitor of NSM, yet its exact mechanism of action is unknown.

SPHINGOMYELIN TRAFFICKING PROTEIN, NIEMANN-PICK TYPE C1 (NPC1) PROTEIN

Because sphingomyelin is a major component mammalian membranes, it is routinely endo- and exocytosed during regular cell membrane recycling. In this process, sphingomyelin is transported through the early endosomes, to the late endosomes. There, Niemann-Pick Type C1 (NPC1) protein routes the sphingolipid to either the lysosomes for degradation by ASM, or to the plasma membrane to replace lost membrane sphingomyelin (Figure 10) (Koivusalo et al., 2007). In ASM-dependent endocytosis, macropinosomes form as a result large ceramide-induced

invaginations of the plasma membrane (Zha et al., 1998). In a similar manner, NSM2-dependent ceramide formation leads to membrane blebbing and shedding (Tepper et al., 2000; van Blitterswijk et al., 2003). In either case, a substantial membrane sphingomyelin is lost, and must be replaced by NPC1-dependent exocytosis (Koivusalo et al., 2007). In NPC1 disease, a rare, often fatal lipid storage disorder, NPC1-dependent trafficking is impaired, causing lysosomes to swell with cholesterol, sphingomyelin, and other cargo. This is due to a mutation in the *NPC1* gene, which prevents the NPC1 protein from associating with the late endosomal and lysosomal membranes. As a result, the detached, mutant protein is proteolytically degraded, leaving the cell without function NPC1 (Ko et al., 2001; Lange et al., 1998; Slotte et al., 1989). Characterization of the NPC1 trafficking defect has helped us to better understand sphingomyelin trafficking, as well as NPC1 function. As additional tool for studying sphingomyelin trafficking, the chemical inhibitor, U18666A, was found to induce a similar trafficking defect as seen in NPC1 disease. More precisely, U18666A inhibits NPC1-dependent trafficking to the plasma membrane (Ko et al., 2001; Liscum, 1990; Liscum and Faust, 1989).

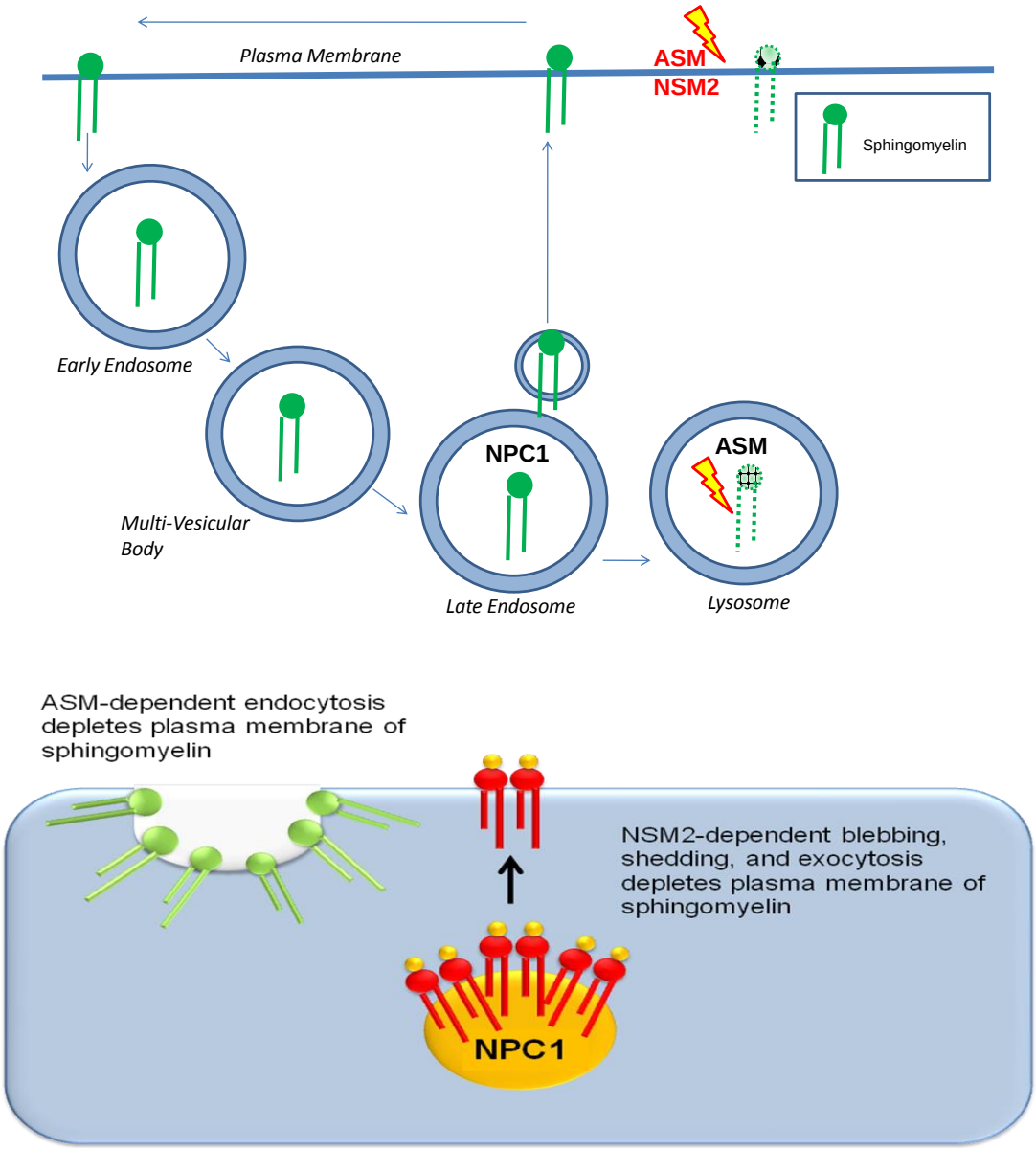

Figure 10. Sphingomyelin trafficking. (Top) Sphingomyelin (SM) is trafficked from the plasma membrane, to the early endosomes, multi-vesicular bodies (MVBs), and late endosomes. NPC1 then routes SM to the plasma membrane or lysosomes. Once in the lysosome, SM is degraded by acid sphingomyelinase (ASM). (Bottom) Under stress-induced conditions, lysosomal ASM is recruited to the outer leaflet of the plasma membrane via lysosomal exocytosis. There, it hydrolyzes SM to ceramide. Additionally, neutral sphingomyelinase 2 (NSM2) is located on the inner leaflet of the plasma membrane where it hydrolyzes SM to ceramide. Through the activation of ASM and/or NSM2, membrane SM is depleted, likely inducing NPC1-dependent repletion of SM to the plasma membrane via exocytosis. Modified from (Koivusalo et al., 2007).

Mechanism of Action for Exocytosis Inhibitors, U18666A and Vacuolin-1

The chemical inhibitor, U18666A, induces a similar trafficking defect as seen in NPC1 disease (Figure 11). Lysosomes swell with sphingomyelin and cholesterol until their NPC1-dependent movement to the plasma membrane is severely reduced. (Ko et al., 2001; Liscum, 1990; Liscum and Faust, 1989). Vacuolin-1 specifically blocks lysosomal exocytosis to the plasma membrane with affecting endocytosis or actin skeleton rearrangement (Cerny et al., 2004; Huynh and Andrews, 2005). Bao used vacuolin-1 to block lysosomal exocytosis of ASM to the plasma membrane. This specifically inhibited ASM-dependent ceramide macrodomain formation on the cell surface (Bao et al., 2010b). Falcone also showed that vacuolin-1 blocks the exocytic, but not the endocytic, function of macropinocytosis (Falcone et al., 2004). Finally, vacuolin-1 has also been used to block histamine release from mast cells (Shaik et al., 2009) (Figure 12).

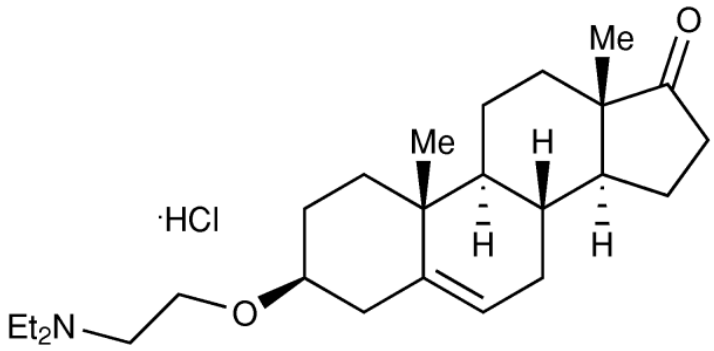

Figure 11. NPC1-trafficking inhibitor, U18666A.

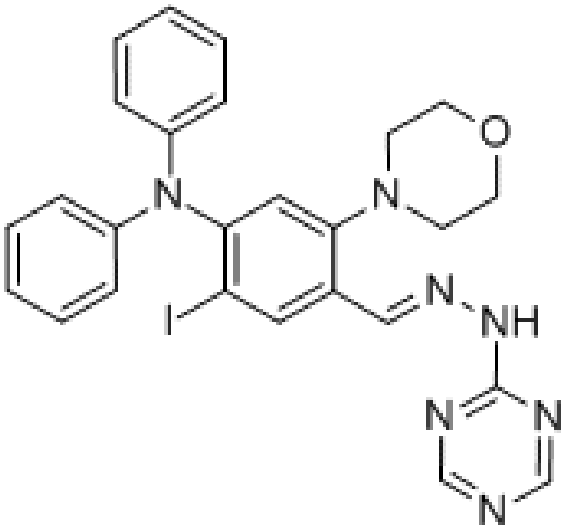

Figure 12. Lysosomal trafficking inhibitor, vacuolin-1.

ROLE OF SPHINGOMYELINASES IN INFECTION

Bacteria

Sphingomyelinases play a direct and important role in many pathogen entry mechanisms. First, many bacteria are known to manipulate sphingomyelinases to enter mammalian cells. Grassme et al. showed that treatment with MβCD, a reagent which selectively extracts cholesterol and sphingomyelin from cell membranes, blocked internalization of *Pseudomonas aeruginosa*. Additionally, *P. aeruginosa* was unable to enter cells lacking acid sphingomyelinase (Grassme et al., 2003; Gulbins et al., 2004; Gulbins and Li, 2006). Grassme et al. suggested that the bacterium induces translocation of acid sphingomyelinase to the cell surface, where the enzyme converts raft sphingomyelin to ceramide. The ceramide enlarges the membrane raft, the raft invaginates, and the pathogen is internalized. Dramatic bacterium-induced raft restructuring occurred with 5 to 10 minutes of infection, and was complete within 30 minutes (Grassme et al., 2003). Electron microscopy shows acid sphingomyelinase accumulating near bacteria still bound to the cell surface (Gulbins et al., 2004).

Falcone et al. found that *Escherichia coli* activate acid sphingomyelinase to form ceramide-rich rafts in human monocyte-derived immature dendritic cells. This leads to apoptosis, sepsis-induced immune suppression. The acid sphingomyelinase inhibitor, imipramine (20 μM), inhibited both acid sphingomyelinase activation, and ceramide formation. Nitric oxide (NO), a natural inhibitor of the sphingomyelinase/ceramide pathway, also blocked ceramide-induced apoptosis. However, neutral sphingomyelinase inhibitors, scyphostatin (1μM) and manumycin A (5μM), had no effect. Acid sphingomyelinase activity increased above basal levels within 5 minutes of LPS or *E. coli* treatment, peaked at 30 minutes, and returned to basal

levels within 60 minutes of initial treatment. Interestingly, mature dendritic cells have significantly less acid sphingomyelinase than immature dendritic cells; and mature dendritic cells were not sensitive to ceramide-induced apoptosis (Falcone et al., 2004).

Neisseria gonorrhoeae enters cells via macropinocytosis, and stimulates host acid sphingomyelinase activity within the first five minutes of host cell invasion. During this process, approximately 35 percent of host membrane sphingomyelin is hydrolyzed to ceramide. Bacteria colocalized with fluid phase markers, and their entry was blocked by inhibitors of PI3K, actin polymerization, and acid sphingomyelinase. Additionally, acid sphingomyelinase-deficient cells were resistant to *N. gonorrhoeae* infection (Grassme et al., 1997; Zenni et al., 2000). Pre-treatment of mammalian cells with acid sphingomyelinase inhibitors, imipramine or SR33557, inhibited internalization of bacteria, but did not prevent binding (Hauck et al., 2000).

Viruses

Several viruses take advantage of sphingomyelinase-induced ceramide production to gain access to mammalian cells. Dreschers et al. showed that rhinoviruses stimulate acid sphingomyelinase to generate ceramide-enriched rafts within minutes of virus being added to cells. Peak ceramide raft formation occurs at 15 minutes post-inoculation, and returns to basal levels within 2 hours. Transfection with siRNA targeting acid sphingomyelinase, or treatment with MβCD, abolished virus infection (Dreschers et al., 2007). More recent work by Grassme et al. shows that rhinovirus entry is also blocked by acid sphingomyelinase inhibitors, imipramine and amitriptyline. Additionally, mutant primary human fibroblasts lacking acid sphingomyelinase activity are resistant to rhinovirus infection. Grassme et al. also found that rhinovirus infection causes immediate acid sphingomyelinase activation, and microtubule-

dependent translocation of the enzyme from an intracellular compartment to the outer leaflet of the plasma membrane. Acid sphingomyelinase then converts raft sphingomyelin to ceramide, causing membrane invagination and endocytosis (Grassme et al., 2005).

Sindbis virus (SINV) entry activates both acid and neutral sphingomyelinase to generate ceramide, but at different time points during infection. SINV binding to the plasma membrane increases acid sphingomyelinase activity with 30 minutes post-inoculation – peaking at 90 minutes in mouse neuroblastoma (N18) cells, and within 4 hours, in primary human fibroblasts. As sphingomyelinase activity begins to wane, neutral sphingomyelinase activity peaks at 4 hours, and again at 8 hours post-inoculation. This is paired by a sharp decrease in total sphingomyelin, and reciprocal increase in ceramide. Treatment with acid ceramidase, a ceramide-degrading enzyme, protects cells from ceramide-induced apoptosis. Additionally, mutant primary human fibroblasts with minimal to no acid sphingomyelinase activity have much early neutral sphingomyelinase activation, and are more susceptible to apoptosis. This suggests that in the absence of acid sphingomyelinase, cells may generate ceramide through neutral sphingomyelinase activation as a compensatory mechanism. The different signaling events required to produce neutral- verses acid sphingomyelinase-derived ceramide in ASM-/- fibroblasts may trigger a pro-apoptotic verses an anti-apoptotic pathway. Smit et al. also found that SINV fusion is receptor-independent, since fusion could occur in low pH liposomes containing cholesterol, sphingomyelin, and other sphingolipids (Smit et al., 1999). From this, it was suggested that SINV entry requires acid sphingomyelinase activation for virus fusion with the endosomal membrane, just prior to viral uncoating (Jan et al., 2000; Ng and Griffin, 2006).

Additionally, pretreatment of cells with desipramine blocks parvovirus trafficking, causing virions to become trapped within intracellular vesicles. Desipramine may disrupt cholesterol/sphingomyelin-rich membranes, or inhibit acid sphingomyelinase-derived ceramide formation (Pakkanen et al., 2009b).

Furthermore, Tani et al. found that treatment with sphingomyelinase notably increased Japanese encephalitis virus infection, while treatment with acid sphingomyelinase inhibitor, imipramine, blocked infection (Tani et al., 2010).

Finally, Gassert et al. used RNA interference and chemical inhibition to show that ASM and NSM2 are required for ceramide raft formation on primary human T cells during measles virus (MV) infection. More recently, Avota et al. found that MV uptake is enhanced through DC-SIGN-mediated sphingomyelinase activation (Avota et al., 2010; Gassert et al., 2009). Furthermore, Frecha et al. found that, like EBOV, MV entry occurs via macropinocytosis, and also requires PI3K, microtubules, and actin (Frecha et al., 2011).

SUMMARY

Because sphingomyelinases and NPC1, play such an integral part in sphingomyelin trafficking and endocytosis, I will investigate their roles in EBOV entry. Initially, I will assess the importance of sphingomyelin in EBOV infection using immunofluorescence assay and EBOVLPs. Additionally, I will show co-localization of ASM and lysosomal marker, lamp1, with EBOVLPs on the plasma membrane. Next, I will evaluate the role of ASM in EBOV infection using recombinant GFP-expression EBOV (EBOV-GFP) and ASM inhibitors. Then, I will use a mechanistic approach to determine which step of entry is affected by ASM inhibition. Using a pseudotyped virus infection assay, I will show that the ASM entry requirement is

specific for EBOV GP. Finally, I will use a mixing contents assay and EBOVLP-Luciferase to show that ASM inhibition blocks a fusion or pre-fusion step. In addition, because lysosomal exocytosis is required to deliver ASM to the outer leaflet of the plasma membrane, I will use EBOV-GFP and inhibitors of lysosomal exocytosis to show that this trafficking pathway is crucial for EBOV infection. Next, I will use the same methods to show that NSM2 inhibition blocks EBOV infection, is GP specific, and that NSM2 is required for a pre-fusion or fusion step. Finally, because NPC1-dependent exocytosis is required to deliver sphingomyelin on the plasma membrane, I will again use EBOV-GFP, pseudotyped viruses, EBOVLPs and NPC1 inhibitors to demonstrate the requirement for NPC1 in EBOV infection.

In summary, no effective drugs treatments exist to prevent or treat EBOV infection. Therefore, we will seek to identify potential drug targets by applying chemical and genetic inhibitors of sphingomyelinases and NPC1-dependent trafficking in the context of EBOV entry. During this process, we will determine whether a novel sphingomyelin-sphingomyelinase-NPC1-dependent entry mechanism is required for EBOV entry and infection, and if this pathway can be exploited for drug development.

CHAPTER 2: RESULTS

SPHINGOMYELIN AND LYSOSOMAL ACID SPHINGOMYELINASE (ASM) ARE IMPORTANT IN EBOV INFECTION.

INTRODUCTION

Sphingomyelin is a prominent lipid found in mammalian cell membranes. It preferentially associates with cholesterol to form lipid rafts on the plasma membrane (McIntosh et al., 1992a, b). These rafts harbor cellular receptors, and form signaling platforms important for entry (Kiyokawa et al., 2005). It has been previously shown that EBOV binds lipid rafts, and is sensitive to cholesterol extraction by MβCD treatment (Bavari et al., 2002; Saeed et al., 2010). Because MβCD has also been shown to extract sphingomyelin from cell membranes (Giocondi et al., 2004), it was unclear whether sphingomyelin was also important in EBOV entry. For this, we looked at the whether EBOV co-associates with sphingomyelin.

To test if EBOV requires sphingomyelin rafts for entry, HeLa cells were incubated with EBOVLPs for 90 minutes, rinsed once, and then immediately fixed with formalin. A 90 minute time point was used since previous work from our lab showed that EBOVLP co-localization with trans-Golgi marker, GM130, occurred within 90 minutes of VLPs being added to cells. Therefore, it was assumed that any co-localization event at the plasma membrane would occur no later than this time point. Cells were not permeabilized in order to show only co-localization events which occurred at the cell surface. To label sphingomyelin rafts, a unique sphingomyelin binding protein was used called lysenin. This protein is derived from the coelomic fluid of earthworms, and is a toxin which specifically binds clustered sphingomyelin, or sphingomyelin rafts. After fixation, cells were incubated with lysenin, followed by anti-lysenin antibody and

then a conjugated secondary antibody. Cells were then DAPI-stained and imaged with a Nikon T7 and Zeiss LSM 510 confocal immunofluorescence microscope using a 100x oil lens.

EBOVLPs Co-localize with Sphingomyelin rafts

EBOVLPs co-associated with sphingomyelin rafts at the earliest time point of 15 min, with the number of these events increasing with time. There appeared to be a correlation between the number of EBOVLPs bound, and the amount of sphingomyelin associated with them. Essentially, the more EBOVLPs that bind to the membrane, the more sphingomyelin is co-localized with them. Figure 13 shows co-localization of EBOVLPs with sphingomyelin at 90 minutes.

Because the hydrolysis of sphingomyelin leads to macropinosome formation, we next looked at whether ASM was involved in EBOV infection.

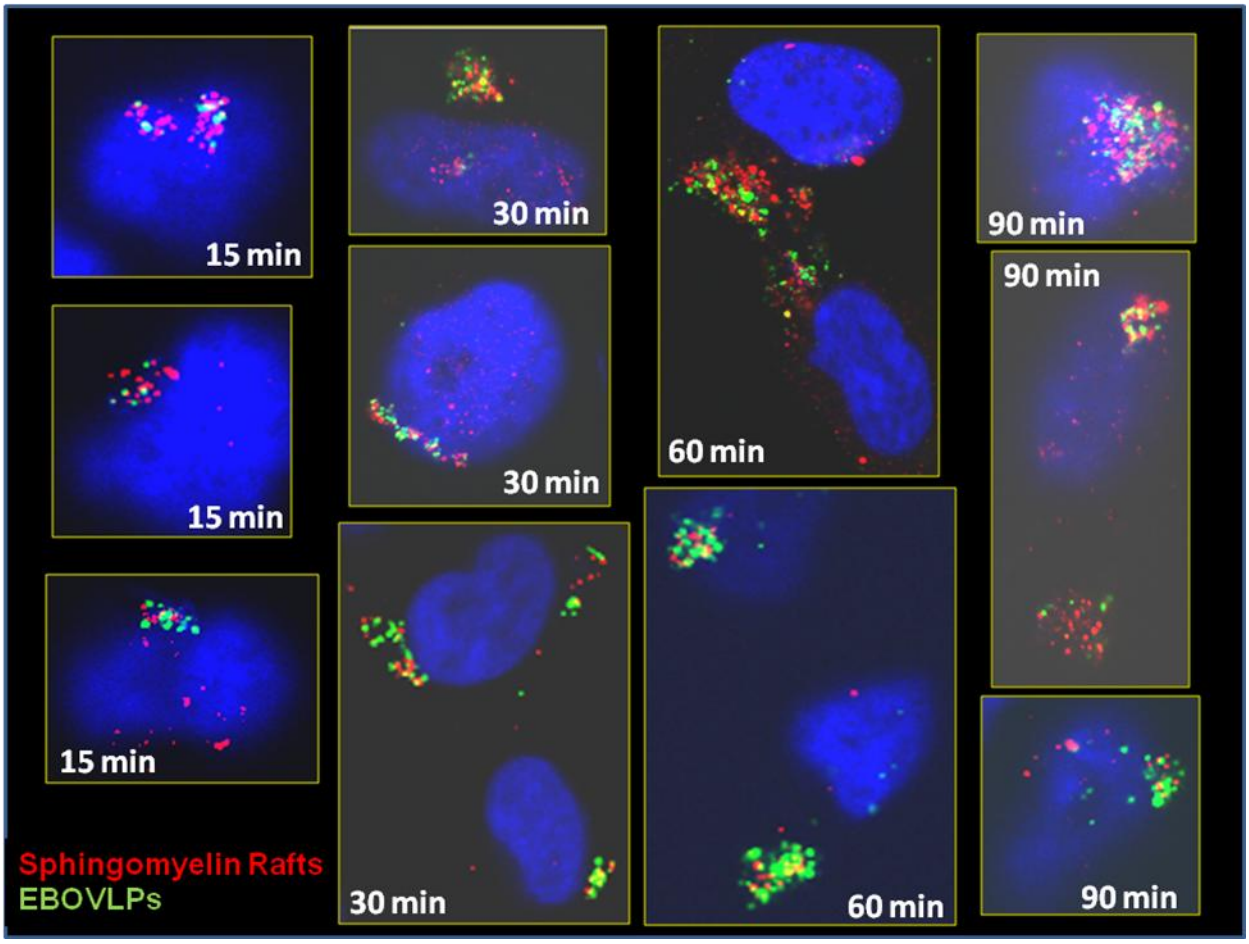

Figure 13. EBOVLPs co-localize with sphingomyelin rafts. HeLa cells were incubated with EBOVLPs for 15, 30, 60, or 90 minutes, rinsed once, and fixed with formalin. Cells were not permeabilized to show co-localization events on the cell surface. Cells were then incubated with lysenin, a toxin which specifically binds clustered sphingomyelin. After incubation with anti-lysenin antibody and Alexa Fluor 594 secondary antibody, cells were DAPI-stained and imaged with a 100x oil lens using a Zeiss LSM 510 confocal immunofluorescence microscope. Images reflect one "slice" of a cell, showing co-localization of EBOVLPs with sphingomyelin on the same plane.

EBOVLPs Co-localize with Lysosomal Acid Sphingomyelinase (ASM) at the Plasma Membrane

Lysosomal acid sphingomyelinase (ASM) is an enzyme which hydrolyzes sphingomyelin on the outer leaflet of the plasma membrane. In order for ASM to access its substrate, lysosomal fusion with the plasma membrane must occur. Once ASM removes sphingomyelin's

phosphocholine headgroup, ceramide is formed (Tepper et al., 2000; Zeidan and Hannun, 2010; Zeidan et al., 2008). Ceramide, due its structure, forms large macrodomains which invaginate to form macropinosomes approximately 400 nm in diameter. This process is clathrin- and caveolin-independent (Zha et al., 1998). With regard to EBOV, it was recently shown that entry occurs via macropinocytosis-like mechanism, independent of clathrin and caveolin (Nanbo et al., 2010; Saeed et al., 2010). These findings are consistent with a role for ASM in infection. I therefore tested if ASM could be found at the cell surface with virus particles.

Indeed, Figure 14 shows co-localization of EBOVLPs with ASM at various time points during entry. HeLa cells were incubated with EBOVLPs for 15, 30, 60, or 90 minutes, rinsed once with PBS, and then formalin-fixed. Cells were not permeabilized to show co-localization events on the cell surface. Cells were then incubated with anti-ASM antibody, followed by a conjugated secondary antibody. Cell nuclei were DAPI-stained and imaged with a 100x oil lens using a Nikon T7 immunofluorescence microscope. Images were then processed using Autoquant deconvolution software as described in Methods to delineate VLP and ASM overlap.

ASM co-localized with EBOVLPs at the earliest time point of 15 minutes, and continued through the last time point of 90 minutes. As with sphingomyelin, there appeared to be a correlation between the number of EBOVLPs bound and the amount of ASM associated with them – the more EBOVLPs that were bound to the cell surface, the more ASM that was present, suggesting that EBOV particles induced ASM localization to the cell surface. Because other pathogens have been shown to recruit ASM to the plasma membrane via lysosomal exocytosis, I next tested whether EBOVLPs would also stimulate lysosomal recruitment to the cell surface.

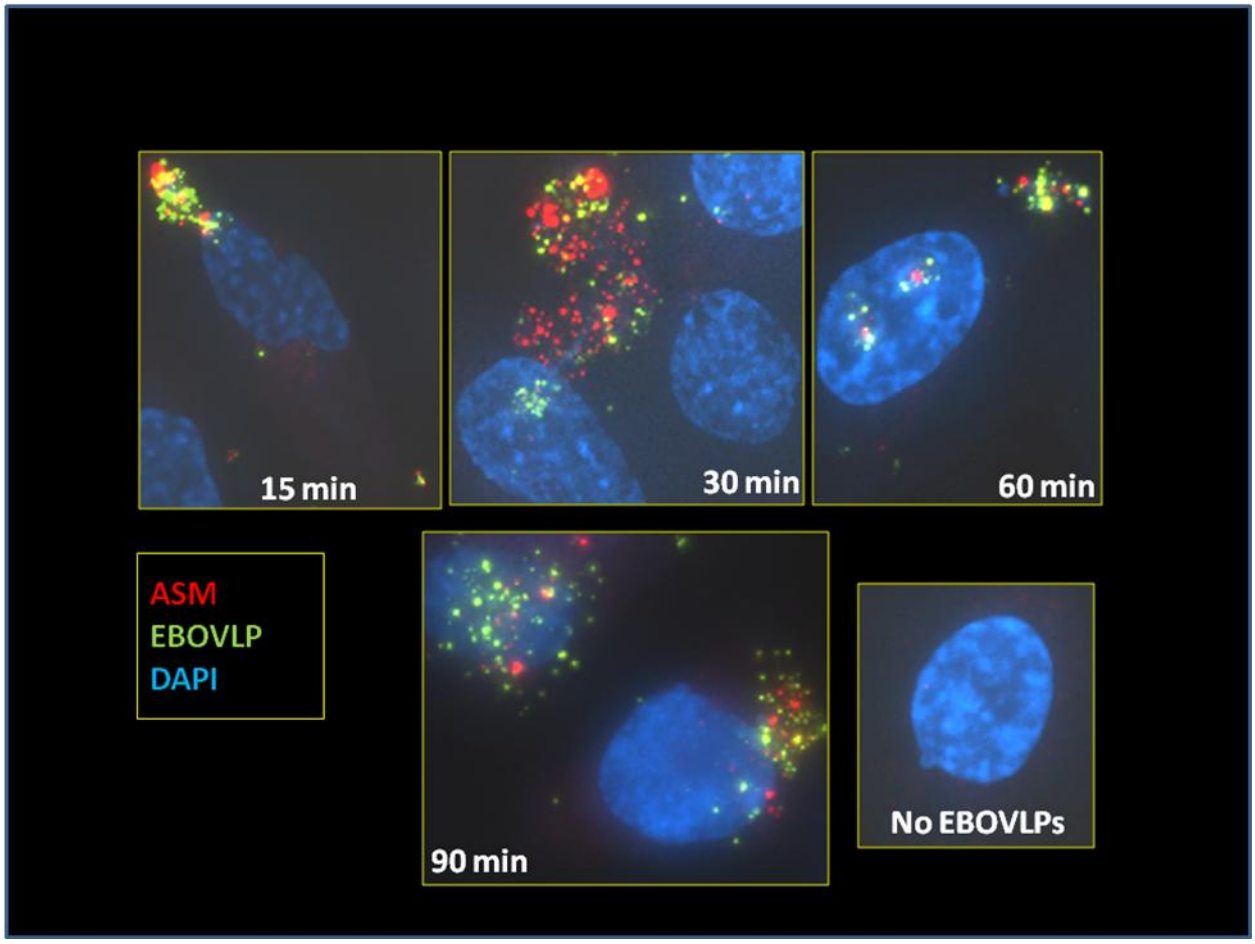

Figure 14. EBOVLPs co-localize with lysosomal ASM at the cell surface. HeLa cells were incubated with EBOVLPs for 15, 30, 60, or 90 minutes, rinsed once, and fixed with formalin. Cells were not permeabilized to show co-localization events on the cell surface. Cells were then incubated with anti-ASM antibody, and then conjugated Alexa Fluor 594 secondary antibody. Cells were DAPI-stained and imaged with a 100x oil lens using a Nikon T7 immunofluorescence microscope. Images were then processed using Autoquant deconvolution software as described in Methods.

EBOVLPS CO-LOCALIZE WITH LYSOSOMAL MARKER, LAMP1, AT THE PLASMA MEMBRANE.

To further verify that lysosomal exocytosis of ASM was occurring, non-permeabilized HeLa cells were stained for the lysosomal marker, Lamp1, using the same methods are described for ASM. Similar to ASM, Lamp1 was co-localized with EBOVLPs at the plasma membrane

within 15 min of VLP addition. This indicates that EBOVLPs trigger lysosomal exocytosis during entry, and further supports the premise that lysosomal ASM translocates to the plasma membrane upon EBOVLP stimulation (Figure 15).

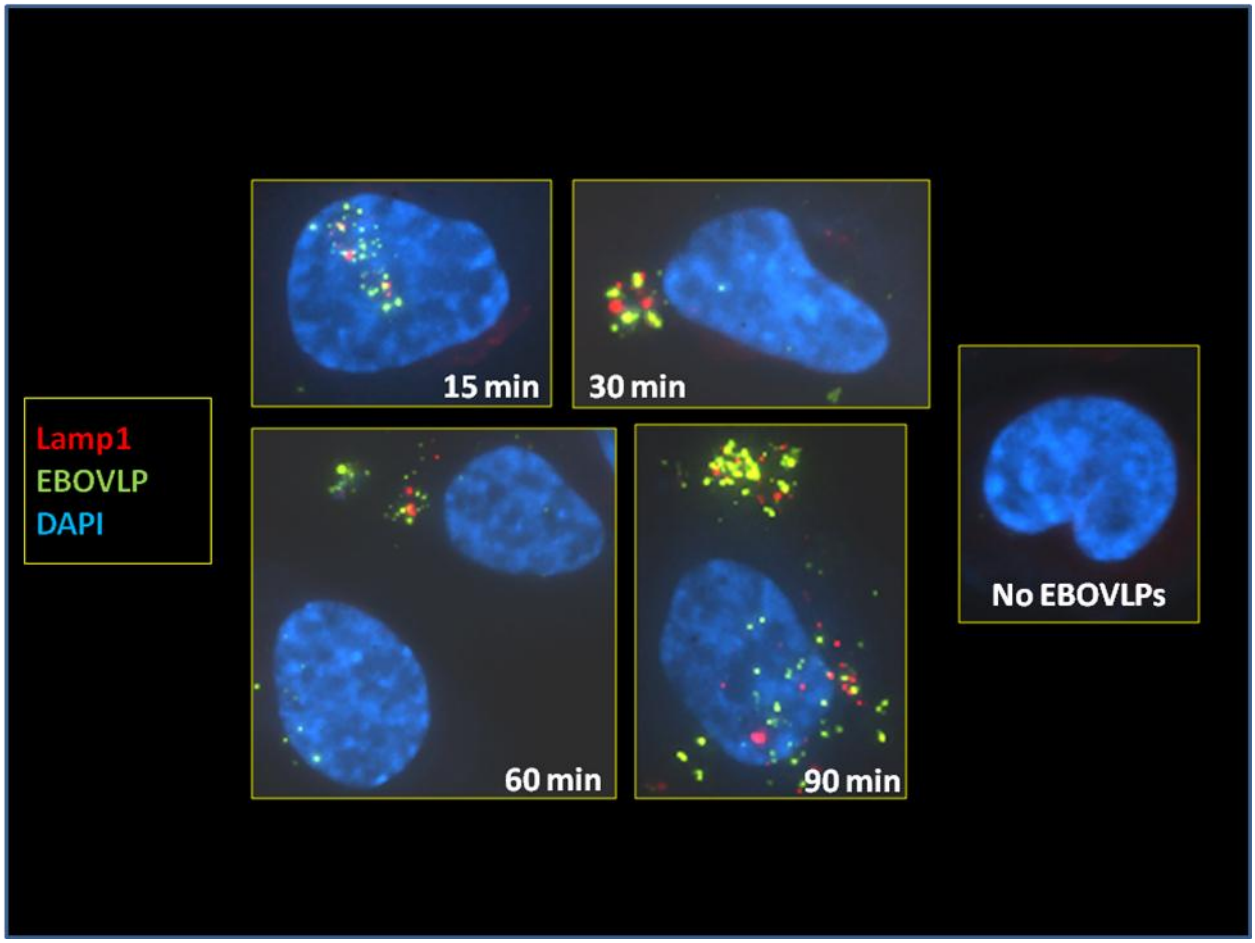

Figure 15. EBOVLPs co-localize with lysosomal marker, Lamp1, at the cell surface. HeLa cells were incubated with EBOVLPs for 15, 30, 60, or 90 minutes, rinsed once, and fixed with formalin. Cells were not permeabilized to show co-localization events on the cell surface. Cells were then incubated with anti-Lamp1 antibody, and then conjugated Alexa Fluor 594 secondary antibody. Cells were DAPI-stained and imaged with a 100x oil lens using a Nikon T7 immunofluorescence microscope. Images were then processed using Autoquant deconvolution software as described in Methods.

LYSOSOMAL ASM IS IMPORTANT IN EBOV-GFP INFECTION

$ASM^{-/-}$ Primary Human Skin Fibroblasts Are Resistant to EBOV-GFP Infection

Next, we investigated the requirement for ASM in EBOV infection. Primary human fibroblasts with a homozygous ASM mutation ($ASM^{-/-}$) and no detectable ASM activity were incubated for 24 h with EBOV-GFP, formalin-fixed, imaged, and analyzed using Cell Profiler image analysis software to determine infection efficiency. Surprisingly, EBOV-GFP infection was reduced by over 40% compared to normal fibroblasts (Figure 16). Because these cells have evolved to function in the absence of ASM activity, they have likely developed a mechanism, such as enhanced NSM activity, to compensate for the defect. This may explain why there is not a complete inhibition of EBOV infection.

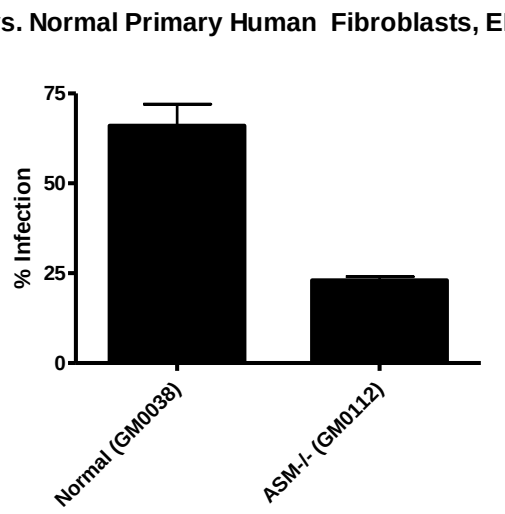

Figure 16. ASM-/- fibroblasts are resistant to EBOV-GFP infection. EBOV-GFP infection was reduced by nearly 40% in $ASM^{-/-}$ fibroblasts compared to normal fibroblasts. Primary human fibroblasts from a donor with ASM deficiency and a normal donor were inoculated with EBOV-GFP (MOI = 0.8). Cells were then fixed in formalin, stained with DAPI, and analyzed to count total cell nuclei and infected cells. Percent infection data was analyzed by one-way ANOVA with Tukey post-test using GraphPad Prism analysis software (see Methods).

Cells Treated with the ASM Inhibitor, Imipramine, Resist EBOV-GFP Infection

To further elucidate the requirement for ASM in EBOV infection, specific ASM inhibitors, imipramine, desipramine, and amitriptyline were used. Imipramine was 2-fold serially diluted in molecular grade water with a starting concentration of 100 μM. HeLa cells were incubated with drug dilutions for 1 h prior to inoculation with EBOV-GFP. Cells were incubated for 24 h with titrated EBOV-GFP, formalin-fixed, DAPI-stained, imaged, and analyzed using Cell Profiler image analysis software to determine infection efficiency. To determine drug concentrations required to reduce infection by 50% of control, or effective concentrations (EC_{50}), a sigmoidal dose-response curve with non-linear regression was fitted to infection efficiency data using GraphPad Prism analysis software.

As shown in Figure 17, 3.7 μM imipramine reduced EBOV-GFP infection by 50% compared to cells treated with water only. And at 6.25 μM, imipramine completely blocked infection. Additionally, only concentrations of 50 μM or greater were toxic to cells according to an Alamar Blue cytotoxicity assay. This is a fluorescence-based assay that measures cellular metabolic activity. Imipramine, as well as desipramine and amitriptyline, also effectively blocked EBOV-GFP infection at similar concentrations. Additionally, these drugs worked equally well in 293 human embryonic kidney (HEK) cells (EC_{50} data is summarized in Discussion). Although these drugs inhibited infection in Vero E6 cells as well, their potency was reduced by 2 to 3 times. Of note, only impramine HCl inhibits infection. When cells were treated with the same concentrations of impramine N-oxide, infection did not appear to be inhibited at all (data not shown). Usually the body metabolizes imipramine to desipramine, so perhaps the N oxide form cannot be metabolized properly to generate desipramine.

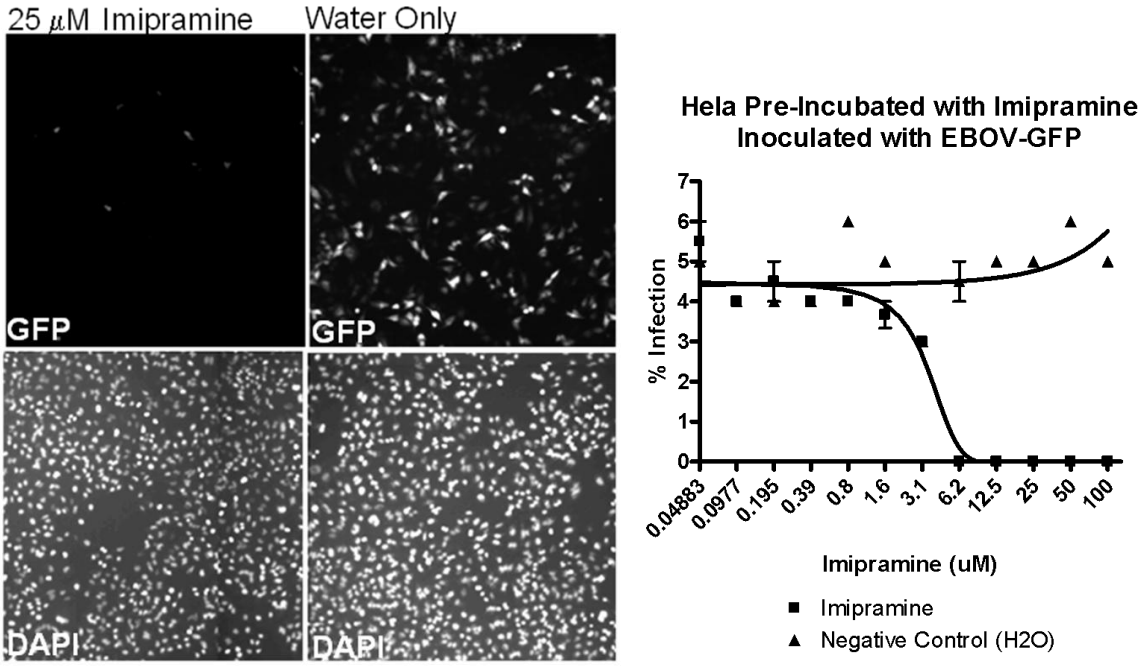

Figure 17. ASM inhibitor, imipramine, inhibits EBOV infection. (Left) HeLa cells were plated in a 96-well plate, and then incubated with 2-fold serially diluted drug for 1 h prior to inoculation with EBOV-GFP. Cells then fixed, DAPI-stained, and imaged for DAPI and GFP. To determine infection efficiency, images were analyzed using Cell Profiler image analysis software as described in Methods (MOI 0.3). (Right) EC_{50} was calculated by fitting infection efficiency data to a sigmoidal dose-response (variable slope) and non-linear regression using GraphPad Prism analysis software. At an MOI of 0.05, 3.7 μM of imipramine inhibited infection by 50% compared to a negative control.

ASM Inhibitor, Imipramine, Reduces EBOV-GFP Replication

Because the previous assay relied on GFP expression as an infection marker, an independent measure of EBOV infection was used. Therefore, we tested the inhibitory effect of imipramine on viral replication; HeLa cells were plated in a 6-well plate, and then pre-incubated with 25 μM drug for 1h prior to inoculation with EBOV-GFP. This concentration was used because it was previously determined to provide the greatest inhibitory effect without toxicity. Cells were incubated with virus and drug for 24 h, and then lysed with 1 mL per well of BioRad guanidine cell lysis buffer. RNA was purified using an Aurum RNA purification kit as described

in Methods. qRT-PCR was performed using EBOV-Zaire Mayinga NP primers (see Methods) (Figure 18). Compared to cells treated only with water, 25 μM imipramine inhibited EBOV NP vRNA expression by nearly 64-fold.

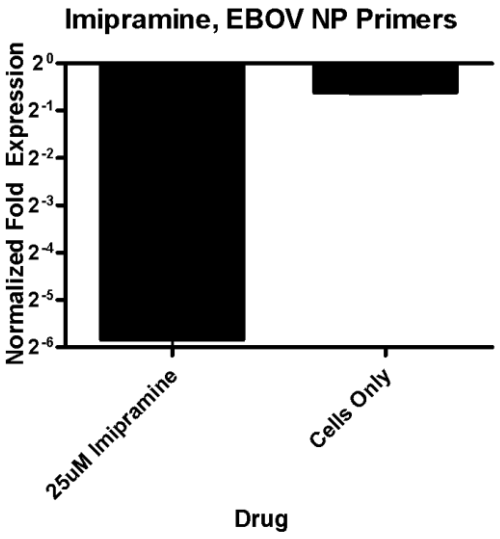

Figure 18. ASM inhibitor, impramine, reduces EBOV replication. HeLa cells were plated in a 6-well plate, and then pre-incubated with 25 μM drug for 1h prior to inoculation with EBOV-GFP. This concentration was used because it was previously determined to provide the greatest inhibitory effect without toxicity. Cells were incubated with virus and drug for 24 h, and then lysed with 1 mL per well of BioRad guanidine cell lysis buffer. Supernatant was placed in tubes, and stored at 4^{o} C for at least 24 h. RNA was purified using an Aurum RNA purification kit as described in Methods. qRT-PCR was performed using EBOV-Zaire Mayinga NP primers (see Methods). Compared to cells treated only with water, 25 μM impramine inhibited EBOV NP vRNA expression by nearly 64-fold.

Cells Transfected with ASM-Specific siRNA Are Resistant to EBOV-GFP Infection

Because chemical inhibitors can have non-specific effects, we further assessed the role of ASM in EBOV infection using RNA interference. HeLa cells were inoculated with EBOV-GFP in BSL4 at 48 h post-transfection with ASM-targeting siRNA. At 24 h post-inoculation (pi),

cells were formalin-fixed, and stored at 4^{o} C for at least 24 h in BSL4. Cell nuclei were then DAPI-stained, imaged, and analyzed with Cell Profiler cell image analysis software to determine infection efficiency. Data was analyzed with GraphPad Prism analysis software, using a one-way ANOVA with Tukey post-test. EBOV-GFP infection in ASM-transfected cells was reduced by more than 50% by all 5 sequences tested, as compared to All Stars negative siRNA control (Figure 18). Ctbp1 siRNA was used as positive control against EBOV-GFP infection due its potent inhibition of EBOV-GFP infection (Saeed et al., 2010). To quantify the reduction of ASM mRNA expression by RNA interference, qRT-PCR was performed. Change in threshold cycles, ΔCt, was determined by normalizing ASM expression to GAPDH. $\Delta\Delta$Ct values were calculated by normalized ΔCt values to an All Stars negative siRNA control. Untransfected cells ("cells only") showed similar ASM mRNA expression compared to All Stars control. As compared to an All Stars negative siRNA control, the most effective sequence reduced ASM mRNA expression by nearly 32-fold, which corresponds to this sequence also having the greatest inhibition on EBOV-GFP infection. Although mRNA suppression varied between ASM siRNA sequences, the amount of mRNA suppression correlated with suppression of EBOV-GFP infection for each siRNA type (Figure 19).

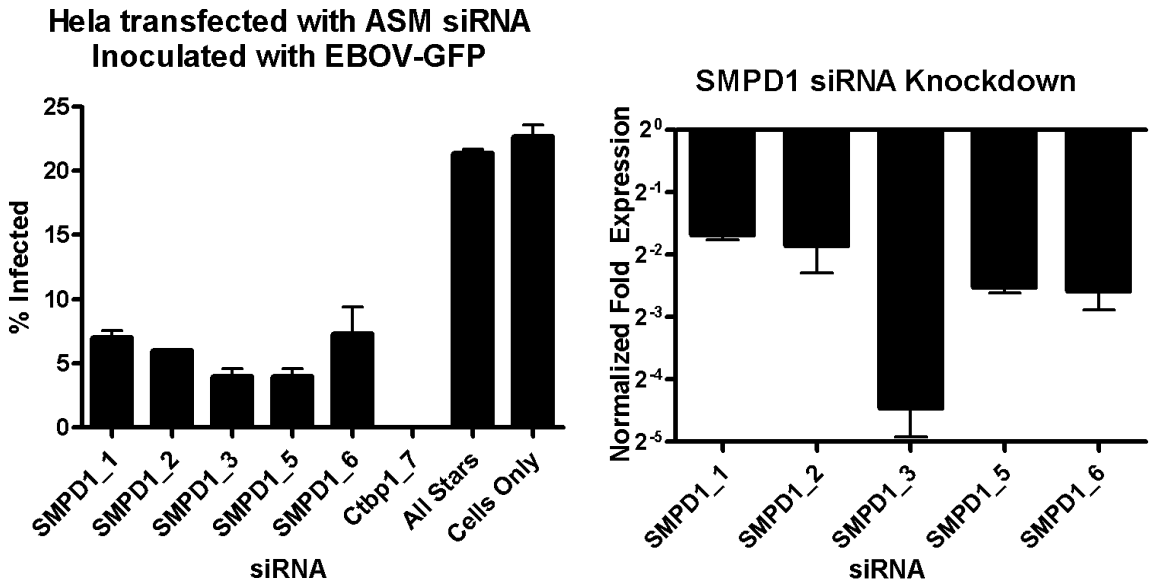

Figure 19. ASM siRNA inhibits EBOV-GFP infection. (Left) HeLa cells were transfected with ASM-specific siRNA. At 48 h post-transfection, cells were incubated with EBOV-GFP for 24 h (MOI = 0.1). EBOV-GFP infection was reduced by more than 50% in ASM-transfected cells compared to All Stars negative siRNA control. Ctbp1-targeting siRNA was used a positive control since it was previously shown to block EBOV infection. (Right). ASM siRNA knocks down ASM mRNA expression. ASM mRNA was purified from HeLa cells at 48 h post-transfection with ASM siRNA, and amplified using ASM-specific primers. Change in threshold cycles, ΔCt, was determined by normalizing ASM expression to GAPDH. ΔΔCt values were calculated by normalizing ΔCt values to an All Stars negative siRNA control. Untransfected cells ("cells only") showed similar ASM mRNA expression compared to All Stars control. There was approximately a 4- to 32-fold decrease ASM mRNA expression compared to the All Stars negative siRNA control. Although sequences varied in their suppression of ASM mRNA, these values corresponded with the amount of virus suppression for each sequence.

CELLS TREATED WITH ASM INHIBITOR, IMIPRAMINE, BLOCKED INFECTION AT THE FUSION STEP

After identifying a role for ASM in EBOV infection, we next looked at what step of infection was being blocked by ASM inhibitors. First, we looked at the fusion step, using a fusion assay (detailed in Methods – Figure 42). For this assay, we used EBOVLPs containing nef-luciferase fusion proteins beneath the viral envelope. When the VLPs fuse with cell membranes, the luciferase within the VLPs is exposed to a luciferin-containing buffer,

generating luminescence, which can be measured and quantified by luminometer. HeLa cells were pre-incubated with 20 μM imipramine for 1 h, before 3 h incubation with EBOVLP-Luciferase. As shown in Figure 20, 20 μM imipramine reduced contents mixing signal by over 90% as compared to a water-treated control. This suggested that imipramine is acting on a step leading up to or including membrane fusion step during infection. Additionally, 20 μM imipramine reduced fusion of EBOVLP-luciferase in Vero E6 and 293HEK cells, as well, showing that this suppression was not cell type specific (data not shown).

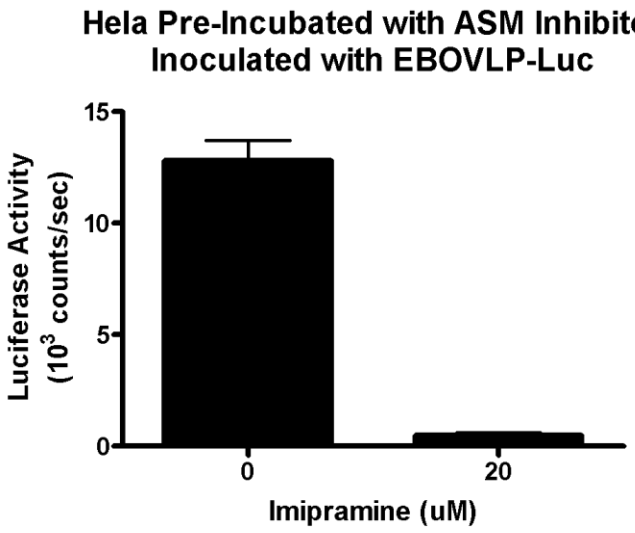

Figure 20. ASM inhibitor, impramine, reduces EBOVLP-Luciferase fusion. HeLa cells were pre-incubated with 20 μM imipramine for 1 h, before 3 h incubation with EBOVLP-Luciferase. 20 μM imipramine reduces viral fusion with cell membranes by over 90% as compared to a water-treated control.

ASM-DEPENDENT INFECTION IS EBOV-GP SPECIFIC

Next, we assessed if the requirement for ASM in EBOV entry was GP-specific. We used Vesicular Stomatitis Virus-Luciferase pseudotyped virus (VSV-Luc) cores encoated with either EBOV, Venezuelan Equine Encephalitis Virus (VEEV), or Lassa virus (LASV) glycoproteins.

VEEV- and LASV-VSV-Luc viruses were chosen as negative controls because preliminary data showed that $ASM^{-/-}$ fibroblasts were susceptible to infection by pseudotyped viruses, while strongly resistant to EBOV-GFP infection. HeLa cells were pre-incubated for 1 h with either 25 μM imipramine, 25 μM desipramine, or 25 nM Bafilomycin A prior to an 8 h incubation with virus. At termination, luciferase buffer was added, and luciferase activity measured with a luminometer. Bafilomycin A is an H^+ V-ATPase inhibitor, which causes lysosomal dysfunction by increasing vesicle pH. It was used as a positive control because it potently blocks each of the viruses, including EBOV-GFP infection at low concentrations.

As shown in Figure 21, 25 μM imipramine or desipramine reduces EBOV-VSV-Luc infection (luciferase activity) in treated cells to background levels, whereas water-treated cells still generate nearly 20,000 luciferase counts per second. This shows that the complete block of EBOV-VSV-Luc infection is due to the ASM inhibitor. When compared to VEEV- and LASV-VSV-Luc, 25 μM imipramine or desipramine results in a more than 10-fold decrease in EBOV GP-specific infection. This shows that the inhibitory effect of ASM inhibitors is potent against EBOV GP, since the only difference between the pseudotyped viruses is their glycoprotein.

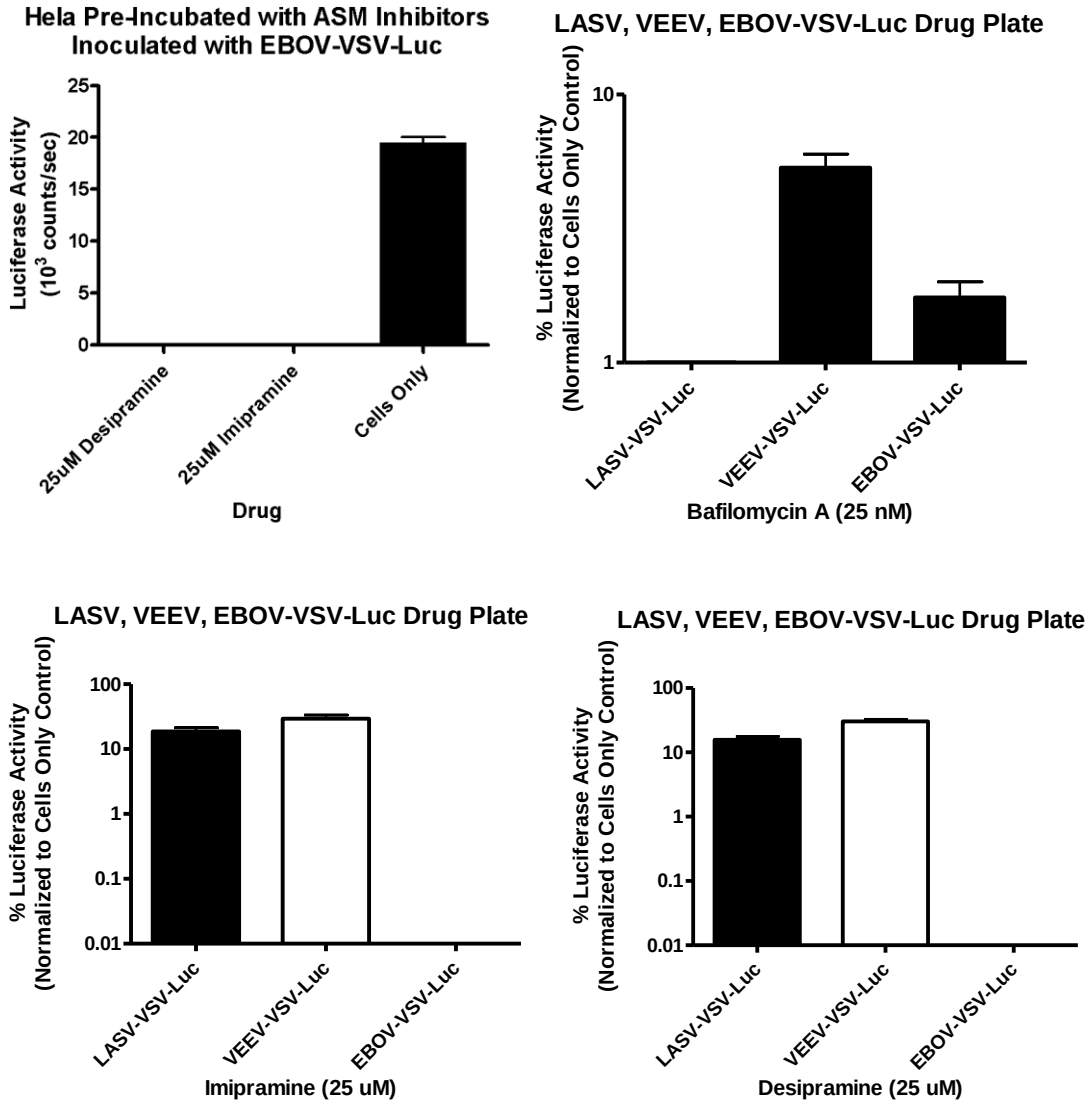

Figure 21. Inhibitory effect of ASM inhibitors, imipramine and desipramine, on VSV-pseudotyped viruses. HeLa cells were pre-incubated with 25 μM drug for 1 h prior to 8 h incubation with VEEV-, LASV-, or EBOV-VSV-Luc. (Top) 25 μM of either ASM inhibitor reduces EBOV-VSV-Luc activity in treated cells to background levels, whereas water-treated cells still show significant luciferase activity – a complete block in infection. Positive control, Bafilomycin A, potently blocks all 3 viruses, with less than a 10-fold difference between viruses. (Bottom) Compared to VEEV- and LASV-VSV-Luc, EBOV-VSV-Luc luciferase activity is reduced by more than 10-fold, showing EBOV GP-specific inhibition by either ASM inhibitor.

To confirm the GP-specific inhibition seen with the ASM chemical inhibitors, we next transfected HeLa cells with the same ASM siRNA sequences previously used in the EBOV-GFP infection assay to see if EBOV-VSV-Luc pseudotyped virus infection would be inhibited. As shown in Figure 22, different ASM-targeting siRNA sequences inhibited infection between 10 to 50%. Initially, it would appear that ASM siRNA inhibition is not as potent in blocking EBOV-VSV-Luc as compared to EBOV-GFP. However, this can be accounted for by different detection methods for each assay. The readout of the luciferase assay is much more sensitive than the EBOV-GFP infection assay because it measures the luciferase production of every replicating virus particle. In contrast, the EBOV-GFP infection assay is measuring the number of infected cells as a function of fluorescence intensity. If the viral replication is not sufficient to generate GFP fluorescence intensity above a set threshold, it is not measured. However, in the luciferase assay, such minimal replication would be detected. Most importantly, the trend seen between the EBOV-GFP infection assay and the EBOV-VSV-Luciferase infection assay is the same. Sequence SMPD1_5 has previously been shown to most potently suppress ASM mRNA expression; it most sharply decreased EBOV-GFP infection; and it generated the greatest decrease in EBOV-VSV-Luciferase infection.

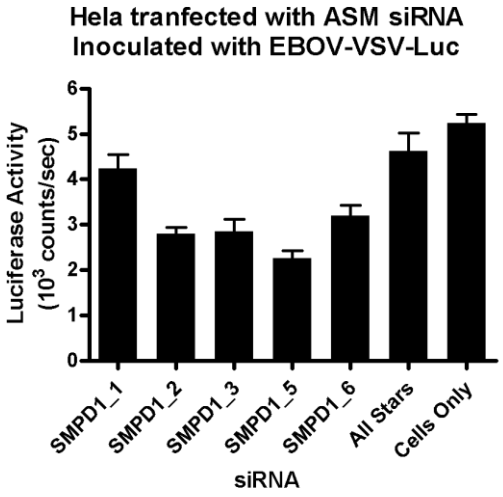

Figure 22. ASM-specific siRNA reduces EBOV-VSV-Luciferase pseudotyped virus infection. HeLa cells were transfected with ASM-specific siRNA. At 48 h post-transfection, cells were incubated with EBOV-VSV-Luc pseudotyped virus for 8 h. Upon termination, luciferase buffer was added to the cells, and luciferase activity was measured with a luminometer. Cells transfected with different ASM-siRNA sequences showed between a 10-50% reduction in infection compared to cells transfected with All Stars – a negative siRNA control.

DISCUSSION:

In summary, we have shown that within 15 minutes of being added to cells, EBOVLPs co-localize with sphingomyelin-rich rafts, ASM, and Lamp1 on the cell membrane. This suggests that EBOVLP binding to sphingomyelin rafts, stimulates lysosomal exocytosis, and subsequent activation of ASM, which would permit ASM-dependent macropinosome formation, and EBOVLP internalization. Our ASM infection data support this. First, $ASM^{-/-}$ fibroblasts with no detectable ASM activity, showed a 40% decrease in EBOV-GFP infection as compared to normal fibroblasts. Second, the ASM inhibitor, imipramine, reduces EBOV-GFP infection by 50% of control at 3.7 μM. Additionally, 25 μM imipramine inhibits EBOV-GFP replication by 64-fold as compared to a water-treated control. Third, 5 different ASM-targeting siRNA sequences reduced EBOV-GFP infection by more than 50%. Because ASM clearly played a role

in EBOV infection, we next assessed what step in EBOV entry was affected by ASM inhibition. A fusion assay determined that 20 μM imipramine decreases EBOVLP-Luciferase fusion with cell membranes by more than 90%. Additionally, imipramine reduced VLP fusion in 293HEK and Vero E6 cells in a similar manner. Finally, we showed that the requirement for ASM in EBOV entry is GP-specific by using VSV-Luciferase-expressing pseudotyped viruses which only differ by their surface glycoproteins. Although LASV- and VEEV-VSV-Luciferase infection was also inhibited by imipramine and desipramine to some extent, the inhibition of EBOV-VSV-Luc was 10-fold greater.

This data supports the current model of EBOV entry by providing a mechanism for lipid raft-dependent binding, and macropinocytosis-like internalization of virus, which is independent of clathrin and caveolin (Bavari et al., 2002; Nanbo et al., 2010; Saeed et al., 2010; Zha et al., 1998). First, it highlights the importance of lipid raft composition in virus entry. Previous work focused only on the cholesterol component of rafts, since it was thought that MβCD selectively extracted cholesterol. However, more recent work has shown that MβCD also extracts sphingomyelin (Giocondi et al., 2004). Sphingomyelin is a major lipid in mammalian membranes that preferentially associates with cholesterol to form lipid rafts (McIntosh et al., 1992b). Unlike cholesterol, the hydrolysis of sphingomyelin to ceramide results in dynamic changes in the plasma membrane such as macrodomain formation, receptor clustering, changes in membrane fusogenicity, and membrane invagination – all of which are important in pathogen entry (Bollinger et al., 2005; Gulbins and Li, 2006). Second, the rapid cell surface recruitment of ASM, hydrolysis of sphingomyelin to ceramide, and subsequent internalization of the virus are in agreement with previously described ASM-dependent macropinocytosis-like entry for *P.*

aeruginosa, rhinoviruses, Sindbis virus, measles virus, *N. gonorrheoeae*, and *E. coli* (Avota et al., 2010; Avota et al., 2011; Avota et al., 2004; Falcone et al., 2004; Grassme et al., 1997; Grassme et al., 2003; Grassme et al., 2005; Jan et al., 2000; Ng and Griffin, 2006; Zha et al., 1998). Finally, the requirement for ASM-dependent macropinocytosis defines an additional virus entry step which can be targeted by drug treatments. ASM inhibitors such as imipramine, desipramine, and amitriptyline are FDA-approved anti-depressants that could potentially be re-purposed for preventing and treating EBOV infection (Kornhuber et al., 2010).

Because sphingomyelin and acid sphingomyelinase were shown to be important in EBOV entry and infection, we next looked at the role of another sphingomyelinase, neutral sphingomyelinase 2 (NSM2), in EBOV infection.

NEUTRAL SPHINGOMYELINASE 2 IS (NSM2) REQUIRED IN EBOV INFECTION

INTRODUCTION

Because acid sphingomyelinase (ASM) was found to be important in EBOV infection, we tested if other sphingomyelinases may also be required. Of the four known neutral sphingomyelinases, only neutral sphingomyelinase 2 (NSM2) is associated with the plasma membrane and multi-vesicular bodies, making it the best candidate. When NSM2 hydrolyzes sphingomyelin to ceramide on the inner leaflet of the plasma membrane, it causes bleb formation. However, the same enzymatic reaction in multi-vesicular bodies results in exosome formation (Tani and Hannun, 2007; Tepper et al., 2000; Trajkovic et al., 2008; van Blitterswijk et al., 2003).

CYTOSOLIC NEUTRAL SPHINGOMYELINASE 2 (NSM2) IS REQUIRED FOR EBOV-GFP INFECTION

Cells Treated with NSM Inhibitor, Manumycin A, Are Resistant to EBOV-GFP Infection

To test NSM's in EBOV infection, the specific, irreversible inhibitor, manumycin A, was used. Manumycin A was 2-fold serially diluted in DMSO with a starting concentration of 100 μM. HeLa cells were incubated with drug dilutions for 1 h prior to inoculation with EBOV-GFP. Cells were incubated for 24 h with titrated EBOV-GFP, formalin-fixed, DAPI-stained, imaged, and analyzed using Cell Profiler image analysis software to determine infection efficiency. To determine concentrations required to reduced infection by 50% of control, or effective concentrations, (EC_{50}), infection data was fitted to a sigmoidal dose-response curve (variable slope) and non-linear regression using GraphPad Prism analysis software.

As shown in Figure 23, manumycin A was a potent inhibitor of infection with 5 μM reducing EBOV-GFP infection by 50% compared to cells treated with water only. Additionally, drug concentrations up to 50 μM had similar cell density compared to negative controls, suggesting that this inhibitory effect was not due to toxicity. Manumycin A inhibited EBOV-GFP infection by 50% of control in 293 human embryonic kidney (HEK) cells at an EC_{50} of 3.4 μM (data not shown). This suggests that either 293HEK cells are more sensitive to this drug, or that NSM activity is more important during infection in these cells. (EC_{50} data summarized in Discussion).

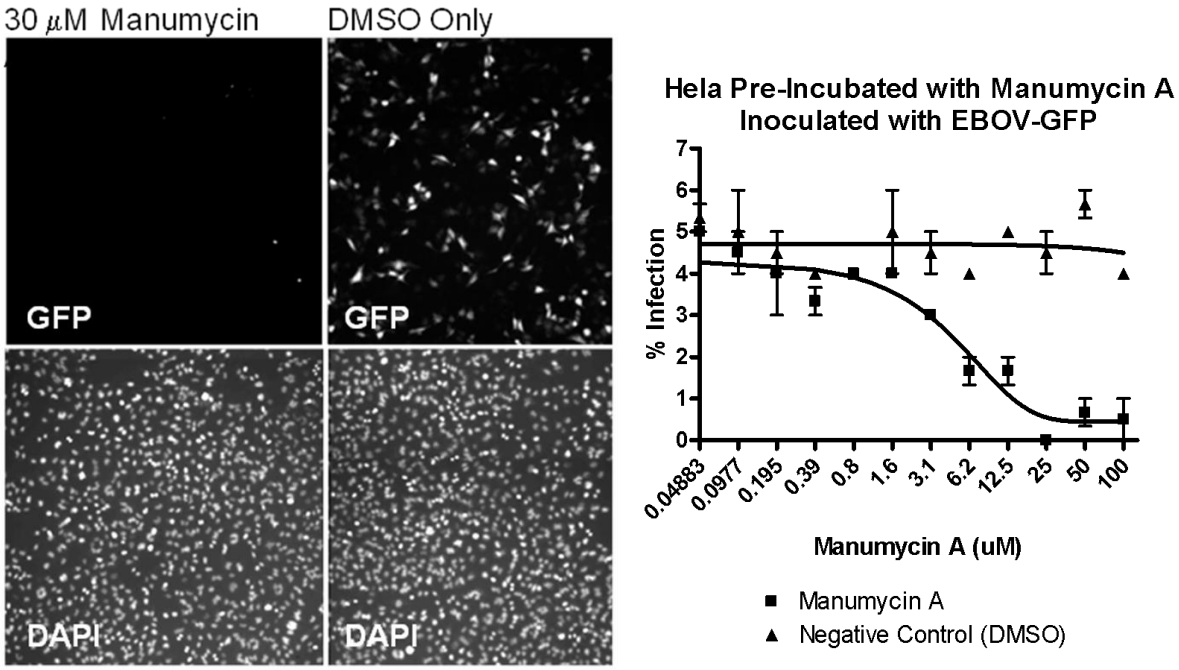

Figure 23. NSM inhibitor, manumycin A, inhibits EBOV infection. (Left) HeLa cells were plated in a 96-well plate, and then incubated with 2-fold serially diluted drug for 1 h prior to inoculation with EBOV-GFP. Cells then fixed, DAPI-stained, and imaged for DAPI and GFP. To determine infection efficiency, images were analyzed using Cell Profiler image analysis software as described in Methods (MOI 0.3). (Right) EC_{50} was calculated by fitting infection efficiency data to a sigmoidal dose-response (variable slope) and non-linear regression using GraphPad Prism analysis software. At an MOI of 0.05, 5 μM of manumycin A inhibited infection by 50% compared to a negative control.

NSM Inhibitor, Manumycin A, Reduces EBOV-GFP Replication

Next, we tested the inhibitory effect of manumycin A on viral replication, HeLa cells were plated in a 6-well plate, and then pre-incubated with 30 μM drug for 1 h prior to inoculation with EBOV-GFP. This concentration was used because it was previously determined to provide the greatest inhibitory effect without toxicity. Cells were incubated with virus and drug for 24 h, and then lysed with 1 mL per well of BioRad guanidine cell lysis buffer. Supernatant was placed in tubes, and stored at 4^{o} C for at least 24 h. RNA was purified using an Aurum RNA purification kit as described in Methods. qRT-PCR was performed using EBOV-Zaire Mayinga

NP primers (see Methods) (Figure 24). Compared to cells treated only with water, 30 μM manumycin A inhibited EBOV NP vRNA expression by more than 64-fold.

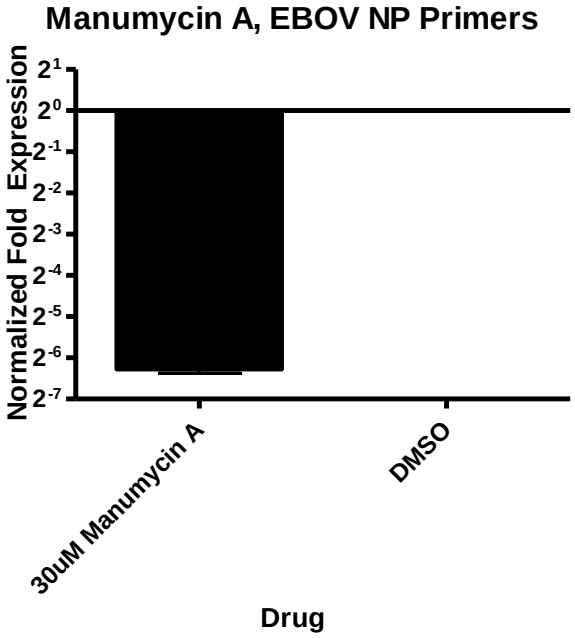

Figure 24. NSM inhibitor, manumycin A, inhibits EBOV-GFP replication. HeLa cells were plated in a 6-well plate, and then pre-incubated with drug for 1h prior to inoculation with EBOV-GFP. Cells were incubated with virus and drug for 24 h, and then lysed with 1 mL per well of BioRad guanidine cell lysis buffer. Supernatant was placed in tubes, and stored at 4^{o} C for at least 24 h. RNA was purified using an Aurum RNA purification kit as described in Methods. qRT-PCR was performed using EBOV-Zaire Mayinga NP primers (see Methods). 30 μM Manumycin A reduces expression of EBOV NP vRNA by more than 64-fold.

Cells Transfected with NSM2-Specific siRNA Are Resistant to EBOV-GFP Infection

Because chemical inhibitors can have off-target effects, we tested the role of NSM2 in EBOV infection using RNA interference. HeLa cells were inoculated with EBOV-GFP in BSL4 at 48 h post-transfection with ASM-targeting siRNA. At 24 h post-inoculation (pi), cells were formalin-fixed, and stored at 4^{o} C for at least 24 h in BSL4. Cells were then DAPI-stained, imaged, and analyzed with Cell Profiler cell image analysis software to determine infection

efficiency. Data was analyzed with GraphPad Prism analysis software, using a one-way ANOVA with Tukey post-test. EBOV-GFP infection in NSM2-transfected cells was reduced by more than 70% by all 4 sequences tested, as compared to All Stars negative siRNA control (Figure 25). Ctbp1 siRNA was used as positive control against EBOV-GFP infection due its potent inhibition of EBOV-GFP infection (Saeed et al., 2010). To quantify the reduction of NSM2 mRNA expression by RNA interference, qRT-PCR was performed. Change in threshold cycles, ΔCt, was determined by normalizing NSM2 expression to GAPDH. ΔΔCt values were calculated by normalized ΔCt values to an All Stars negative siRNA control. Untransfected cells ("cells only") showed similar NSM2 mRNA expression compared to All Stars control. As compared to an All Stars negative siRNA control, the most effective sequence reduced NSM2 mRNA expression by more than 4-fold, which corresponds to this sequence also having the greatest inhibition on EBOV-GFP infection. Although mRNA suppression varied between NSM2 siRNA sequences, the amount of mRNA suppression corresponded with suppression of EBOV-GFP infection for each sequence, with the exception of sequence SMPD3_7. For this sequence, there appears to be an off-target effect since it suppressed NSM2 mRNA the least, while inhibiting EBOV-GFP infection the most. Cell toxicity did not appear to be the cause, since cell density of NSM2 siRNA-transfected cells was at least 80% of the All Stars negative control. Admittedly, qRT-PCR of NSM2 mRNA proved challenging. During the optimization process, multiple primer sets were assessed. Additionally, different annealing temperatures, mRNA concentrations, cell densities were tested. However, the remaining 3 siRNA sequences show corresponding mRNA suppression with inhibition of EBOV-GFP infection. (Figure 25).

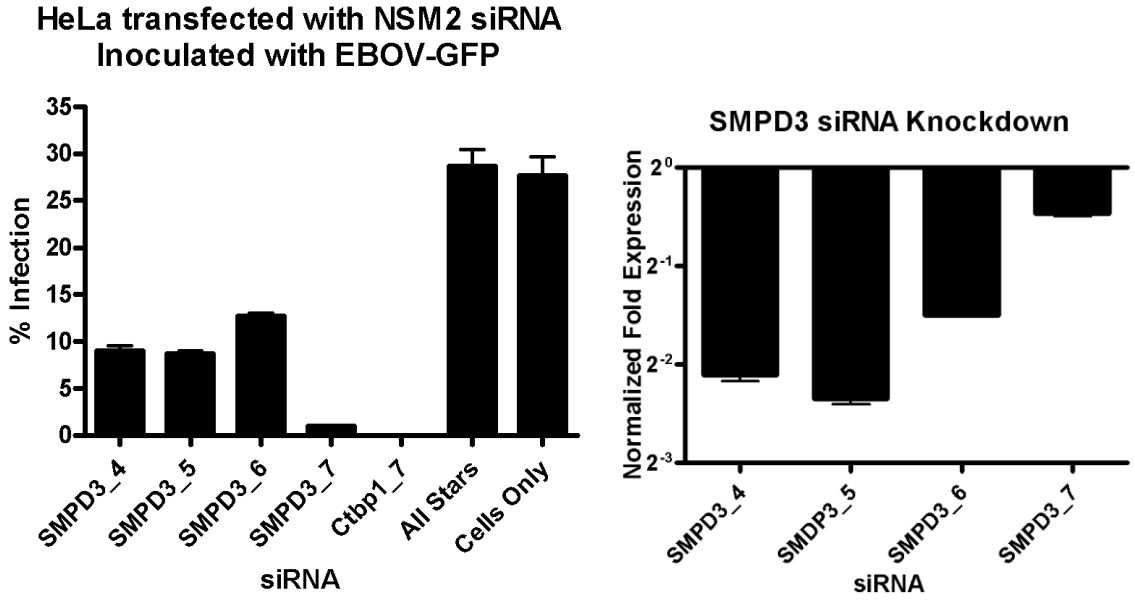

Figure 25. NSM2 siRNA inhibits EBOV-GFP infection. (Left) HeLa cells were transfected with NSM2-specific siRNA. At 48 h post-transfection, cells were incubated with EBOV-GFP for 24 h (MOI = 0.1). EBOV-GFP infection was reduced by at least 70% in NSM2-transfected cells compared to All Stars negative siRNA control. Ctbp1-targeting siRNA was used a positive control since it was previously shown to block EBOV infection. (Right) NSM2 siRNA knocks down NSM2 mRNA expression. NSM2 mRNA was purified from HeLa cells at 48 h post-transfection with NSM2 siRNA, and amplified using NSM2-specific primers. Change in threshold cycles, ΔCt, was determined by normalizing NSM2 expression to GAPDH. ΔΔCt values were calculated by normalized ΔCt values to an All Stars negative siRNA control. Untransfected cells ("cells only") showed similar NSM2 mRNA expression compared to All Stars control. With the exception of sequence SMPD3_7, there was approximately a 4-fold decrease in NSM2 mRNA expression compared to the All Stars negative siRNA control. Although sequences varied in their suppression of NSM2 mRNA, these values corresponded with the amount of virus suppression for each sequence, with the exception of SMPD3_7.

CELLS TREATED WITH NSM INHIBITOR, MANUMYCIN A, ARE RESISTANT TO EBOVLP-LUCIFERASE FUSION

Because NSM2 was shown to be important in EBOV infection, we next looked at what step of entry was being blocked by NSM inhibition. To assess NSM2's role in the fusion step, we used EBOVLPs containing nef-luciferase fusion proteins beneath the viral envelope in a mixing contents fusion assay. When the VLPs fuse with cell membranes, the luciferase within

the VLPs is exposed to a luciferin-containing buffer, generating luminescence, which can be measured and quantified by luminometer. HeLa cells were pre-incubated with 30 μM manumycin A for 1 h, before 3 h incubation with EBOVLP-Luciferase. As shown in Figure 26, 30 μM manumycin A reduces viral fusion with cell membranes by nearly 50% as compared to a DMSO-treated control. This inhibition is not as potent as that seen with ASM inhibitors. There are several possible explanations for this result. First, NSM-dependent membrane blebbing and shedding may be detrimental to fusion, and therefore, partial inhibition of this activity aids in virus fusion with cell membranes. Second, it may indicate that the NSM inhibitor is blocking exosome formation from multi-vesicular bodies, which may be important in virus trafficking with regards to replication, assembly, budding. Lastly, virus-induced NSM2 activity may be so enhanced that it overcomes the drug's inhibitory effect.

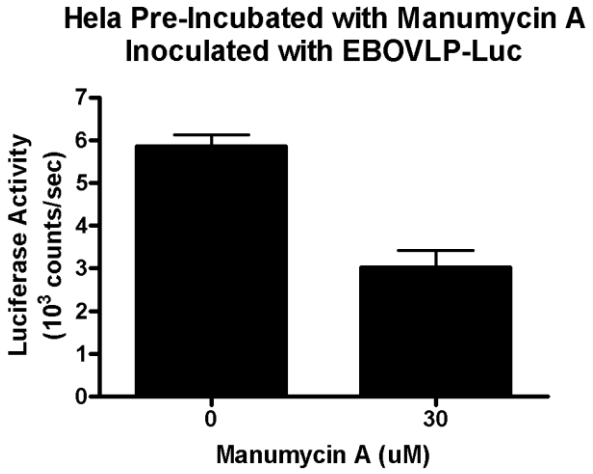

Figure 26. NSM inhibitor, manumycin A, reduces EBOVLP-Luciferase fusion. HeLa cells were pre-incubated with 30 μM manumycin A for 1 h, before 3 h incubation with EBOVLP-Luciferase. 30 μM manumycin A reduces viral fusion with cell membranes by approximately 50% as compared to a DMSO-treated control.

NSM2-DEPENDENT INFECTION IS EBOV-GP SPECIFIC

Next, we tested the specificity of NSM2-dependent entry to EBOV GP. We used Vesicular Stomatitis Virus-Luciferase pseudotyped viruses (VSV-Luc) viruses encoated with either EBOV, Venezuelan Equine Encephalitis Virus (VEEV), or Lassa virus (LASV) glycoproteins. VEEV- and LASV-VSV-Luc viruses were chosen as negative controls because our previous work showed that these viruses were not as susceptible to ASM inhibition as EBOV. Therefore, it was assumed that these viruses would also make suitable controls for testing NSM2. HeLa cells were pre-incubated for 1 h with either 30 μM manumycin A or 25 nM Bafilomycin A prior to an 8 h incubation with virus. At termination, luciferase buffer was added, and luciferase activity measured with a luminometer. Bafilomycin A is an H^+ V-ATPase inhibitor, which causes lysosomal dysfunction by increasing vesicle pH. It was used as a positive control because it potently blocks EBOV-GFP infection at low concentrations.

As shown in Figure 27, 30 μM manumycin A decreases EBOV-VSV-Luc infection (luciferase activity) in treated cells to non-detectable levels, whereas DMSO-treated cells still generate nearly 6,000 luciferase counts per second. This shows that the inhibition of EBOV-VSV-Luc infection is due to the NSM inhibitor, not DMSO. When compared to VEEV- and LASV-VSV-Luc, 30 μM manumycin A results in a nearly 100-fold decrease in EBOV GP-specific infection. This shows that the inhibitory effect of manumycin A is more specific to EBOV GP, since the only difference between the pseudotyped viruses is their glycoprotein. This suggests that the role of NSM2 in EBOV infection may be more specific to EBOV GP than that of ASM.

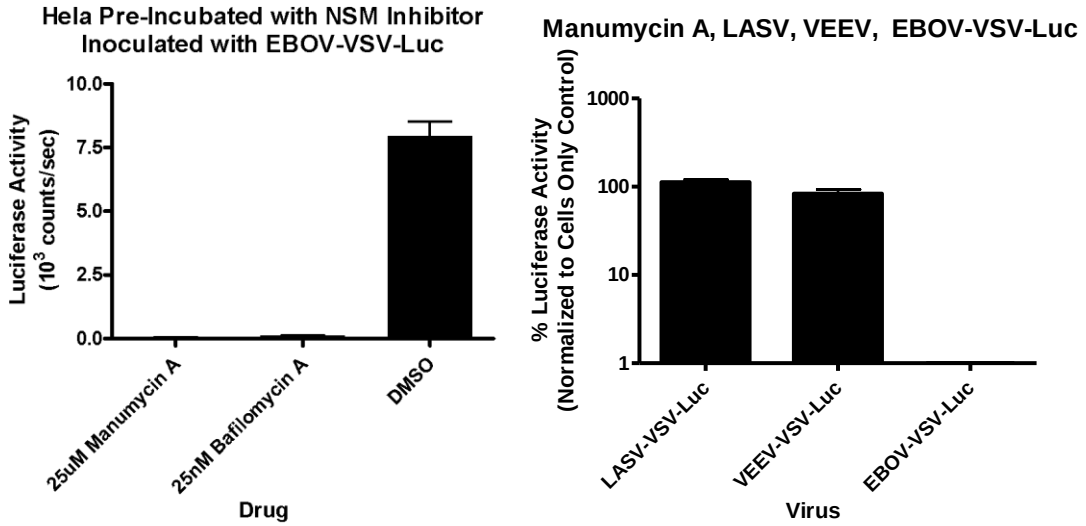

Figure 27. Inhibitory effect of NSM inhibitor, manumycin A, on VSV-pseudotyped viruses. HeLa cells were pre-incubated with 30 μM drug for 1 h prior to 8 h incubation with VEEV-, LASV-, or EBOV-VSV-Luc. (Left) 30 μM of manumycin A decreases EBOV-VSV-Luc activity in treated cells to non-detectable levels, whereas DMSO-treated cells still show significant luciferase activity. (Right) Compared to VEEV- and LASV-VSV-Luc, EBOV-VSV-Luc luciferase activity is reduced by nearly 100-fold, showing EBOV GP-specific inhibition by manumycin A.

To verify our chemical inhibitor data, we next transfected HeLa cells with the same NSM2 siRNA sequences previously used in the EBOV-GFP infection assay to test whether EBOV-VSV-Luc pseudotyped virus infection would be blocked in the same manner. As shown in Figure 28, different NSM2-targeting siRNA sequences inhibited infection between approximately 30 to 60%. At first glance, it would seem that NSM2 siRNA inhibition is not as potent in blocking EBOV-VSV-Luc as compared to EBOV-GFP. However, this can be explained by the different detection methods used for each assay. The readout of the luciferase assay is much more sensitive than the EBOV-GFP infection assay because it measures the luciferase production of every replicating virus particle. In contrast, the EBOV-GFP infection assay is measuring the number of infected cells as a function of fluorescence intensity. If the

viral replication is not sufficient to generate GFP fluorescence intensity above a set threshold, it is not measured. However, in the luciferase assay, such minimal replication would be detected. Most importantly, the trend seen between the EBOV-GFP infection assay and the EBOV-VSV-Luc infection assay is the same. All sequences except SMPD3_7 have previously been shown to suppress NSM2 mRNA expression; and the amount of mRNA suppression for each sequence corresponds to the level of inhibition of EBOV-GFP and EBOV-VSV-Luc infection. Again, although sequence SMPD3_7 most potently blocked EBOV-VSV-Luc infection, it was previously shown to have the least impact of NSM2 mRNA suppression as compared to the other 3 sequences. Therefore, its inhibitory effect on EBOV infection is not necessarily due to its ability to suppress NSM2 mRNA, and should be interpreted with caution.

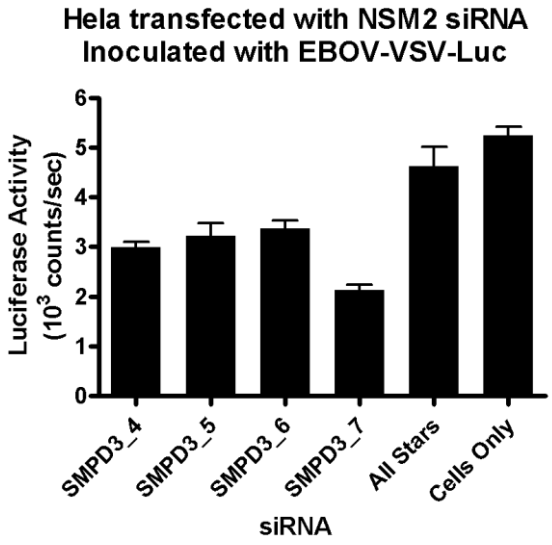

Figure 28. NSM2-specific siRNA reduces EBOV-VSV-Luciferase pseudotyped virus infection. HeLa cells were transfected with NSM2-specific siRNA. At 48 h post-transfection, cells were incubated with EBOV-VSV-Luc pseudotyped virus for 8 h. Upon termination, luciferase buffer was added to the cells, and luciferase activity was measured with a luminometer. Cells

transfected with different NSM2-siRNA sequences showed between a 30-60% reduction in infection compared to cells transfected with All Stars – a negative siRNA control.

DISCUSSION:

To summarize our findings, we have shown that the NSM inhibitor, manumycin A, inhibits EBOV-GFP infection by 50% of control at 5 μM in HeLa cells. Next, we showed that 30 μM manumycin A decreases EBOV-GFP replication by 64-fold as compared to a DMSO-treated control. Furthermore, at least 3 different NSM2-targeting siRNA sequences reduced EBOV-GFP infection by more than 50%. Because NSM2 played a role in EBOV-GFP infection, we looked at which step of entry was effected by NSM inhibition. A fusion assay determined that 30 μM manumycin A reduces EBOVLP-Luciferase fusion with cell membranes by approximately 50%. Lastly, we showed that NSM2-dependent mechanism for entry is EBOV GP-specific. For this assay, we used VSV-Luciferase-expressing pseudotyped viruses, which only differ by their surface glycoproteins. Inhibition of EBOV-VSV-Luc was 100-fold greater than that of LASV- or VEEV-VSV-Luciferase infection, showing that NSM2's role in infection is GP-dependent.

Compared to ASM, NSM2 appears to have a less important role in virus entry; but its inhibition still has a strong inhibitory effect on infection. This suggests that NSM2 may be more involved in a post-entry step, such as virus assembly and budding. This is agrees with the model for NSM-dependent Sindbis virus entry, which shows an increase in ASM activity, followed by an increase in NSM activity (Jan et al., 2000). Additionally, because NSM2 activity results in exosome formation from multi-vesicular bodies (Trajkovic et al., 2008), this may be beneficial to virus formation at the cell surface. During virus assembly and budding, VP40 matrix proteins

are routed through multi-vesicular bodies prior to being exocytosed to the plasma membrane (Jasenosky and Kawaoka, 2004). So, in this way, NSM2 activity would be beneficial. However, NSM2 also induces membrane blebbing and shedding (Tepper et al., 2000; van Blitterswijk et al., 2003). Recently, blebbing has been described a cell defense mechanism. By forming a bleb, the cell can pinch off, isolate, and shed the pathogen before entry occurs (Babiychuk et al., 2011). Therefore, overstimulation of NSM2-dependent blebbing and membrane shedding may actually hinder virus entry. This suggests that moderate NSM2 stimulation may enhance virus infection, but only when it occurs after ASM-dependent internalization of virus.

Because sphingomyelin and sphingomyelinases were shown to be important in EBOV entry and infection, we next assessed the role of sphingomyelin-trafficking protein, Niemann-Pick Type C1 (NPC1) in EBOV infection. Additionally, because repletion of sphingomyelin requires NPC1-dependent exocytosis; and translocation of lysosomal ASM to the cell surface also requires exocytosis, we also looked at the requirement for exocytosis in EBOV infection.

EBOV ENTRY REQUIRES SPHINGOMYELIN TRAFFICKING PROTEIN, NIEMANN-PICK TYPE C1 (NPC1), FOR INFECTION

INTRODUCTION:

Sphingomyelin is a prominent sphingolipid found in mammalian cell membranes. It preferentially associates with cholesterol to form lipid rafts on the plasma membrane (McIntosh et al., 1992a, b; Shakor et al., 2003; Shogomori and Kobayashi, 2008). Sphingomyelinase activation results in conversion of sphingomyelin to ceramide; thereby, depleting sphingomyelin in the plasma membrane (Jenkins et al., 2010; Tani and Hannun, 2007). To replace hydrolyzed sphingomyelin, Niemann-Pick Type C1 (NPC1)-dependent exocytosis of sphingomyelin is

required. NPC1 is a transmembrane protein localized to late endosomes and lysosomes, and has been well-studied for its role in transporting cholesterol and sphingomyelin to the cell surface (Gong et al., 2006; Koivusalo et al., 2007; Lange et al., 1998; Lusa et al., 2001; Sugimoto et al., 2001). Because EBOV requires rafts for entry, and we have previously shown that EBOVLPs co-localize with sphingomyelin rafts and ASM on the cell surface, we investigated the role of sphingomyelin trafficking protein, NPC1, in EBOV infection.

EBOVLPs Co-Associate with Sphingomyelin Trafficking Protein, NPC1, at the Plasma Membrane

To determine whether NPC1 was involved in EBOV infection, we first incubated HeLa cells with EBOVLPs for 15, 30, 60, or 90 minutes. At termination, cells were rinsed to remove unbound VLPs, and then immediately fixed. Non-permeabilized cells were incubated with anti-NPC1 antibody, and then with a fluorescently labeled secondary antibody. Cell nuclei were stained with DAPI prior to cells being imaged with a Nikon T7 immunofluorescent microscope, using a 100x oil lens. As shown in Figure 29, NPC1 strongly co-localized with EBOVLPs between 15 to 30 minutes after VLP addition. Because this co-association at the plasma membrane occurs after ASM and Lamp1 recruitment, it suggests that NPC1-dependent exocytosis is a later event in entry, and may even be in response to ASM and/or Lamp1 recruitment.

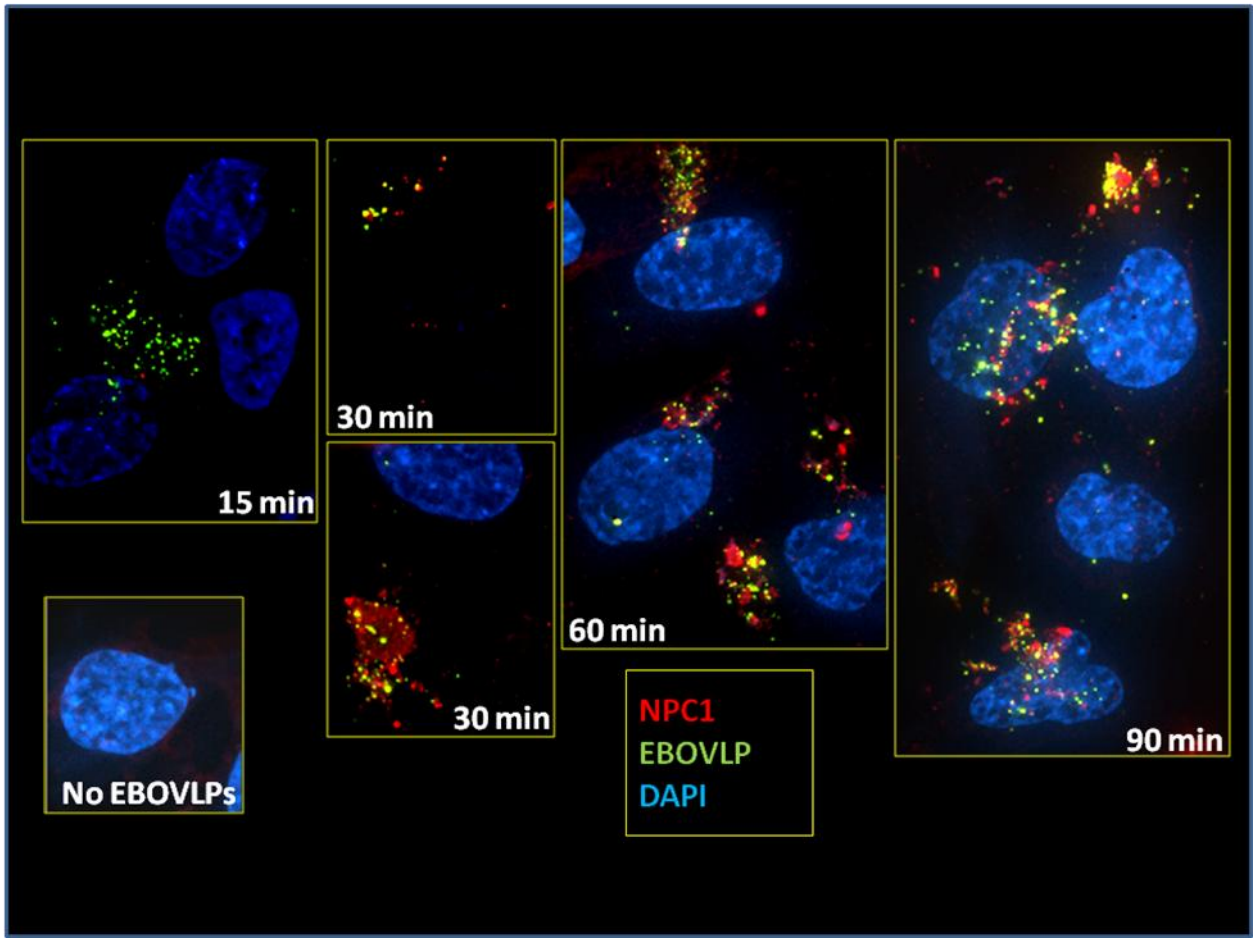

Figure 29. Sphingomyelin-trafficking protein, NPC1, co-localizes with EBOVLPs at the plasma membrane. HeLa cells were incubated with EBOVLPs for 15, 30, 60, and 90 minutes, and then immediately fixed. Non-permeabilized cells were incubated with anti-NPC1 antibody, a fluorescently labeled secondary antibody, and finally DAPI. Cells were imaged with a Nikon T7 immunofluorescent microscope, using a 100x oil lens.

SPHINGOMYELIN TRAFFICKING PROTEIN, NPC1, IS REQUIRED FOR EBOV-GFP INFECTION

Because we have previously shown that EBOVLPs co-localize with sphingomyelin rafts, and that EBOVLP binding recruits NPC1 to the plasma membrane, we next tested whether sphingomyelin-trafficking protein, NPC1, was also involved in EBOV infection.

NPC1$^{-/-}$ Primary Human Skin Fibroblasts Are Resistant to EBOV-GFP Infection

EBOVLP co-localization with sphingomyelin on the plasma membrane suggests that sphingomyelin is involved in EBOV entry. For this, we investigated the role of the sphingomyelin trafficking protein, Niemann-Pick Type C1 (NPC1) in EBOV infection. NPC1 is a transmembrane protein which exocytoses sphingomyelin, cholesterol, and other cargo from the late endosomes/lysosomes to the plasma membrane (Gong et al., 2006; Koivusalo et al., 2007; Lange et al., 1998; Lusa et al., 2001; Sugimoto et al., 2001). In Niemann-Pick Type C1 disease, a rare genetic mutation results in a defective NPC1 protein which cannot bind to late endosomal/lysosomal membranes. This unbound form of NPC1 is proteolytically degraded, leaving the cell without functional NPC1. As a result, the lysosomes swell with cholesterol and other cargo, which severely retards their movement to the plasma membrane (Lange et al., 1998; Liscum et al., 1989). To determine whether NPC1-dependent trafficking was required for EBOV infection, we inoculated primary human skin fibroblasts with a compound heterozygous NPC1 mutation, NPC1$^{-/-}$ (GM0110) (Slotte et al., 1989), with recombinant EBOV expressing GFP, and compared the infection efficiency to normal human fibroblasts (GM0038) inoculated under the same conditions. Surprisingly, EBOV-GFP infection was reduced by 95% in primary human NPC1$^{-/-}$ fibroblasts compared to normal fibroblasts (Figure 30).

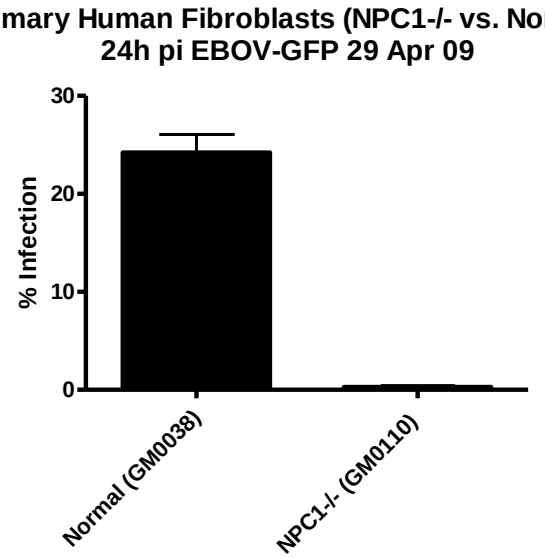

Figure 30. NPC1-/- fibroblasts are resistant to EBOV-GFP infection. Primary human fibroblasts from a donor with NPC1 deficiency and a normal donor were inoculated with EBOV-GFP (MOI = 0.3). Cells were then fixed in formalin, stained with DAPI, and analyzed to count total cell nuclei and infected cells. Percent infection data was analyzed by one-way ANOVA with Tukey post-test using GraphPad Prism analysis software (see Methods).

Cells Treated with U18666A, a Drug Which Mimics the NPC1$^{-/-}$ Phenotype, Are Resistant to EBOV-GFP Infection

To further elucidate the requirement for NPC1 in EBOV infection, we incubated HeLa cells with U18666A - a chemical inhibitor commonly used to mimic the NPC1$^{-/-}$ phenotype (Harmala et al., 1994; Liscum and Faust, 1989). More specifically, U18666A blocks vectorial movement of lysosomes from the perinuclear region to the plasma membrane (Ko et al., 2001). At 830 nM, U18666A inhibits EBOV-GFP infection by 50% compared to DMSO control in a dose-responsive manner (Figure 31). Cell cytotoxicity assay results indicated that there was no reduction in cell metabolic activity at drug concentrations of 25 μM or less, and this concentration effectively blocked infection in all cell types tested. After 24 h post-inoculation (pi), cells were formalin-fixed, DAPI-stained, imaged, and analyzed with Cell Profiler image

analysis software to determine infection efficiency. Using GraphPad Prism analysis software, data was fitted to a sigmoidal dose-response curve with variable slope.

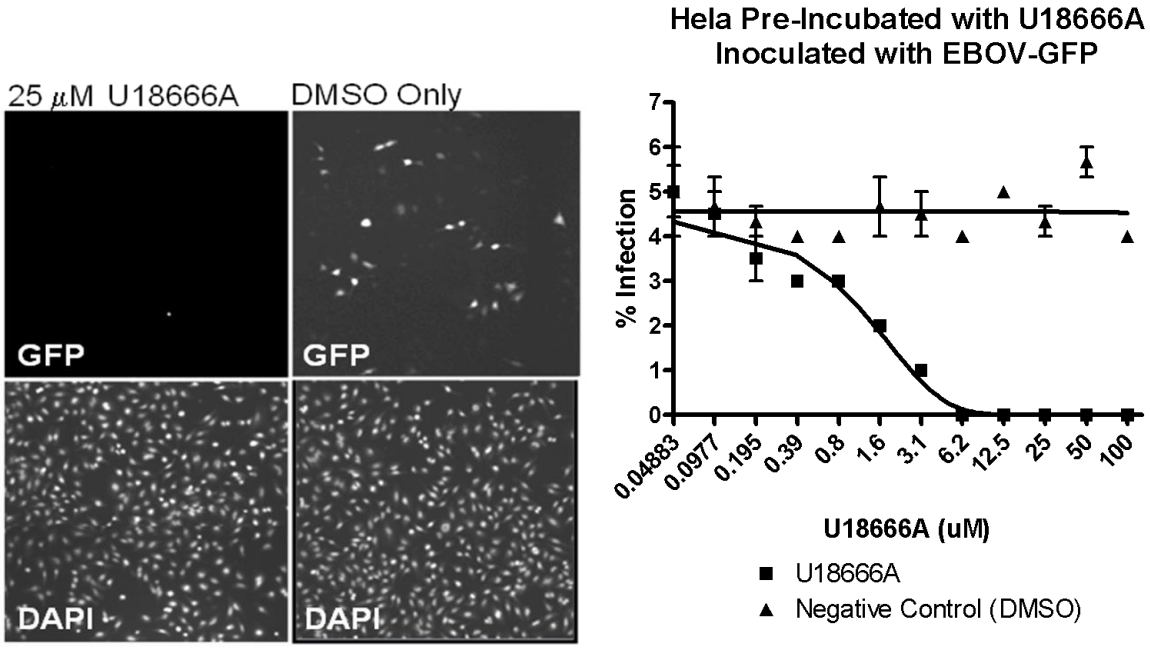

Figure 31. U18666A inhibits EBOV-GFP infection. (Left) HeLa cells were plated in 96-well plate, and then incubated with 2-fold serially diluted drug for 1 h prior to inoculation with EBOV-GFP. Cells then fixed, DAPI-stained, and imaged for DAPI and GFP. To determine infection efficiency, images were analyzed using Cell Profiler image analysis software as described in Methods (MOI 0.1). (Right) EC_{50} was calculated by fitting infection efficiency data to a sigmoidal dose-response (variable slope) and non-linear regression using GraphPad Prism analysis software. At an MOI of 0.05, 830 nM of U18666A inhibited infection by 50% compared to DMSO control.

U18666A, a Drug Which Mimics the NPC1$^{-/-}$ Phenotype, Reduces EBOV-GFP Replication

To assess the inhibitory effect of 25 μM U18666A on viral replication, HeLa cells were plated in a 6-well plate, and then pre-incubated with drug for 1h prior to inoculation with EBOV-GFP. Cells were incubated with virus and drug for 24 h, and then lysed with 1 mL per well of BioRad guanidine cell lysis buffer. Supernatant was placed in tubes, and stored at 4^{o} C for at least 24 h. RNA was purified using an Aurum RNA purification kit as described in Methods.

qRT-PCR was performed using EBOV-Zaire Mayinga NP primers (see Methods) (Figure 32). Compared to DMSO control, 25 μM U18666A inhibited EBOV NP vRNA expression by more than 128-fold.

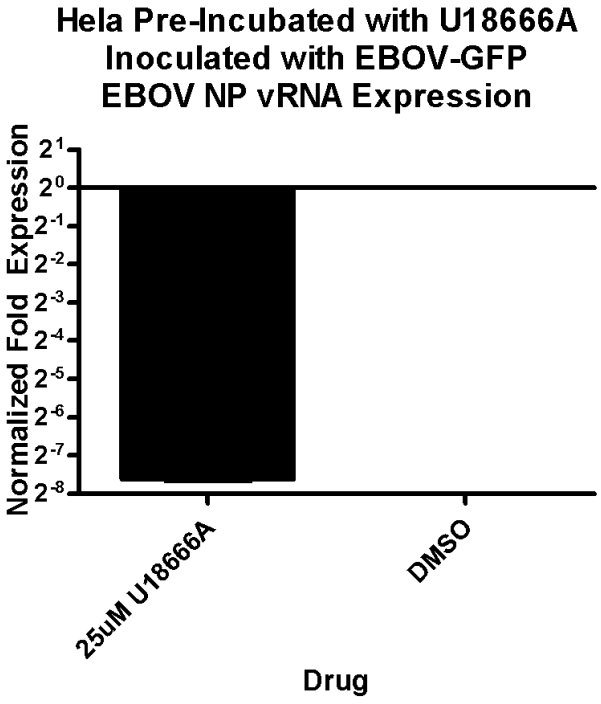

Figure 32. U18666A inhibits EBOV-GFP replication. HeLa cells were plated in a 6-well plate, and then pre-incubated with drug for 1h prior to inoculation with EBOV-GFP. Cells were incubated with virus and drug for 24 h, and then lysed with 1 mL per well of BioRad guanidine cell lysis buffer. Supernatant was placed in tubes, and stored at 4^{o} C for at least 24 h. RNA was purified using an Aurum RNA purification kit as described in Methods. qRT-PCR was performed using EBOV-Zaire Mayinga NP primers (see Methods). 25 μM U18666A reduces expression of EBOV NP vRNA by more than 128-fold.

Cells Transfected with NPC1-Specific siRNA Are Resistant to EBOV-GFP Infection

Because chemical inhibitors are known to have pleiotropic effects, we further tested NPC1's role in EBOV infection using RNA interference. This sequence was used because it was previously shown to potently inhibit NPC1 expression in HeLa cells (Ganley and Pfeffer, 2006). HeLa cells were inoculated with EBOV-GFP at 48 h post-transfection with NPC1-specific

siRNA. At 24 h pi cells were formalin-fixed, DAPI-stained, imaged, and analyzed with Cell Profiler cell image analysis software to determine infection efficiency. Data was analyzed with GraphPad Prism analysis software, using a one-way ANOVA with Tukey post-test. EBOV-GFP infection in NPC1-transfected cells was reduced by greater than 95% compared to All Stars negative siRNA control (Figure 33). Ctbp1 siRNA was used as positive control against EBOV-GFP infection due its potent inhibition of EBOV-GFP infection (Saeed et al., 2010). To quantify the reduction of NPC1 mRNA expression by RNA interference, qRT-PCR was performed. Change in threshold cycles, ΔCt, was determined by normalizing NPC1 expression to GAPDH. ΔΔCt values were calculated by normalized ΔCt values to an All Stars negative siRNA control. Un-transfected cells ("cells only") showed similar NPC1 mRNA expression compared to All Stars control. This data showed that NPC1-specific siRNA was reduced by more than 8-fold compared to an All Stars negative siRNA control (Figure 33).

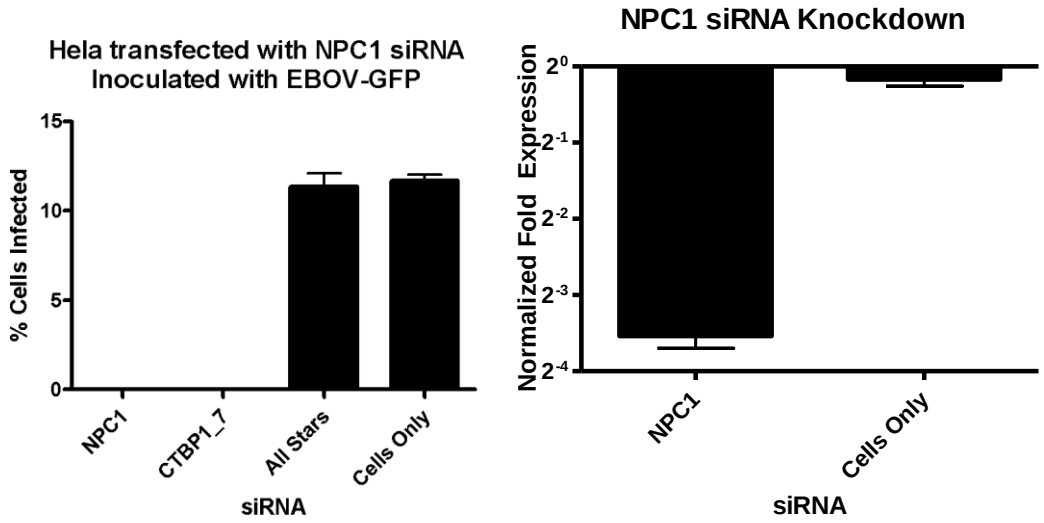

Figure 33. NPC1 siRNA inhibits EBOV-GFP infection. (Left) HeLa cells were transfected with NPC1-specific siRNA. At 48 h post-transfection, cells were incubated with EBOV-GFP for 24 h (MOI = 0.1). EBOV-GFP infection was reduced by over 95% in NPC1-transfected cells

compared to All Stars negative siRNA control. Ctbp1-targeting siRNA was used a positive control since it was previously shown to block EBOV infection. (Right) NPC1 siRNA knocks down NPC1 mRNA expression. NPC1 mRNA was purified from HeLa cells at 48h post-transfection with NPC1 siRNA, and amplified using NPC1-specific primers. Change in threshold cycles, ΔCt, was determined by normalizing NPC1 expression to GAPDH. ΔΔCt values were calculated by normalized ΔCt values to an All Stars negative siRNA control. Untransfected cells ("cells only") showed similar NPC1 mRNA expression compared to All Stars control. There was more than an 8-fold decrease in NPC1 mRNA expression compared to the All Stars negative siRNA control.

NPC1-DEPENDENT INFECTION IS EBOV GP SPECIFIC

After demonstrating the importance of NPC1 in EBOV infection, we tested whether this requirement was EBOV GP-specific by using Vesicular Stomatitis Virus-Luciferase pseudotyped viruses (VSV-Luc) viruses encoated with either EBOV, Venezuelan Equine Encephalitis Virus (VEEV), or Lassa virus (LASV) glycoproteins. VEEV- and LASV-VSV-Luc viruses were chosen as negative controls because preliminary data showed that $NPC1^{-/-}$ fibroblasts were susceptible to infection by pseudotyped viruses, while strongly resistant to EBOV-GFP infection. HeLa cells were pre-incubated for 1 h with either 25 μM U18666A or 25 nM Bafilomycin A prior to an 8 h incubation with virus. At termination, luciferase buffer was added, and luciferase activity measured with a luminometer. Bafilomycin A is an H^+ V-ATPase inhibitor, which causes lysosomal dysfunction by increasing vesicle pH. It was used as a positive control because it potently blocks EBOV-GFP infection at low concentrations.

As shown in Figure 34, 25 μM U18666A reduces EBOV-VSV-Luc infection (luciferase activity) in treated cells to background levels, whereas DMSO-treated cells still generate up to 7,500 luciferase counts per second. This shows that the complete block of EBOV-VSV-Luc infection is due to U18666A, and not due to its solvent, DMSO. When compared to VEEV- and LASV-VSV-Luc, 25 μM U18666A causes nearly a 100-fold decrease in EBOV GP-specific

infection. This shows that the inhibitory effect of U18666A is specific to EBOV GP, since the only difference between the pseudotyped viruses in their glycoprotein.

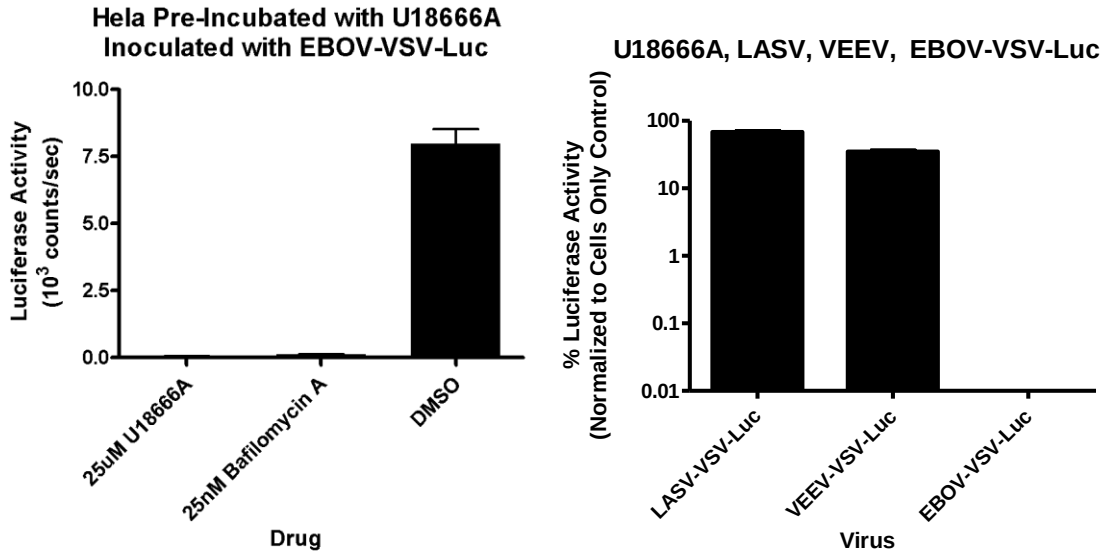

Figure 34. Inhibitory effect of U18666A on VSV-pseudotyped viruses. HeLa cells were pre-incubated with drug for 1h prior to 8h incubation with VEEV-, LASV-, or EBOV-VSV-Luc. Bafilomycin A was used as positive control since it potently blocks EBOV infection. (Left) 25 μM U18666A reduces EBOV-VSV-Luc activity in treated cells to background levels, whereas DMSO-treated cells still show significant luciferase activity – a complete block in infection. (Right) Compared to VEEV- and LASV-VSV-Luc, EBOV-VSV-Luc luciferase activity is reduced by nearly 100-fold, showing EBOV GP-specific inhibition by U18666A.

In Figure 35, HeLa cells were transfected with NPC1-specific siRNA. At 48 h post-transfection, cells were inoculated with EBOV-VSV-Luc pseudotyped virus. After an 8 h incubation, luciferase buffer was added to the cells, and luciferase activity measured. A 48% decrease infection was seen in cells transfected with NPC1-siRNA as compared to cells transfected with the negative siRNA control, All Stars. According to these results, it would appear that NPC1 siRNA inhibition is not as potent in blocking EBOV-VSV-Luc as compared to EBOV-GFP. However, this can be accounted for by different detection methods for each assay. The readout of the luciferase assay is much more sensitive than the EBOV-GFP infection assay

because it measures the luciferase production of every replicating virus particle. In contrast, the EBOV-GFP infection assay is measuring the number of infected cells as a function of fluorescence intensity. If the viral replication is not sufficient to generate GFP fluorescence intensity above a set threshold, it is not measured. However, in the luciferase assay, such minimal replication would be detected.

Taken together, this data suggests that NPC1-dependent trafficking is required for EBOV infection in a sphingomyelin-dependent manner. Because NPC1 specifically exocytoses sphingomyelin to the plasma membrane, we wanted to further investigate the requirement for exocytosis in EBOV infection.

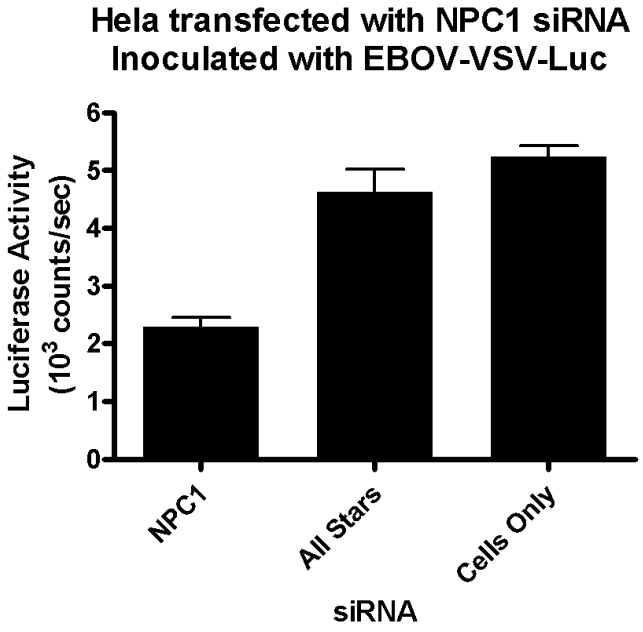

Figure 35. HeLa cells were transfected with NPC1-specific siRNA. At 48 h post-transfection, cells were incubated with EBOV-VSV-Luc pseudotyped virus for 8 h. Upon termination, luciferase buffer was added to the cells, and luciferase activity was measured with a luminometer. Cells transfected with NPC1-siRNA showed a 48% reduction in infection compared to cells transfected with All Stars – a negative siRNA control.

LYSOSOMAL EXOCYTOSIS INHIBITOR, VACUOLIN-1, BLOCKS EBOV-GFP INFECTION.

To further elucidate the requirement for exocytosis during EBOV entry, we used the chemical, vacuolin-1, which specifically and potently blocks lysosomal exocytosis without affecting actin cytoskeleton rearrangement or endocytosis (Cerny et al., 2004). After 1h pre-incubation with 10 μM of 2-fold serially diluted vacuolin-1, HeLa cells were inoculated with EBOV-GFP (Figure 36). After 24 h pi cells were formalin-fixed, DAPI-stained, imaged, and analyzed with Cell Profiler cell counting software to determine infection efficiency. Data was analyzed with GraphPad software, using a one-way ANOVA with Tukey post-test. EBOV-GFP infection was reduced by 50% of control at a concentration of 370 nM. Even at 100 μM, there was no significant decrease in cellular metabolic activity as indicated by Alamar Blue cytotoxicity assay. In HeLa cells, 370 nM, vacuolin-1 inhibits EBOV-GFP infection by 50% compared to DMSO control in a dose-responsive manner. Cell cytotoxicity assay results indicated that there was no reduction in cell metabolic activity at drug concentrations as high as 100 μM. After 24 h post-inoculation (pi), cells were formalin-fixed, DAPI-stained, imaged, and analyzed with Cell Profiler image analysis software to determine infection efficiency. Using GraphPad Prism analysis software, data was fitted to a sigmoidal dose-response curve with variable slope.

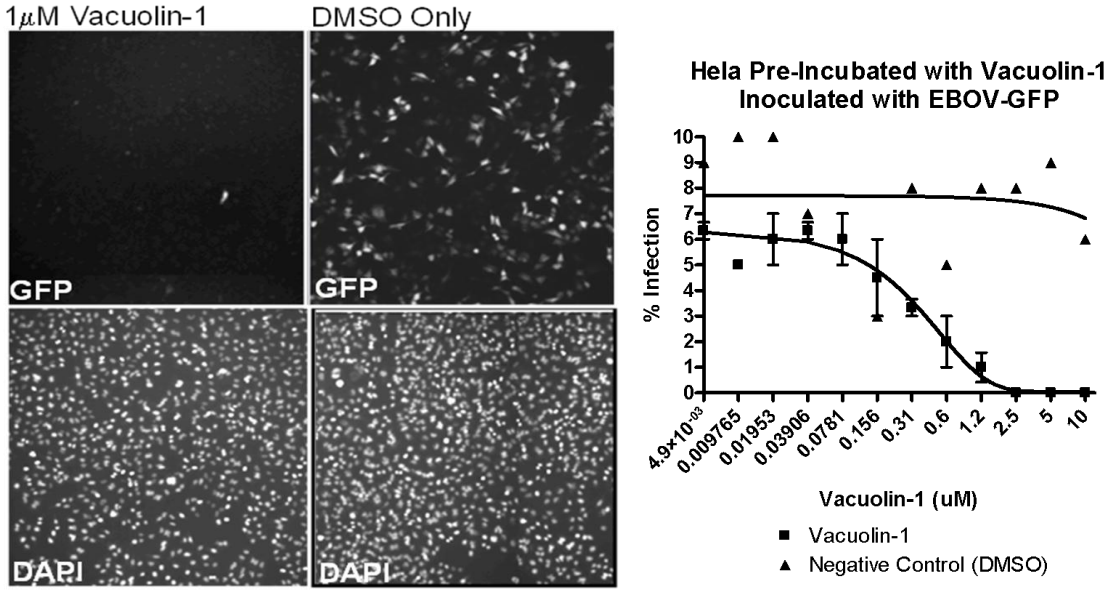

Figure 36. Lysosomal exocytosis inhibitor, vacuolin-1, inhibits EBOV-GFP infection. (Left) HeLa cells were plated in 96-well plate, and then incubated with 2-fold serially diluted drug for 1 h prior to inoculation with EBOV-GFP. Cells then fixed, DAPI-stained, and imaged for DAPI and GFP. To determine infection efficiency, images were analyzed using Cell Profiler image analysis software as described in Methods (MOI 0.3). (Right) EC_{50} was calculated by fitting infection efficiency data to a sigmoidal dose-response (variable slope) and non-linear regression using GraphPad Prism analysis software. At an MOI of 0.1, 370 nM of vacuolin-1 inhibited infection by 50% compared to DMSO control.

Lysosomal Exocytosis Inhibitor, Vacuolin-1, inhibits EBOV-GFP Replication.

To assess the inhibitory effect of vacuolin-1 on viral replication, HeLa cells were pre-incubated with 1 μM vacuolin-1 for 1h before inoculation with EBOV-GFP. Cells were incubated with virus for 24 h to allow for one complete round of viral replication. Expression of EBOV nucleoprotein (NP) vRNA was determined using RT-PCR with EBOV Zaire-Mayinga NP primers (Figure 37). Compared to DMSO control, vacuolin-1 inhibited EBOV NP vRNA expression by more than 128-fold.

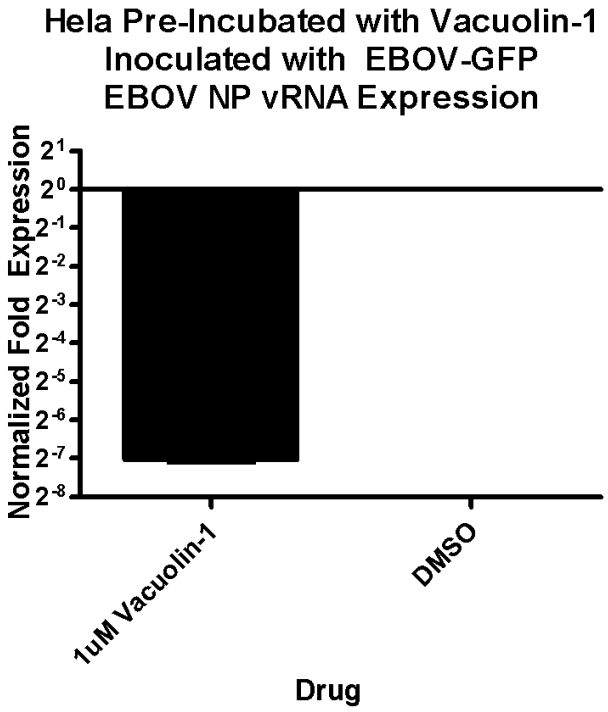

Figure 37. Lysosomal exocytosis inhibitor, vacuolin-1, blocks EBOV-GFP replication. HeLa cells were plated in a 6-well plate, and then pre-incubated with drug for 1 h prior to inoculation with EBOV-GFP. Cells were incubated with virus and drug for 24 h. 1 μM vacuolin-1 reduces expression of EBOV NP vRNA by more than 128-fold.

LYSOSOMAL EXOCYTOSIS REQUIREMENT IS EBOV GP-SPECIFIC

After demonstrating the importance of lysosomal exocytosis in EBOV infection, we wanted to test if this requirement was EBOV GP-specific by using VSV-Luciferase pseudotyped viruses encoated with either EBOV, Venezuelan Equine Encephalitis Virus (VEEV), or Lassa virus (LASV) glycoproteins. VEEV- and LASV-VSV-Luc viruses were chosen as negative controls because previous data showed that HeLa cells treated with lysosomal trafficking and exocytosis inhibitor, U18666A, were susceptible to infection by pseudotyped viruses, but resistant to EBOV-GFP infection. HeLa cells were pre-incubated for 1 h with either 1 μM vacuolin-1 or 25 nM Bafilomycin A, and then inoculated with either VEEV-, LASV-, or EBOV-

VSV-Luc pseudotyped viruses. After 8 h incubation, luciferase buffer was added, and luciferase activity measured by luminometer. Bafilomycin A is an H^+ V-ATPase inhibitor, which causes lysosomal dysfunction by increasing vesicle pH. It was used as a positive control because it potently blocks EBOV-GFP infection at low concentrations.

As shown in Figure 38, 1 μM vacuolin-1 reduces EBOV-VSV-Luc infection (luciferase activity) in treated cells to background levels, whereas DMSO-treated cells still generate up to 7,500 luciferase counts per second. This shows that the complete block of EBOV-VSV-Luc infection is due to vacuolin-1, and not due to its solvent, DMSO. When compared to VEEV- and LASV-VSV-Luc, 1 μM vacuolin-1 causes nearly a 100-fold decrease in EBOV GP-specific infection. This shows that the inhibitory effect of vacuolin-1 is specific to EBOV GP, since the only difference between the pseudotyped viruses in their glycoprotein.

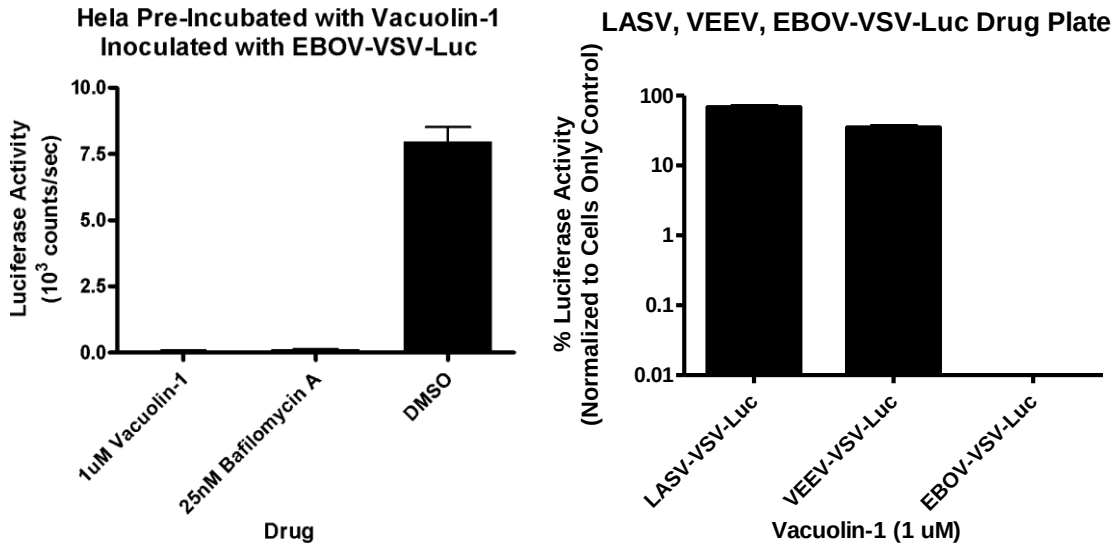

Figure 38. Inhibitory effect of lysosomal exocytosis inhibitor, vacuolin-1, on VSV-pseudotyped viruses. HeLa cells were pre-incubated with drug for 1 h prior to 8 h incubation with VEEV-, LASV-, or EBOV-VSV-Luc. (Left) 1 μM vacuolin-1 reduces EBOV-VSV-Luc activity in treated cells to background levels, whereas DMSO-treated cells still show significant luciferase activity – a complete block in infection. (Right) Compared to VEEV- and LASV-VSV-Luc,

EBOV-VSV-Luc luciferase activity is reduced by nearly 100-fold, showing EBOV GP-specific inhibition by vacuolin-1.

EXOCYTOSIS INHIBITORS, U18666A AND VACUOLIN-1, BLOCK LAMP1, ASM, AND NPC1 RECRUITMENT TO THE PLASMA MEMBRANE

To further confirm the function of the exocytosis inhibitors on EBOV entry, we incubated HeLa cells with either 1 μM vacuolin-1 or 25 μM U18666A for 1 h prior to the addition of EBOVLPs. Cells were then incubated with VLPs for 90 minutes, rinsed, and then immediately fixed. Non-permeabilized cells were then incubated with either anti-Lamp1, anti-ASM, or anti-NPC1 as previously described. As shown in Figure 39, vacuolin-1 blocked recruitment of Lamp1, ASM, and NPC1 to the cell surface, while U18666A only blocked recruitment of NPC1. This is consistent our infection data, since vacuolin-1 was the most potent inhibitor of EBOV infection, and U18666A was the second most potent inhibitor.

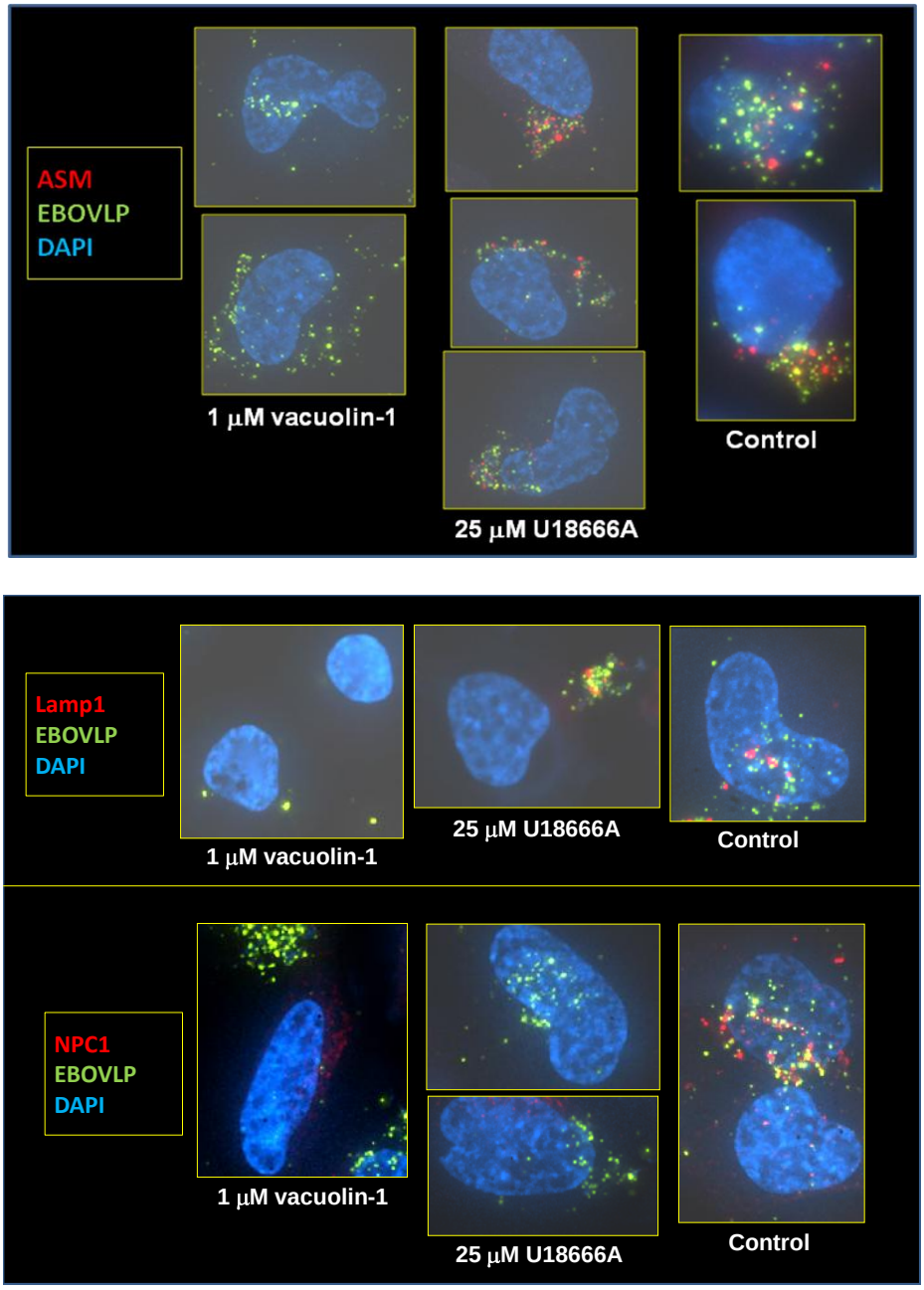

Figure 39. Exocytosis inhibitors, vacuolin-1 and U18666A, block recruitment of ASM, Lamp1, and/or NPC1 to the plasma membrane. HeLa cells were incubated with either 1 μM vacuolin-1 or 25 μM U18666A for 1 h prior to incubation with EBOVLPs for 90 minutes. Cells were then rinsed, and fixed. Non-permeabilized cells were incubated with either anti-ASM, anti-Lamp1, or anti-NPC1 antibodies as previously described. Cell nuclei were DAPI-stained prior to cells being imaged with a Nikon T7 immunofluorescent microscope. (Top) Vacuolin-1 inhibits ASM recruitment to the cell surface, whereas U18666A does not. (Bottom) Vacuolin-1 inhibits Lamp1 and NPC1 recruitment to the cell surface, whereas U18666A only inhibits NPC1.

DISCUSSION:

NPC1-dependent exocytosis is important in EBOV infection. First, EBOV-GFP infection was reduced by 95% in NPC1$^{-/-}$ fibroblasts compared to normal fibroblasts. Second, when HeLa cells were treated with U18666A, a drug which mimics the lysosomal trafficking defect in NPC1$^{-/-}$ cells, EBOV-GFP infection was blocked completely at 6.25 μM, with an EC_{50} of 870 nM. Additionally, 25 μM U18666A reduced EBOV infection in HeLa cells by 128-fold, compared to DMSO-treated cells. Third, EBOV-GFP infection was reduced by over 95% in HeLa cells transfected with NPC1-specific siRNA, as compared to cells transfected with a negative siRNA control. To show that NPC1 inhibition had an EBOV-GP-specific inhibitory effect, HeLa were cells inoculated with VSV pseudotyped viruses which only differ in their surface glycoproteins. It was found that EBOV-VSV-Luc infection was reduced by nearly 100-fold compared to VEEV- and LASV-VSV Luc pseudotyped viruses. Additionally, NPC1 siRNA inhibited EBOV-VSV-Luc infection by nearly 50%. This difference in this result compared to the EBOV-GFP infection assay is due to the differing sensitivities of the luciferase- verses GFP-expressing assays. Luciferase detection is much more sensitive, detecting even one virus replicating; whereas, detection of GFP-expression requires fluorescence intensity to reach at least 18% above background before it is counted.

These results also suggest that lysosomal exocytosis is important for EBOV infection. First, EBOV-GFP infection was completely inhibited in HeLa cells pre-incubated with 2.5 μM of vacuolin-1. At 370 nM, infection was still blocked by 50% as compared to DMSO-treated cells. Second, HeLa cells pre-incubated with 1 μM vacuolin-1 showed a 128-fold reduction in viral replication as compared to DMSO-treated controls. Finally, lysosomal exocytosis is specific for

EBOV entry. When pseudotyped viruses differing only by their surface glycoprotein were incubated with HeLa cells treated with 1 μM vacuolin-1, EBOV-VSV-Luc infection was decreased nearly 50- and 100-fold as compared to VEEV- and LASV-VSV-Luc pseudotyped viruses, respectively.

Finally, vacuolin-1 inhibited recruitment of ASM, lysosomes, and NPC1 to the cell surface. This was consistent with our infection data, which showed that vacuolin-1 was the most potent inhibitor of EBOV infection. It also confirmed previous work by Bao et al., which showed that 1 μM vacuolin-1 blocked ASM-dependent ceramide macrodomain formation on the plasma membrane (Bao et al., 2010b). Additionally, U18666A blocked only NPC1 recruitment to the plasma membrane, as expected. This is supported by previous work by Ko et al., which showed that U18666A specifically inhibits the movement of NPC1 to the plasma membrane (Ko et al., 2001). Furthermore, U18666A was the second most potent inhibitor of EBOV infection.

Taken together, these results indicate that exocytosis is an important process in EBOV infection. First, inhibition of NPC1 function nearly abolishes infection. NPC1 is a late endosomal/lysosomal trafficking protein which delivers long chain sphingomyelin and cholesterol to the plasma membrane via exocytosis (Koivusalo et al., 2007). Therefore, inhibition of NPC1-dependent exocytosis of sphingomyelin and cholesterol may reduce the number of rafts available for virus binding. This is supported by our previous data which showed strong co-association of EBOVLPs with sphingomyelin-rich rafts. Also, one cannot rule out a more specific role for NPC1 in EBOV entry. Recently, Cunningham et al. suggested that NPC1 may be a receptor for EBOV (WRCE Conference, Denver, CO). Second, with regards to infection, inhibition of exocytosis may also negatively impact NSM2-dependent exocytosis – a

process which may be required for routing VP40 matrix proteins to the plasma membrane for virus assembly and budding. Third, inhibition of lysosomal exocytosis would block ASM recruitment to the plasma membrane, and subsequent ASM-dependent ceramide macrodomain formation, receptor clustering, and macropinosome formation. Finally, because lysosomal cathepsins B and L are required to proteolytically cleave the EBOV GPs prior to fusion, and the site of virus fusion has yet to be identified, this suggests that lysosomal recruitment may also expose EBOV GPs to cathepsins at the cell surface. If this is true, then it is possible that virus fusion could occur at the plasma membrane shortly after lysosomal exocytosis, or shortly after internalization via ASM-dependent macropinocytosis.

CHAPTER 3: DISCUSSION

OVERVIEW

EBOV is a filamentous, negatively sensed, single-strand RNA virus which causes up to 90% mortality in man. To date, there are no FDA-approved vaccines or drug treatment therapies. As a strategy for finding new drug treatments to prevent EBOV infection, we investigated potential targets in virus entry. From previous work, EBOV enters via a macropinocytosis-like mechanism which requires cholesterol-rich rafts; pH-dependent cellular enzymes such as cathepsins; PI3K; actin; calmodulin and calmodulin kinase II; and microtubules (Bavari et al., 2002; Chandran et al., 2005; Hood et al., 2010; Kaletsky et al., 2007; Kolokoltsov et al., 2009; Nanbo et al., 2010; Saeed et al., 2010; Saeed et al., 2008; Sanchez, 2007; Schornberg et al., 2006). Because the first step in virus entry is binding to lipid rafts, we chose to investigate EBOV's association with another prominent lipid raft component – sphingomyelin.

Sphingomyelin is a major lipid found in mammalian cells. It preferentially associates with cholesterol to form lipid rafts on the outer leaflet of the plasma membrane. These rafts serve as signaling platforms for cellular entry (McIntosh et al., 1992a, b). Sphingomyelin, unlike cholesterol, is a substrate for sphingomyelinases. These enzymes remove sphingomyelin's phosphocholine headgroup to form ceramide – an important molecule in both pro- and anti-apoptotic pathways. Because the ceramide molecule lacks phosphocholine, it is narrower on one end than the other. This causes unequal spacing in the lipid bilayer, lipid flipping between inner and outer leaflets, and subsequent pinching or invagination of the membrane (Tani and Hannun, 2007; Tepper et al., 2000; van Blitterswijk et al., 2003). Lysosomal acid sphingomyelinase

(ASM), as its name suggests, is localized to lysosomes. However, when activated, ASM translocates to the plasma membrane via lysosomal exocytosis (Bao et al., 2010b; Tam et al., 2010). Once the lysosome fuses with the outer membrane, ASM is released to outside the cell where it hydrolyzes sphingomyelin on the outer leaflet to ceramide. This, in turn, causes macropinsome formation as the ceramide-macrodomain invaginates into the cell. This process is clathrin and caveolin-independent (Zha et al., 1998).

Neutral sphingomyelinase 2 (NSM2) is located on the cytosolic side of the plasma membrane, where it hydrolyzes sphingomyelin which has been flipped inside the cell in response to a pro-apoptotic event. As a result, phosphatidylserine flips to the outer leaflet. Ceramide formation destabilizes the membrane further by loosening the once tight junctions formed between sphingomyelin and cholesterol. As a result of ceramide being generated on the inner leaflet, the membrane pinches outward from the cell, forming a bleb. In a similar manner, hen NSM2 hydrolyzes sphingomyelin on multi-vesicular bodies within the cell, the pinched off membrane forms exosomes which are released to the plasma membrane (Tani and Hannun, 2007; Tepper et al., 2000; van Blitterswijk et al., 2003).

Because sphingomyelin plays such an important role in raft formation, endocytosis, and exocytosis, its concentration on the plasma membrane is carefully maintained. When sphingomyelin on the plasma membrane is depleted due to ASM-dependent macropinosome formation or NSM2-dependent blebbing and membrane shedding, it is restored by Niemann-Pick Type C1 (NPC1)-dependent exocytosis. NPC1 is a transmembrane protein that is found in late endosomes and sometimes lysosomes. It has been well-studied in its role in lipid trafficking. When NPC1 function is lost, lysosomes swell with cholesterol, sphingomyelin, and other cargo,

and vesicle movement to the plasma membrane is blocked (Harmala et al., 1994; Koivusalo et al., 2007; Lange et al., 1998; Lusa et al., 2001).

Because sphingomyelin, sphingomyelinases, and NPC1 are so intimately involved in raft formation, cell signaling, and membrane dynamics, we chose to investigate their role in EBOV entry and infection.

SUMMARY OF RESULTS

After showing that EBOVLPs associated with sphingomyelin rafts, we further showed that lysosomal marker, Lamp1, and ASM similarly co-localized with EBOVLPs on the cell surface. This demonstrated that EBOVLP binding stimulates lysosomal ASM translocation to the cell membrane, and subsequent release via lysosomal exocytosis. This in line with previous studies, which showed that lysosomal exocytosis is required to deliver lysosomal ASM to sphingomyelin on the plasma membrane's outer leaflet. (Bao et al., 2010a; Bao et al., 2010b; Tam et al., 2010).

Because ASM translocation suggested ASM activity was important in EBOV entry, we next looked at what effect ASM chemical and genetic inhibitors had on infection. ASM inhibitor, impramine, inhibited EBOV-GFP infection as well as viral replication. $ASM^{-/-}$ fibroblasts were also resistant to EBOV-GFP infection, with a 40% reduction compared normal fibroblast controls. Additionally, 5 different ASM-targeting siRNA reduced EBOV-GFP infection by at least 50%. Impramine also sharply decreased EBOVLP-Luciferase fusion with cell membranes, suggesting ASM activity is involved in a fusion or pre-fusion step. Lastly, the ASM-dependent mechanism in entry is EBOV GP-specific, in that EBOV-VSV-Luciferase

pseudotyped virus infection was reduced 10-fold by ASM inhibitors, desipramine and imipramine, as compared to LASV- and VEEV-VSV-Luciferase pseudotyped viruses.

Next we tested if NSM2 was equally necessary for EBOV entry. Manumycin A is a specific, potent irreversible inhibitor of NSM. At a concentration of 5 μM, manumycin A blocked EBOV-GFP infection by 50% as compared to DMSO-treated cells. Additionally, 30 μM manumycin A sharply inhibited EBOV-GFP replication. To ensure that this effect was specific for NSM2, NSM2 mRNA expression was suppressed by NSM2-specific siRNA. This suppression corresponded to a similar decrease in EBOV-GFP infection. Manumycin A reduced EBOVLP-Luciferase fusion, but only by about 50%. This suggests that NSM2 is not as important in fusion or a pre-fusion step; or that NSM activity is so intense that it overcomes the inhibitory effect of the drug. Finally, NSM inhibition is EBOV GP-specific as evidenced by a nearly 100-fold decrease in EBOV-VSV-Luciferase pseudotyped virus infection as compared to VEEV- and LASV-VSV-Luciferase pseudotyped viruses treated with the same concentration of manumycin A.

Finally, we assessed the role of sphingomyelin-trafficking protein, NPC1, in EBOV entry. Unlike ASM, $NPC1^{-/-}$ fibroblasts sharply resisted EBOV-GFP infection – with an over 95% reduction in infection as compared to normal fibroblast controls. Similarly, NPC1-exocytosis inhibitor, U18666A, required less than 1 μM to generate 50% inhibition of EBOV-GFP infection as compared to a DMSO control. In contrast, ASM inhibitor, imipramine, required over 3 times this concentration under similar conditions to generate the same level of inhibition. Similarly, NSM inhibitor, manumycin A, required a concentration 5 times greater than that of U18666A to block EBOV-GFP infection by 50% compared to control. In line with

this, NPC1-targeting siRNA blocked EBOV-GFP infection by more than 95%, mimicking the inhibition seen in the mutant fibroblasts. U18666A also reduced EBOV-GFP replication with slightly greater potency than for ASM or NSM inhibitors. Finally, U18666A inhibition of NPC1-trafficking and EBOV-VSV-Luciferase pseudotyped virus infection is specific to EBOV GP. In addition, the lysosomal exocytosis inhibitor, vacuolin-1, also potently blocked EBOV-GFP infection – even more so than U18666A. At only 370 nM, vacuolin-1 blocked 50% of EBOV-GFP infection as compared to a DMSO control. 1 μM vacuolin-1 also potently suppressed EBOV-GFP replication – decreasing nucleoprotein vRNA expression by 128-fold compared to a DMSO control. Finally, it was shown that vacuolin-1-dependent exocytosis is specific for EBOV GP. When compared to VEEV- and LASV-VSV-Luciferase pseudotyped viruses, EBOV-VSV-Luciferase infection was reduced by 50- and 100-fold, respectively (Table 1).

Table 1. Summary of EC50 values for cells and drugs tested in this work. Concentrations are in μM, except Bafilomycin A, which is in nM.

Drug	Cell Type	EC_{50}	EC_{50} 95% Confidence Interval	Standard Error LogEC_{50}	R^2
Imipramine	293 HEK	4.863	4.108 – 5.758	0.03546	0.9728
	Hela	3.617	2.966 – 4.411	0.04165	0.9488
	Vero E6	5.560	4.686 – 6.596	0.03643	0.9651
Desipramine	Hela	3.314	2.546 – 4.314	0.05450	0.9812
	Vero E6	11.34	8.697 – 14.80	0.05534	0.9555
Manumycin A	293 HEK	3.387	3.088 – 3.715	0.01940	0.9895
	Hela	5.024	2.777 – 9.089	0.1248	0.8524
Vacuolin-1	293 HEK	0.1300	0.1106 – 0.1527	0.03413	0.9750
	Hela	0.3678	0.2472 - 0.5473	0.08396	0.9220
U18666A	293 HEK	1.716	1.376 – 2.140	0.04663	0.9799
	Hela	0.8273	0.4366 – 1.568	0.1345	0.9389
Bafilomycin A	293 HEK	3.416	2.757 – 4.232	0.04528	0.9707
	Hela	1.680	0.9486 – 2.974	0.1207	0.9254

INTERPRETATION OF RESULTS

Because sphingomyelin concentrations on the plasma membrane can be depleted by sphingomyelinases and subsequently replaced by NPC1-dependent exocytosis, we looked at the possibility that EBOV binding might over-stimulate this process in a GP-dependent manner (Figure 40).

First, desipramine, imipramine, and manumycin A, as well as genetic inhibition of ASM and NSM2, likely all inhibit sphingomyelinase activity; and, therefore, subsequent depletion of

sphingomyelin on the plasmid membrane. In short, they prevent the requirement for sphingomyelin repletion by NPC1-dependent exocytosis. Because ASM inhibitors negatively impact fusion of EBOVLPs, this suggests that they are involved in step leading up to the fusion step during EBOV entry. NSM inhibitor, manumycin A, did not potently inhibit fusion, suggesting that NSM2 may a role in a post-fusion step. In addition, because inhibition of ASM and NSM reduced EBOV entry in a GP-dependent manner, this suggests that sphingomyelinases are stimulated by EBOV GP. Interestingly, NPC1-targeting siRNA blocked EBOV-GFP infection more potently than ASM- and NSM2-targeting siRNA. There are many explanations for this. First, both sphingomyelinases are important in EBOV infection, so blocking only ASM or NSM2 still leaves the other sphingomyelinase to deplete sphingomyelin. Second, the SMPD1 gene also produces a secretory form of acid sphingomyelinase that has a much longer half-life (>24 h) than the lysosomal isoform. Unlike the lysosomal isoform, the secretory isoform is insensitive to desipramine. Also, because EBOV-GFP was added at 48 h post-transfection, this may not have allowed sufficient time for complete ASM suppression to occur. Third, other neutral sphingomyelinases besides NSM2, may be contributing to sphingomyelin depletion. Finally, sphingomyelin depletion may be caused by other mechanisms that have yet to be defined.

Second, U18666A, as previously shown (Ko et al., 2001; Liscum, 1990; Liscum and Faust, 1989), blocks movement of NPC1-dependent trafficking from late endosomes/lysosomes to the plasma membrane. Therefore, this chemical inhibitor, as well as genetic inhibition of NPC1, blocks NPC1-dependent delivery of sphingomyelin to the plasma membrane. This, in turn, reduces the number of sphingomyelin-rich rafts available for EBOVLP binding. A more

specific role for NPC1 in EBOV infection cannot be ruled out, however. Because cells lacking functional NPC1 are almost completely resistant to infection, this suggests that NPC1 specifically, not just NPC1-dependent exocytosis, is required for EBOV infection. In line with this, Cunningham et al. recently proposed that NPC1 is an EBOV receptor because it binds EBOV GP (WRCE conference, Denver, CO).

Finally, the lysosomal exocytosis inhibitor, vacuolin-1, likely blocks EBOV infection is many ways. First, by blocking lysosomal fusion with the plasma membrane, ASM as well as lysosomal cathepsins B and L, no longer have access sphingomyelin or EBOV GPs, respectively. Second, because ASM release to the outer membrane is inhibited, ASM-dependent ceramide macrodomain formation, receptor clustering, and macropinosome formation are also blocked. Third, vacuolin-1 may also directly block NPC1-dependent exocytosis of sphingomyelin. In this way, vacuolin-1 is a potent inhibitor of EBOV entry and infection in that it blocks both ASM-dependent depletion of sphingomyelin, ASM-dependent macrodomain formation, ceramide-induced clustering of receptors, and subsequent macropinosome formation; as well as NPC1-dependent repletion of sphingomyelin to the plasma membrane. Like ASM and NSM, vacuolin-1-dependent lysosomal exocytosis is stimulated by a EBOV-GP-specific mechanism, as shown by vacuolin-1's nearly 50- and 100-fold decrease in EBOV-VSV-Luc infection as compared to VEEV- and LASV-VSV-Luc pseudotyped viruses, respectively.

In summary, these results suggest that EBOV binding to sphingomyelin-rich rafts activates sphingomyelinases through a yet undetermined mechanism. Because sphingomyelinases deplete membrane sphingomyelin through macropinosome formation, and membrane blebbing and shedding, NPC1-dependent exocytosis is required to replace the lost

sphingomyelin. This, in turn, creates a continuous feedback loop. As more sphingomyelin is brought to the surface by $NPC1^+$ vesicles, more sphingomyelin rafts form, allowing more EBOVLPs to bind. As more EBOVLPs bind, more sphingomyelinase activation occurs. As sphingomyelinase activity increases, so does the demand to bring more sphingomyelin to the cell surface via NPC1-dependent exocytosis. Over-stimulation of this feedback loop may contribute to EBOVLP clustering on the plasma membrane. Although more work needs to be done to define the specific role of NSM2 in EBOV infection, it appears that NSM2 may be important in virus assembly and budding. By inducing exosome formation in multi-vesicular bodies, NSM2 may aid in trafficking VP40 matrix proteins to the plasma membrane.

UNRESOLVED ISSUES AND FUTURE WORK

Because we have shown that EBOV binding recruits lysosomes to the plasma membrane, and that lysosomal enzyme, ASM, can be delivered to the plasma membrane, we next will look at whether EBOV binding can stimulate exocytosis of cathepsins B and L to the cell surface. We will incubate fixed, non-permeabilized, EBOVLP-treated HeLa cells with anti-cathepsin B antibodies which bind both secreted and intracellular forms of the enzyme. We expect to see co-localization of only secreted cathepsin B with EBOVLPs at the plasma membrane within 15 minutes, similar to ASM and Lamp1. In addition, we will incubate cells with anti-cathepsin L antibodies, and expect similar results. To further assess the role of secreted cathepsin B in EBOV infection, we will also perform a cathepsin cleavage assay, using a specific EBOV GP which will allow us to differentiate between cleaved verses uncleaved GP protein using a Western blot. We will use the macropinocytosis inhibitor, EIPA, as a positive control, while testing inhibitory effects of U18666A and vacuolin-1 on cathepsin B secretion and cleavage of

EBOV GP. Finally, we will stimulate HeLa cells with EBOVLPs for 90 minutes, and then measure secreted verses non-secreted cathepsin B activity using a FRET/fluorescence-based cathepsin B activity assay using a commercially available kit specifically designed for this purpose. Through these experiments, we intend to determine whether cathepsin-induced GP fusion can occur at the plasma membrane.

Because the hydrolysis of sphingomyelin results in ceramide macrodomain formation, we attempted to stain ceramide using a ceramide-specific antibody. This antibody was previously used by Grassme et al. to show co-localization of *P. aeruginosa* with ASM and ceramide on the membrane surface (Grassme et al., 2003). However, in our hands, it only produced an intense membrane-like stain, rather than the expected punctate, raft-like stain. This may be due to differences in blocking methods.

Additionally, because EBOV entry is so dependent on sphingomyelinase activation, we intend to perform a sphingomyelinase activity assays at various time points after VLP addition to determine when activity peaks. As a reference, *E. coli* activate ASM within minutes of binding to host cells, with activity peaking around 30 minutes (Falcone et al., 2004).

Finally, the chemical, vacuolin-1, induces lysosomal enlargement and inhibits lysosomal exocytosis similarly to the vacuolin $B^{-/-}$ phenotype of *Dictyostelium*, an amoeba which is used as a model for studying human phagocytic cell function. It is thought that vacuolin-1 competes with native vacuolins to disrupt vesicle integrity, specifically late endosomes and lysosomes (Cerny et al., 2004; Huynh and Andrews, 2005; Morrow and Parton, 2005). There are no known mammalian vacuolins; however, flotillins, are the closest homologs (Jenne et al., 1998; Rauchenberger et al., 1997). Flotillins are associated with lipid rafts on the plasma membrane,

as well as in cell vesicles (Wienke et al., 2006). Because vacuolin-1 has such a potent effect on EBOV infection, we intend to investigate the role of flotillins in EBOV entry.

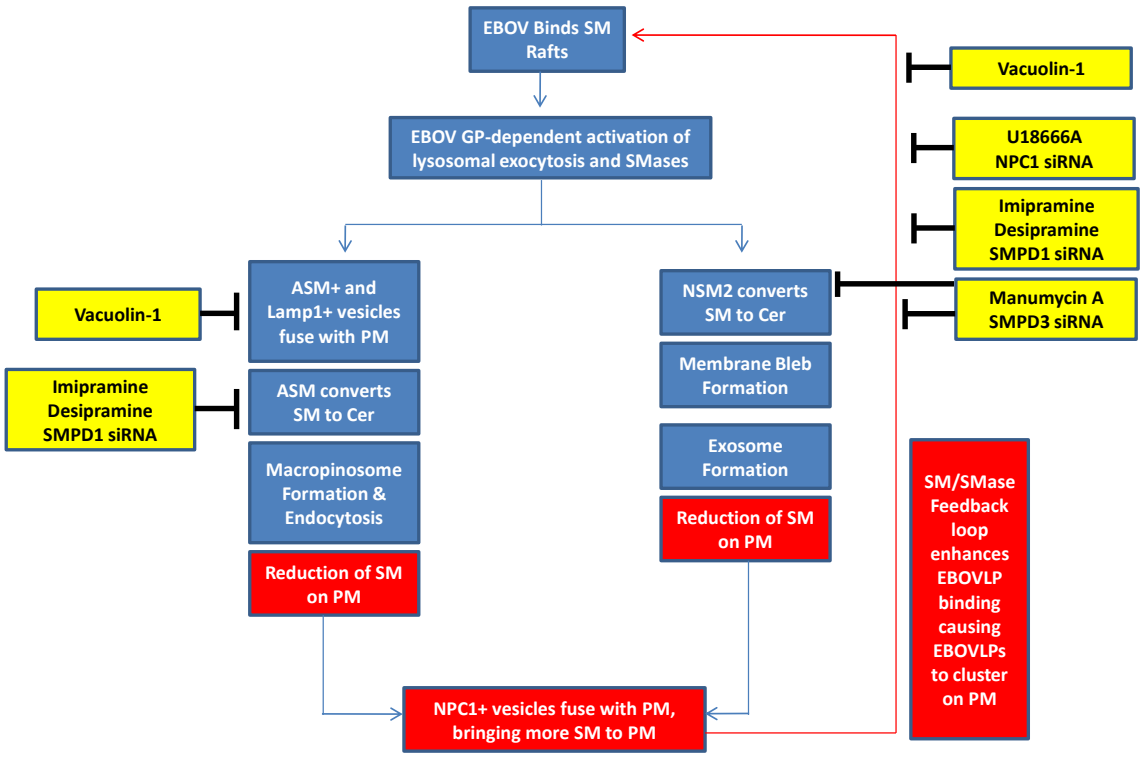

Figure 40. Summary of sphingomyelin-dependent EBOV entry. Refer to detailed description in text.

HOW THESE FINDINGS CONTRIBUTE TO WHAT WE KNOW TO ABOUT EBOV ENTRY SO FAR

First, it was previously assumed that EBOV entry was cholesterol-dependent because EBOV associates with GM_1-positive lipid rafts, and is sensitive to cholesterol extraction by MβCD (Bavari et al., 2002; Saeed et al., 2010). However, a further investigation of lipid raft composition was lacking. In addition, Giocondi et al. showed that MβCD also extracts sphingomyelin from cell membranes (Giocondi et al., 2004); therefore, the assumption that

EBOV entry was strictly cholesterol-dependent was in question. Unlike cholesterol, sphingomyelin is a dynamic molecule. When sphingomyelinases convert sphingomyelin to ceramide, it causes formation of large ceramide macrodomains and clustering of cellular receptors. In addition, ceramide and its metabolites act as signaling molecules in both pro- and anti-apoptotic pathways. Furthermore, sphingomyelinase-induced ceramide production drastically alters the fusogenicity, permeability, and structure of membranes. Also, depending of the subcellular location and pH optima of the sphingomyelinases, ceramide can form either endocytic or exocytic vesicles (Bollinger et al., 2005; Gulbins et al., 2004; Marchesini and Hannun, 2004; Zeidan and Hannun, 2010). Therefore, this current work fills a gap in our understanding about what components of lipid rafts are involved in EBOV binding and entry, and how these lipids contribute to virus internalization.

Second, previous work showed that EBOV enters via a macropinocytosis-like mechanism, which is independent of clathrin and caveolin (Nanbo et al., 2010; Saeed et al., 2010). Previously, Zha et al. showed that ASM can induce macropinosome formation (Zha et al., 1998). Through our work, we have shown a possible mechanism macropinosome formation through stimulation of ASM. Additionally, both macropinocytosis and ASM-dependent macropinosome formation require PI3K and actin rearrangement (Burow et al., 2000; Saeed et al., 2010; Saeed et al., 2008; Sanchez, 2007; Zeidan et al., 2008). Furthermore, because ASM translocation to the outer leaflet of the plasma membrane requires microtubule-dependent lysosomal exocytosis, this process, like EBOV entry, is blocked by microtubule inhibitor, nocodazole (Saeed et al., 2010; Sanchez, 2007). Finally, NPC1-dependent exocytosis of sphingomyelin may also rely on microtubules.

Third, we knew that EBOV entry requires pH-dependent lysosomal cathepsins B and L to proteolytically cleave the GP prior to fusion (Martinez et al., 2010; Schornberg et al., 2006); however, we had not defined a role for lysosomes in EBOV infection. Additionally, we assumed that fusion could only occur within the cell because cathepsins B and L are localized to lysosomes. Our work filled this gap by first showing co-association of lysosomes with EBOVLPs. However, this co-localization occurred at the plasma membrane, not within the cell. Work by Haka et al. as well as Tam et al. shows that lysosomal enzymes can be exocytosed to the plasma membrane, and remain active within "pH pockets" along the cell surface (Haka et al., 2009; Tam et al., 2010). More specifically, lysosomal cathepsin B can be exocytosed from the cell, leading to degradation of the extracellular matrix. In fact, cathepsin B exocytosis is well-studied for its role in cancer metastasis (Cavallo-Medved and Sloane, 2003). Therefore, it is a logical to assume that because EBOV binding can stimulate the recruitment of both lysosomes and the lysosomal enzyme, ASM, to the plasma membrane; EBOV binding likely also recruits lysosomal enzymes, cathepsins B and L to the cell surface in a similar manner. In theory, this would allow proteolytic processing of the virus GPs at the cell surface. Therefore, fusion of virus membranes could occur with the plasma membrane after binding, or with endosomal membranes shortly after virus internalization.

Fourth, EBOV entry requires calmodulin and calmodulin kinase II (CAMKII) (Kolokoltsov et al., 2009). Calmodulin and CAMKII, along with synaptotagmin VII, calcium, and SNARE complexes, are required for fusion of lysosomal and plasma membranes during lysosomal exocytosis (Tchernev et al., 2002). Calmodulin and CAMKII may also be required for fusion of NPC1-dependent exosomes with the plasma membrane. In light of this, calmodulin

and CAMKII may be required for lysosomal fusion, and subsequent release of ASM and cathepsins B and L to the outer leaflet of the plasma membrane prior to endocytosis and/or virus fusion. They may also be important in the fusion of $NPC1^{+}$ vesicles with the plasma membrane, and subsequent repletion of sphingomyelin to the outer leaflet, or possibly even the introduction of NPC1 to EBOV GP.

Finally, because recruitment of ASM, NPC1, and lysosomes to the plasma membrane specifically requires stimulation by EBOV GP, this suggests that GP expressed on the outside of infected cells, as well as secreted GPs, may initiate a similar recruitment of ASM, NPC1, and lysosomes on neighboring cells. In this way, the two forms of GP would, in a sense, 'prime' nearby un-infected cells for virus entry by stimulating exocytosis of sphingomyelin for binding; NPC1 as a possible receptor; ASM for ASM-dependent ceramide macrodomain formation, receptor clustering, and macropinosome formation; and cathepsins B and L for GP cleaving prior to fusion.

In summary, the addition of NPC1, sphingomyelin, and sphingomyelinases in EBOV entry reinforces the pre-existing model by adding to what we know about the binding and internalization steps. However, this work still leaves many unanswered questions. Do cathepsins B and L co-localize with EBOV on the cell surface like ASM, Lamp1, and NPC1? Is NPC1 a receptor for EBOV? Can fusion between the virus membrane and cell membrane occur at the cell surface?

HOW THESE FINDINGS RELATE TO WHAT WE KNOW TO ABOUT OTHER PATHOGENS

Sphingomyelinase-dependent entry is not unique to EBOV. Previously, it has been shown that bacteria such as *Pseudomonas aeruginosa*, *Escheria coli*, and *Neisseria gonorrheoeae* stimulate ASM activity during entry, with ASM being recruited to the outer leaflet within 15 to 30 minutes of the bacterium binding (Falcone et al., 2004; Grassme et al., 2003; Hauck et al., 2000). Viruses such as rhinoviruses (Bollinger et al., 2005; Dreschers et al., 2007; Grassme et al., 2005), Sindbis virus (SINV) (Jan et al., 2000) and measles virus (MV) require ASM for entry, with the latter two also requiring NSM for infection. In fact, MV has been shown to specifically activate NSM2 (Avota et al., 2011; Gassert et al., 2009). And just recently, the protozoan, *Trypanosoma cruzi*, was shown to stimulate ASM upon entry (Fernandes et al., 2011). Because many pathogens exploit sphingomyelinases for entry and infection, they make ideal targets for sphingomyelinase inhibitors.

Additionally, lysosomal exocytosis is not unique to EBOV entry either. *N. gonorrheoeae* recruits lysosomes to the plasma membrane, in addition to entering via macropinocytosis (Ayala et al., 2001; Ayala et al., 2002; Zenni et al., 2000). *Mycobacterium tuberculosis* and *T. cruzi* also stimulate lysosomal movement to the plasma membrane to gain entry in host cells (Divangahi et al., 2009; Gaspar et al., 2009; Kima et al., 2000; Rachman et al., 2006; Woolsey et al., 2003). Again, because so many pathogens rely on lysosomal exocytosis to access host cells, it makes an excellent target for drug development.

Finally, with regard to entry, measles virus (MV) bears the most similarities with EBOV. As a fellow member of the order *Mononegavirales*, MV also requires PI3K, ASM, NSM2, microtubules and actin during entry. Furthermore, MV has recently been shown to enter cells via macropinocytosis like EBOV (Avota et al., 2011; Frecha et al., 2011; Gassert et al., 2009).

Even more intriguing is that MV binds DC-SIGN, a molecule which has also been show to enhance EBOV infection (Alvarez et al., 2002; Avota et al., 2011; de Witte et al., 2006; Marzi et al., 2007; Simmons et al., 2003a). By binding DC-SIGN, MV induces ASM and NSM2 activity, which requires lysosomal exocytosis of ASM. Coincidentally, through this process, MV's lysosomal receptor, SLAM (CD150), is also brought to the cell surface, facilitating virus binding and internalization (Avota et al., 2011). In light of the other similarities with MV entry, we speculate that EBOV may also be recruiting a secondary receptor to the surface via NPC1-dependent exocytosis or lysosomal exocytosis. Recent work by Cunningham et al. supports this idea, by showing that EBOV GP binds NPC1 (WRCE conference, Denver, CO).

HOW THESE FINDINGS CAN BE USED FOR FUTURE RESEARCH

Our goal was to identify potential targets for drug therapies in EBOV entry and infection. During this process, we have identified a novel sphingomyelin-sphingomyelinase-NPC1-dependent entry mechanism which can be exploited for developing drug treatment strategies. Of the potential targets, we have identified ASM as a primary target for drug treatment therapies for several reasons. First, our results showed that ASM inhibitors specifically block EBOV infection, and do so at relatively low concentrations. Second, many ASM inhibitors, such as desipramine, amitriptyline, and imipramine, are already FDA-approved drugs being prescribed as anti-depressants. Additionally, functional ASM inhibitors largely fall into two main drug classes - anti-histamines (R06), and psychoanaleptics (N06) - suggesting that drugs within these classes could potentially be re-purposed for preventing and treating EBOV infection (Kornhuber et al., 2010). Third, ASM is instrumental in the regulation cytotoxic granule exocytosis in primary $CD8^+$ T cells (Herz et al., 2009). Interestingly, a major characteristic of lethal EBOV

infection is an ineffective $CD8^+$ T cell response (Baize et al., 1999; Bradfute et al., 2008; Gupta et al., 2005; Reed et al., 2004; Sanchez et al., 2004; Warfield et al., 2005; Wilson and Hart, 2001). As shown by our work, ASM is required for EBOV entry in a GP-specific manner. Possibly, EBOV surface and secretory GP stimulate pre-mature release of cytotoxic granules from T cells, leading to a non-targeted, dysfunctional immune response. ASM inhibitors may prevent this pre-mature 'firing' of T cells by reducing the level of GP-dependent ASM activation; resulting in a more controlled immune response. Also, the imipramine concentration used to treat anti-depression is not sufficient to prevent normal T cell granule secretion (Herz et al., 2009), suggesting that ASM inhibitors could safely be used to reduce excessive ASM-dependent release of cytotoxic granules without affecting normal levels of secretion.

Our second, yet equally important, target for a drug treatment therapy is exocytosis. Because EBOV entry requires both lysosomal exocytosis for ASM and translocation to the plasma membrane, as well as NPC1-dependent exocytosis of sphingomyelin, chemicals which target these trafficking pathways also most potently block EBOV entry and infection. In addition, it is possible that if EBOV stimulates lysosomal exocytosis of cathepsins B and L, exocytosis inhibitors could greatly reduce virus entry as well as other negative effects which result from the secretion of cathepsin B. Of the inhibitors tested, lysosomal exocytosis inhibitor, vacuolin-1, was most effective in blocking EBOV infection. At a concentration of only 370 nM, it blocked infection as wells as 3 to 5 μM of either ASM or NSM inhibitors, respectively. Additionally, vacuolin-1 blocks recruitment of NPC1, ASM, lysosomes to the plasma membrane, possibly explaining its greater potency. Furthermore, NPC1-dependent exocytosis inhibitor, U18666A, inhibited EBOV-GFP infection at concentrations less than 1 μM, which is still much

less than the ASM and NSM inhibitors. Like ASM inhibitors, exocytosis inhibitors may be useful in reducing excessive release of cytotoxic granules from T cells during EBOV infection. In addition, vacuolin-1 has previously been show to block histamine release from mast cells (Shaik et al., 2009); and, therefore, may possibly suppress excessive release of histamines during *in vivo* EBOV infection.

Our third target is for drug treatment is NSM because it had the least inhibitory effect on EBOV infection as compared to ASM and exocytosis inhibitors. Because NSM2 activity is not as well-studied as ASM, there are also fewer effective NSM inhibitors available. This was evidenced during the course of our work. We tested many NSM inhibitors – sphingolactone-24, GW4869, and spiroepoxide – before finally achieving highly reproducible results with manumycin A. Sphingolactone-24 and spiroepoxide are sensitive to light and oxygen, making them somewhat unstable; and GW4869 has a crystal-like structure, which causes it to readily precipitate out of solution, even when dissolved in DMSO. For this, we felt that these drugs would likely be equally problematic when being used *in vivo*; and, therefore, less effective than ASM or exocytosis inhibitors. However, the mechanism of NSM inhibition in EBOV entry should explored further, especially in the context of exosome formation and virus assembly and budding.

Finally, by exploring which domains of EBOV GP stimulate NSM2 activity, or recruitment of ASM, lysosomes, and NPC1 to the plasma membrane; perhaps we can develop a better understanding of the role of sGP verses surface GP in infection and disease pathology. Additionally, by identifying these GP domains, it may explain the differences in lethality

between the 5 known EBOV species. This information would allow us to further develop our drug treatment strategy.

In conclusion, no effective drugs treatments exist to prevent or treat EBOV infection. Therefore, we sought to identify potential drug targets by applying chemical and genetic inhibitors of sphingomyelinases and NPC1-dependent trafficking in the context of EBOV entry. During this process, we discovered a novel sphingomyelin-sphingomyelinase-NPC1-dependent entry mechanism, which is specific to EBOV GP. We also identified sphingomyelinases and exocytosis as targets for drug treatment therapies. Furthermore, by investigating the related roles of sphingomyelin, sphingomyelinases, and sphingomyelin-trafficking protein, NPC1, in EBOV entry and infection, our work has added to our understanding of EBOV entry, and may possibly lead us to discover even better drug targets than we have proposed here.

CHAPTER 4: METHODS

CELL CULTURE

HeLa (Ambion, Austin, TX), 293HEK (ATCC, Manassas, VA), 293FT (Invitrogen), and Vero E6 (CDC, Atlanta, GA) were grown in DMEM with 10% FBS and 1% penicillin/streptomycin (P/S) at 37^{o} C at 5% CO2. 293FT were subcultured in 0.5 mg/mL G418. Apparently healthy primary human fibroblasts (GM00038), or fibroblasts lacking ASM function (GM0112) or NPC1 function (GM0110), were purchased from the Coriell Cell Repository (Camden, NJ), and cultured in DMEM as per the provided protocol.

REAGENTS

For drug assays, U18666A was purchased from Cayman Chemical (Ann Arbor, MI). Vacuolin-1 was purchased from Calbiochem (Gibbstown, NJ). Desipramine, imipramine, bafilomycin A, and manumycin A were purchased from Sigma (St. Louis, MO). For immunofluorescence assays, lysenin and rabbit anti-lysensin were purchased from Peptides International (Louisville, KY). Goat anti-lamp1 and anti-ASM antibodies were purchased from Santa Cruz Biotechnology (Santa Cruz, CA). Rabbit anti-goat Alexa Flour 594, goat anti-mouse Alexa Flour 594, anti-NPC1 antibody, Cell Mask membrane stain, DAPI, Lipofectamine 2000, Stealth RNAi SMPD1 (HSS143988), and Alamar Blue were purchased from Invitrogen (Carlsbad, CA). NPC1 RNAi was purchased from ThermoScientific Dharmacon (Lafayette, CO). SMPD3, NPC1, and EBOV Zaire Mayinga NP primers were purchased from IDT (Coralville, IA). SMPD1 primers were

purchased from OriGene (Rockville, MD). Flexitube siRNA for SMPD1 and SMPD3 was purchased from Qiagen (Valencia, CA). PEI for large-scale cDNA transfections was purchased from Polysciences, Inc. (Warrington, PA). pEBOV Zaire GP (generous gift from Dr. Paul Bates, University of Pennsylvania), pVP40-GFP (generous gift from Dr. Christopher Basler, Mount Sinai School of Medicine), pVSV-G (BD Biosciences, San Jose, CA), and pVEEV E1 and E3 (from subtype IC strain 3908) were prepared with Qiagen kits and further purified by CsCl gradient centrifugation (Kolokoltsov et al., 2006b; Kolokoltsov et al., 2005). VSV-VSV-Luc was provided by Sean Whelan, Harvard Medical School, Boston, MA. pNef-Luciferase was constructed as previously described (Kolokoltsov and Davey, 2004; Kolokoltsov et al., 2006a). EBOV-GFP was a generous gift from Dr. Stuart Nichol, CDC, Atlanta, GA. mRNA purification was done using an Aurum Total RNA 96 kit (BioRad, Hercules, CA). qRT-PCR was done using iScript One-Step RT-PCR Kit with SYBR Green (BioRad, Hercules, CA).

GENERATION OF NON-INFECTIOUS EBOLA VIRUS-LIKE PARTICLES (EBOVLPS)

To visualize EBOV entry, non-infectious EBOVLPs were generated using GFP-tagged matrix protein, VP40, and EBOV GP (Jasenosky et al., 2001; Johnson et al., 2006; Martinez et al., 2007; Noda et al., 2002; Timmins et al., 2001). 293FT were plated at 70% confluence in ten 10 cm culture dishes 2 to 4 h prior to transfection. To generate EBOVLPs, each 10 cm plate was transfected with 11.5 μg pVP40-GFP and 0.5 μg pEBOV GP using PEI or $CaPO_4$. At 24 h and 48 h post-transfection, EBOVLP-containing supernatant was collected from ten 10 cm plates, and centrifuged at 1,000 rpm for 10 min to remove cell debris. For further purification, EBOVLPs were ultracentrifuged at 25,000 rpm for 3 h through 20% sucrose. EBOVLP pellets

were resuspended in 5 mL PBS- or DMEM (10% FBS, 1% P/S), aliquoted into 200 μl aliquots, and stored at -80^{o} C until ready for use (Figure 41).

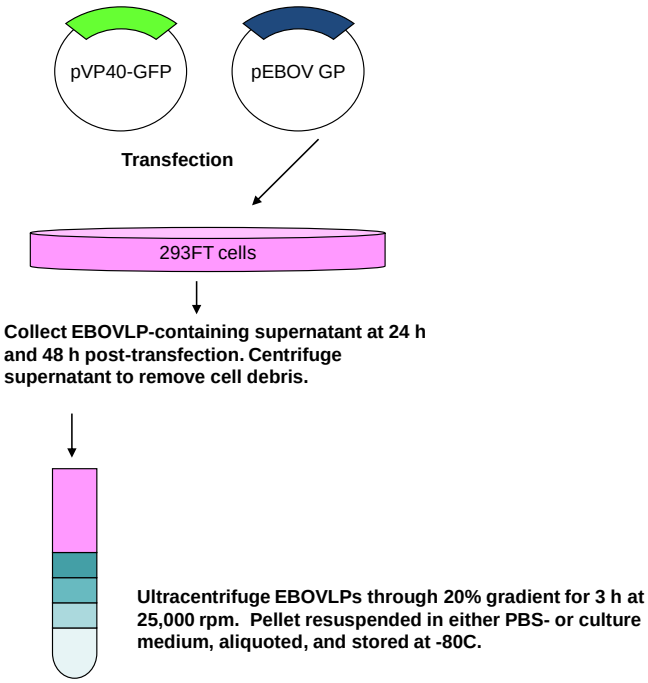

Figure 41. Procedure for generating fluorescently labeled EBOVLPs. Plasmids pVP40-GFP and pEBOV GP are transfected into 293FT cells (top). After 24 h and 48h, the VLP-containing supernatant is collected, and centrifuged to remove cell debris (middle). EBOVLPs are further purified and concentrated via ultracentrifugation (bottom).

GENERATION OF EBOVLP-LUCIFERASE (EBOVLP-LUC)

To measure EBOV fusion via a mixing contents assay, non-infectious EBOVLP-Luc was generated using GFP-tagged matrix protein, VP40; fusion protein, nef-luciferase; and EBOV GP (Saeed et al., 2006; Saeed et al., 2008). 293FT were plated at 90% confluence in five 10 cm culture dishes 2-4 h prior to transfection. To generate EBOVLP-Luc, each 10 cm plate was transfected with 11.5 μg pVP40-GFP, 0.5 μg pEBOV GP, 0.7 μg pNef-Luciferase using PEI, or

a $CaPO_4$ precipitation method At 24 h and 48 h post-transfection, EBOVLP-Luc-containing supernatant was collected from five 10 cm plates, and centrifuged at 1,000 rpm for 10 min to remove cell debris. For further purification, EBOVLP-Luc was ultracentrifuged at 25,000 rpm for 3 h through 20% sucrose. EBOVLP-Luc pellets were resuspended in 2.5 mL PBS- or DMEM (10% FBS, 1% P/S), and used the same day of collection. To confirm luciferase encapsulation into VLPs, an unlysed:lysed ratio was determined by adding 90 μl luciferase buffer to 10 μl concentrated EBOVLP-Luciferase, and immediately measuring counts per second with a luminometer. The unlysed counts were recorded. Next, 10 μl of 1% Triton-X 100 detergent was added to the sample to disrupt the viral envelope and expose the membrane-covered nef-luciferase to the luciferin-containing buffer. The lysed counts were recorded. The number of unlysed counts was divided by the number of lysed counts to determine the unlysed:lysed EBOVLP-Luciferase ratio. EBOVLP-Luc were not used if the unlysed to lysed ratio was less than 1:4 (Figure 42).

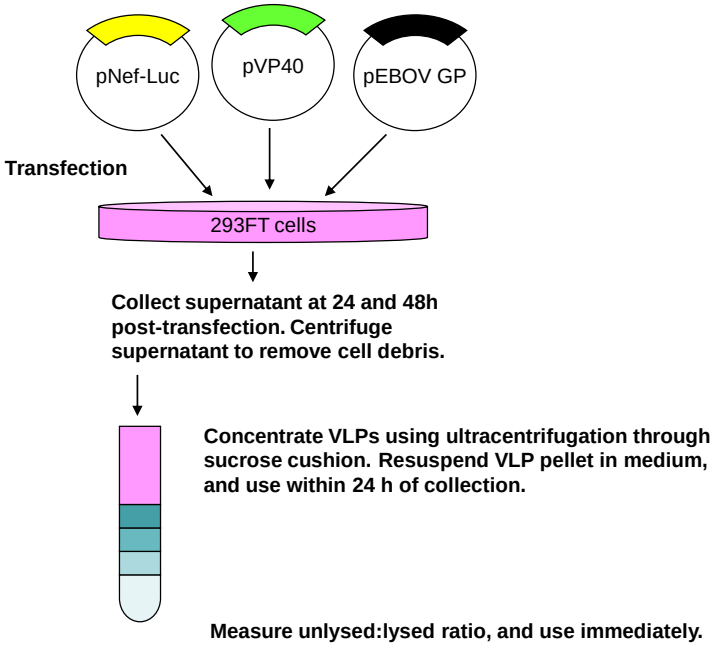

Figure 42. Procedure for generating EBOVLP-Luciferase. This procedure is the same as in Figure 1, for production of VLPs except the plasmid, pNef-luciferase, is added, which encodes firefly luciferase with a C-terminal tag of HIV-nef. The nef tag targets the luciferase to the inner leaflet of the cell membrane, and them into the budding virions.

GENERATION OF EBOV GP-VSV-PSEUDOTYPED VIRUS ENCODING LUCIFERASE (EBOV-VSV-LUC)

To assess EBOV-GP specificity in entry, EBOV pseudotyped virus was generated using a Vesicular Stomatitis Virus (VSV) core virus (Kolokoltsov et al., 2006a; Kolokoltsov et al., 2009; Kolokoltsov et al., 2006b; Kolokoltsov et al., 2005). Since the conformational change of VSV-G is reversible depending on pH, and because VSV-G outcompetes EBOV GP in forming new pseudotyped VSV core virions, it is necessary to first generate a seed stock virus, such as

Venezuelan Equine Encephalitis Virus (VEEV)-VSV-Luc, whose envelope proteins are labile. If EBOV-VSV-Luc is directly generated from VSV-VSV-Luc, significant VSV-VSV-Luc contamination will result. For this reason, we used the VSV core pseudotype bearing the GP of Venezuelan Equine Encephalitis Virus (VEEV). This glycoprotein is labile to pH less than or equal to 5.5, and so can be effectively eliminated during pseudotype formation. To generate the initial seed stock of VEEV-VSV-Luc, 293FT were plated at 70% confluence in ten 10 cm culture dishes 2 to 4 h prior to transfection. Each 10 cm plate was $CaPO_4$-transfected with 10 μg pVEEV E1/E3 and 1 μg pLenti-strawberry (to visualize transfection efficiency). At 36 h post-transfection, transfection efficiency was assessed. If transfection efficiency was at least 70%, 1 mL of VSV-VSV-Luc was added per 10 cm plate at an MOI of 0.1. VSV-VSV-Luc was incubated with pVEEV-transfected cells for 1 h at 37^o C, before cells were rinsed with medium to remove unbound virus. Fresh medium was added to each plate. At 48 h and 72 h pi, VEEV-VSV-Luc was harvested from cell supernatant, passed through a 0.45 μm filter, aliquoted, and stored at -80^o C until use. To generate EBOV-VSV-Luc, each 10 cm plate was $CaPO_4$-transfected with 0.5 μg pEBOV GP, 10 μg pβ-gal (carrier), 1 μg pLenti-strawberry (to visualize transfection efficiency). At 30 h post-transfection, transfection efficiency was determined. If transfection efficiency was 70% or greater, medium was removed, and transfected cells were incubated with 1 mL VEEV-VSV-Luc seed stock (MOI = 1.0) for 1 h. Virus was removed, and cells were rinsed once with DMEM containing citric acid (pH = 5.5), to irreversibly denature the VEEV-E1/E3 on any non-internalized VEEV-VSV-Luc virus. Cells were then incubated with 7 mL DMEM-citric acid per 10 cm plate for 15 min. DMEM-citric acid was removed before cells were rinsed once with DMEM (10% FBS, 1% P/S). Finally, 7 mL DMEM (10% FBS, 1% P/S)

was added per 10 cm plate, and cells were placed in the incubator at 37^{o} C. At 48 h and 72 h post-inoculation, EBOV-VSV-Luc-containing supernatant was harvested, passed through a 0.45 μm filter, divided into 1 mL aliquots, and stored at -80^{o} C until ready for use. Virus titers were determined by inoculating HeLa cells with 2-fold serially diluted virus stock, and then performing a luciferase assay at 8 h post-inoculation. It was determined that for one well of a 96-well plate, 50 μl of concentrated EBOV-VSV-Luc supernatant generated between 5,000 to 25,000 counts per second, depending on the drug or siRNA treatment applied. Using the same method, a Lassa virus (LASV)-VSV-Luc virus stock was also generated by transfecting 293FT with pLASV GP, and then inoculating cells with 1 mL VEEV-VSV-Luc (MOI = 0.1) at 36 h post-transfection (Figure 43).

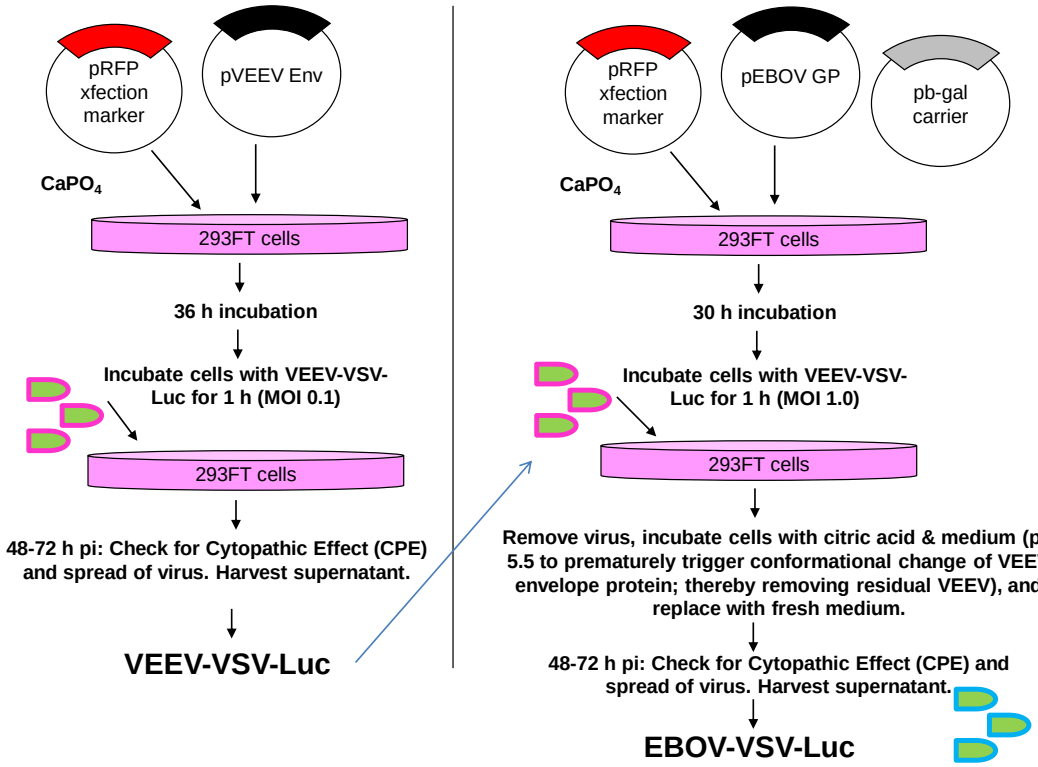

Figure 43. Procedure for generating EBOV-VSV-Luc pseudotyped virus. (Top left) First, to generate VEEV-VSV-Luc seed stock, 293FT cells are tranfected with pLenti-strawberry (transfection efficiency marker) and pVEEV (envelope protein from strain 3908). (Bottom Left) At 36 h post-transfection, cells are incubated with VEEV-VSV-Luc seed stock virus for 1 h at MOI = 0.1. Cells are washed to remove unbound virus. At 48 to 72 h post-inoculation (pi), virus-containing supernatant is collected, passed through a 0.45 μm filter, and stored until use. (Top Right) To generate EBOV-VSV-Luc, 293FT are transfected with pLenti-strawberry, pEBOV GP, and pβ-gal (carrier plasmid). At 30 h post-transfection, cells are incubated with VEEV-VSV-Luc seed stock virus for 1 h, incubated with citric-acid containing medium (to induce rapid pH drop and premature GP activation on unbound virus), and then rinsed with fresh medium. (Bottom Right) At 48 and 72 h pi, virus-containing supernatant is passed through a 0.45 μm filter, aliquoted, and stored at -80^{o} C until use.

siRNA Transfections

HeLa cells were reverse-transfected using Lipofectamine 2000 as per the manufacturer's protocol in either 96-well or 6-well plates. For this, cells were plated into wells containing the

siRNA transfection mixture. In preliminary work, the method was optimized to give greater than 90% suppression of luciferase expression in a cell line stably made to express luciferase. At 24 h post-transfection, cells were visually checked for signs of cytopathic effects (CPE). At 48 h post-transfection, cells were either inoculated with EBOVLPs, EBOV-VSV-Luc, or EBOV-GFP; or lysed for mRNA purification, and subsequent RT-PCR. As a negative control, All Stars siRNA was used since it has no known cellular target. Additionally, Ctbp1 siRNA was used as a positive control since previous work from our lab showed that this siRNA generates up to 90% knockdown of EBOV-GFP infection (Saeed et al., 2010).The siRNA sequences used are shown in Table 2.

Table 2. Sequences of siRNA used in this work.

siRNA name	Vendor	Catalog#	Target Sequence
Hs_SMPD1_1	Qiagen	SI00011557	TGGAATTATTACCGAATTGTA
Hs_SMPD1_2	Qiagen	SI00011564	CTGGTTTAGCTGGATATGGGA
Hs_SMPD1_3	Qiagen	SI00011571	CGGGCTGAAGAAGGAACCCAA
Hs_SMPD1_5	Qiagen	SI03096121	CTGCTGTGGGTAACCATGAAA
SMPD1_6	Invitrogen	SMPD1HSS143988	ACAAAGAGTAGCCAGACGGCAGGGC
Hs_SMPD3_4	Qiagen	SI00727412	AAGAAGGGACTCACAGCATAA
Hs_SMPD3_5	Qiagen	SI03163174	CACGAACGGCCTGTACGATGA
Hs_SMPD3_6	Qiagen	SI04154871	CTCACTCGCCAGGGTCAACAA
Hs_SMPD3_7	Qiagen	SI04299519	CCAGACGGTTCTTCCCTAGAA
NPC1	Dharmacon	MILMK-000001	CCAGGTTCTTGACTTACAATT
Ctbp1_7 (+ control)	Qiagen	SI04301325	CACCGTCAAGCAGATGAGACA
All Stars (- control)	Qiagen	SI1027281	Designed to have no intended target

DRUG TREATMENT AND CYTOTOXICITY ASSAYS

10 mM drug stocks were prepared in either molecular grade water (imipramine and desipramine), or DMSO (U18666A, vacuolin-1, and manumycin A), aliquoted, and stored at -80^{o} C until use. Due to its previously proven potency, a 10 μM stock of bafilomycin A was prepared in DMSO, aliquoted, and stored in -80^{o} C until use. Working drug concentrations were determined by treating cells with 2-fold serially diluted drug stock, starting at 100 μM. Cells were plated at 70% confluence in 96-well plates at least 4 h prior to treatment with drug. Cells were then incubated with serially diluted drugs and 10 μl per well of Alamar Blue cytotoxicity reagent for 24 h. At 24 h, red fluorescence was measured by an Omega plate reader to determine drug toxicity. As an additional measure, during infection assay analysis, cell density was determined for water-treated cells and DMSO-treated verses drug-treated cells using a Nikon T7 fluorescence microscope and Cell Profiler image analysis software (Broad Institute, MIT, Boston, MA). Cell Profiler image analysis software was configured to detect and count cell nuclei. Additionally our lab developed an algorithm enabling the software to measure GFP fluorescence intensity in the cell cytoplasm. Through optimization with several cell types, we determined that GFP expression of at least 18% greater than background was a EBOV-GFP-infected cell. In addition, we further employed the software to count nuclei associated with GFP-expression to determine the infection efficiency in each well of a 96-well plate. If cell density of drug-treated plates was less than 80% of the water- or DMSO-treated control, the drug was considered toxic at that concentration. Effective concentrations, or EC_{50}'s, identify drug concentrations which provide 50% inhibition of EBOV-GFP infection compared to negative control. To determine drug EC_{50}'s, infection efficiency data was fitted to a sigmoidal dose

response curve (with variable slope), and non-linear regression using GraphPad Prism analysis software (version 5.00 for Windows, GraphPad software, San Diego, CA, www.graphpad.com).

INTERNALIZATION ASSAY

For siRNA-treated slides, HeLa cells were Lipofectamine reverse-transfected with non-specific siRNA (All Stars negative control), or siRNA targeting SMPD1 or SMPD3 in 8-well chamber slides 48 h prior to the addition of EBOVLPs. For drug-treated slides, HeLa cells were plated on 8-well chamber slides 4 h prior to the addition of drug. Drug concentrations used were based on 3 to 5 times EC_{50} values, and were previously determined to be non-toxic using an Alamar Blue cytotoxicity assay. Cells were pre-incubated for 1 h with either 25 μM imipramine, 25μM U18666A, 30 μM manumycin A, 1 μM vacuolin-1, DMSO, or culture medium prior to inoculation with EBOVLPs. Chamber slide wells were labeled with time points of either 90, 60, 30, or 15 min. For inoculation, medium was removed from the "90 min" wells, and 100 μl concentrated EBOVLP stock was added per well. After 30 min, "60 min" wells were inoculated. The reverse time course was continued through the 15 min time point. Upon termination, EBOVLPs were removed, and all wells were rinsed with PBS. Cells were fixed with 4% PFA for 10 min at room temperature, and then rinsed 3 times with PBS. Slides were stored at 4^{o} C until prepared for immunofluorescence.

FUSION ASSAY

EBOVLP-Luc unlysed:lysed ratios were determined to be 1:4 or greater prior to initiating the fusion assay to ensure proper function of EBOVLP-Luc. For each drug treatment, one 10 cm plate of confluent cells was resuspended into 1 mL culture medium containing either 20 μM

imipramine or 30 μM manumycin A. Drug concentrations used were based on 3 to 5 times EC_{50} values, and were previously determined to be non-toxic using an Alamar Blue cytotoxicity assay. Cells were then distributed evenly among four 1.7 mL microcentrifuge tubes, generating 4 replicate samples per treatment. As controls, cells were treated with either cell culture medium or DMSO. Cells were pre-incubated with drug for 1 h at 37^{o} C, and rotated continuously to keep cells in suspension. After 1 h, 10 μl of concentrated EBOVLP-Luc was added to each tube of cells with drug. Cells were incubated at 37^{o} C for 3 h, and continuously rotated to ensure optimal interaction between cells and EBOVLP-Luc. At 3 h, each tube of cells was rinsed twice with 1.5 mL PBS, and then centrifuged for 2 min at 800 rpm. PBS was removed, and 90 μl luciferase buffer was added per cell pellet. Cell samples were read immediately, and at 1 min intervals with a luminometer until luciferase activity peaked. Finally, cells and EBOVLP-Luc were lysed with 10 μl of 1% Triton-X 100 detergent. Readings were re-taken to determine the approximate amount of unlysed EBOVLP-Luc in each sample (Saeed et al., 2010). Counts per second were analyzed via student t-test using GraphPad Prism analysis software (version 5.00 for Windows, GraphPad software, San Diego, CA, www.graphpad.com) (Figure 44).

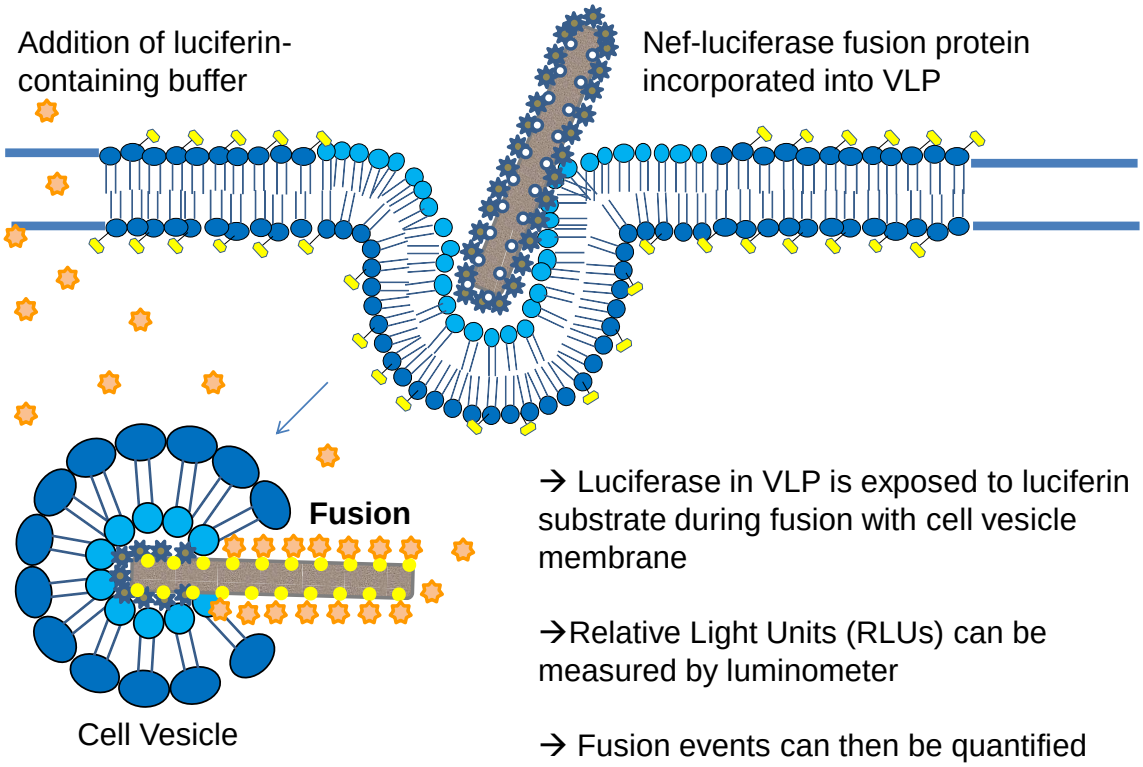

Figure 44. Contents mixing assay. This assay determines the impact of treatments on release of virus contents into the cell cytosol. Because the nef-luciferase fusion protein associates with the inner leaflet of the viral envelope, luciferase cannot interact with its substrate, luciferin, unless the viral envelope fuses with a cellular membrane, exposing the luciferase to the luciferin-containing buffer in the cell cytoplasm. When luciferase encounters luciferin, it generates fluorescence in the form of Relative Light Units (RLUs), which can be measured by a luminometer.

EBOV GP-VSV Core Pseudotyped Virus Luciferase Infection Assay

For siRNA-treated wells, HeLa cells were Lipofectamine reverse-transfected with non-specific siRNA (All Stars negative control), or siRNA targeting SMPD1, SMPD3, and NPC1 in white 96-well luminometer plates 48 h prior to the addition of EBOV-VSV-Luc. For inoculation, medium was removed prior to adding 50 μl concentrated EBOV-VSV-Luc stock and 50 μl

culture medium per well. For drug-treated wells, HeLa cells were plated in white 96-well luminometer plates at 70% confluence 4 h prior to the addition of drug. Cells were pre-incubated for 1 h with either 50 μl 25 μM imipramine, 30 μM manumycin A, 1 μM vacuolin-1, 25 μM U18666A, 25 nM bafilomycin, 25 μM desipramine, DMSO, or culture medium prior to inoculation with EBOV-VSV-Luc. Drug concentrations used were based on 3 to 5 times EC_{50} values, and were previously determined to be non-toxic using an Alamar Blue cytotoxicity assay. For inoculation, medium was removed prior to adding 50 μl concentrated EBOV-VSV-Luc stock and 50 μl 2x concentration of each drug to ensure a 1x concentration of drug with virus. For both siRNA and drug plates, virus was incubated with cells for 8 h at 37^{o} C. At termination, medium was removed, and 100 μl of luciferase buffer was added per well. Cells were gently mixed to ensure optimum luciferase activity, and immediately read by a Veritas plate luminometer. An additional reading of each plate was taken at 1 min to ensure peak luciferase activity had been attained (Kolokoltsov and Davey, 2004). Counts per second were analyzed via one-way ANOVA withTukey post-test using GraphPad Prism statistical analysis software (version 5.00 for Windows, Graphpad Software, San Diego, CA, www.graph.com) (Figure 45).

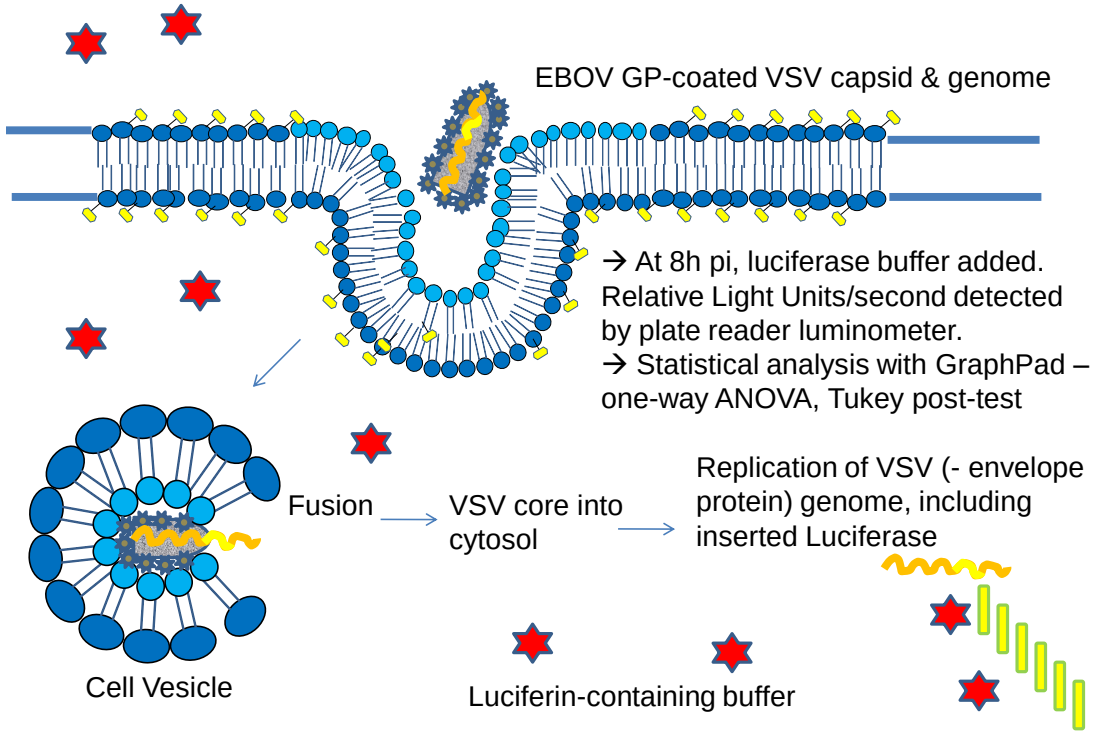

Figure 45. EBOV-VSV-Luciferase infection assay. This assay assesses the specificity of the drug or siRNA treatment against EBOV GP-mediated entry. Because of its VSV core, the virus particle has the bullet-shape of VSV, not the long filamentous structure of EBOV. Because virus morphology may play a role in which entry mechanism is used, all pseudotyped virus assay results must be verified using EBOV-GFP or EBOVLPs which has the same morphology as wildtype virus. Once GP-mediated binding and internalization occur, the virus is trafficked to a cellular compartment, where its envelope fuses with the cell membrane. The VSV core is released into the cytosol, where replication occurs. Because the recombinant VSV genome contains a luciferase gene, it expresses luciferase upon replication. When luciferin-containing buffer is added to cells at 8 h pi, the luciferase-luciferin interaction generates fluorescence, which can be measured by a luminometer. Additionally, the VSV-G gene has been deleted, making the virus replication incompetent.

EBOV-GFP Infection Assay

EBOV-GFP is infectious EBOV-Zaire that was generated by inserting GFP directly into the viral genome without loss of other genes. This virus replicates in cells very similarly to wildtype

virus, but expresses GFP as a marker of infection (Ebihara et al., 2007; Towner et al., 2005). All EBOV-GFP inoculations were conducted in BSL4. For siRNA-treated wells, cells were Lipofectamine reverse-transfected with non-specific siRNA (All Stars negative control), or siRNA targeting SMPD1, SMPD3, and NPC1 in 96-well plates 48h prior to the addition of EBOV-GFP. Ctbp1 siRNA was used as a positive siRNA control since previous work from our lab showed that it inhibited EBOV-GFP infection by greater than 90% (Kolokoltsov and Davey, 2004; Saeed et al., 2010). For inoculation, 1:3 or 1:4 dilutions of stock EBOV-GFP was added per well to generate an MOI of 0.05 to 0.3 (depending on cell type and batch of virus stock). For drug-treated wells, cells were plated at 70% confluence 4 h prior to the addition of drug. Cells were pre-incubated for 1 h with either 100 μl 25 μM imipramine, 30 μM manumycin A, 1 μM vacuolin-1, 25 μM U18666A, 25 nM bafilomycin, 25 μM desipramine, DMSO, or culture medium prior to inoculation with EBOV-GFP. Drug concentrations used were based on 3 to 5 times EC_{50} values, and were previously determined to be non-toxic using an Alamar Blue cytotoxicity assay. For inoculation, concentrated EBOV-GFP stock was added to each well to generate an MOI between 0.05 and 0.3 (depending on cell type and batch of virus stock). For both siRNA and drug plates, virus was incubated with cells for 24 h at 37^{o} C to allow for at least one round of viral replication and optimal GFP expression. At termination, plates were submerged in 10% formalin for more than 24 h. Upon return to BSL2, samples were rinsed 3 times with PBS, and stained with 100 μl of 20 mg/mL DAPI diluted 1:50,000. Plates were then imaged using a Nikon T7 fluorescence microscope using a 16-bit camera and a 10x objective lens. For each well of a 96-well plate, 9 images were taken first of DAPI-, and then of GFP-expressing cells. NIS Elements ND2 images were then converted to .tif files, and processed

using Cell Profiler image analysis software (Broad Institute, MIT, Boston, MA). Cell Profiler image analysis software was originally configured to detect and count cell nuclei; however, our lab developed an algorithm enabling the software to measure GFP fluorescence intensity in the cell cytoplasm. Through optimization with several cell types, we determined that GFP expression of at least 18% greater than background was an EBOV-GFP-infected cell. In addition, we further employed the software to count nuclei associated with GFP-expression to determine the infection efficiency in each well of a 96-well plate. Percent infection data was then analyzed via one-way ANOVA with Tukey post-test using GraphPad Prism statistical analysis software (version 5.00 for Windows, GraphPad Software, San Diego, CA, www.graphpad.com) (Figure 46).

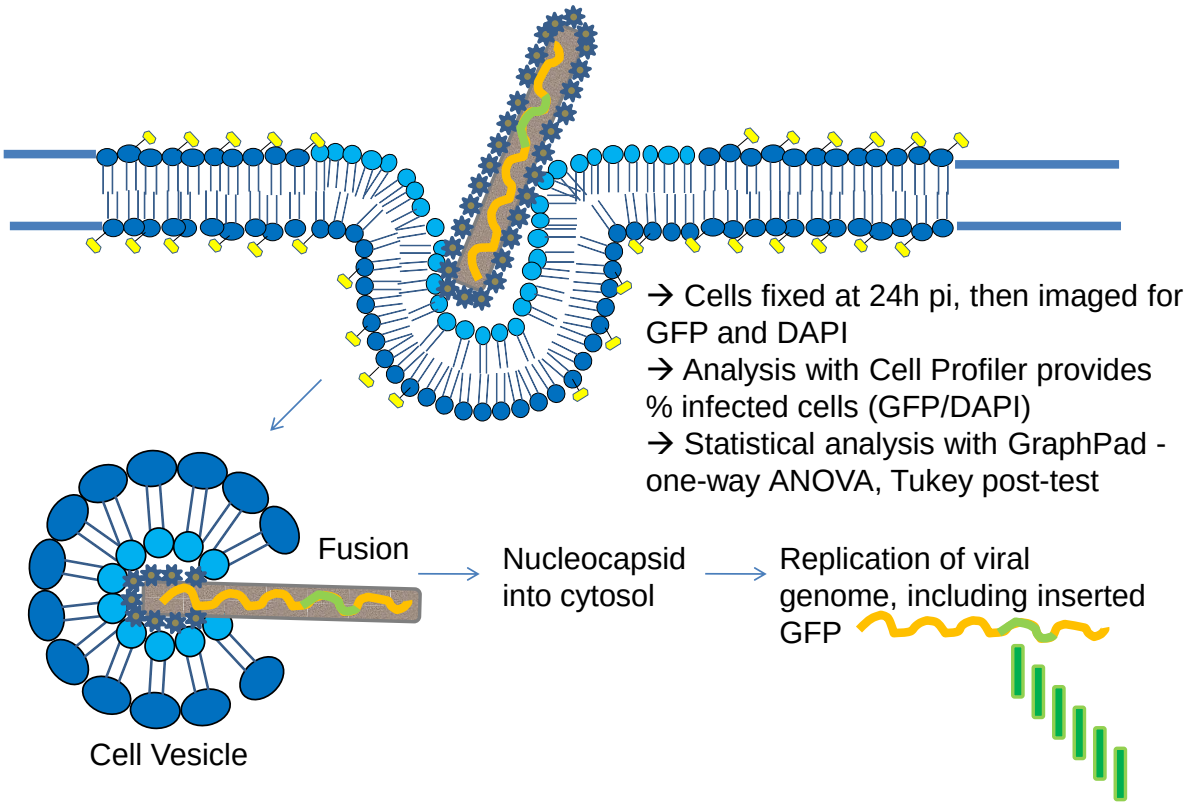

Figure 46. EBOV-GFP infection assay. EBOV-GFP is recombinant EBOV-Zaire with GFP inserted into the viral genome. Its replication is similar to wildtype EBOV, but additionally expresses GFP during viral replication, allowing for visual detection of viral infection. Cells are plated in 96-well plates, and incubated with virus in BSL4 for 24 h. At termination, cells are submerged in 10% formalin for at least 24 h, and then stained with DAPI prior to imaging with an immunofluorescent microscope. Images are then processed using Cell Profiler image analysis software to determine infection efficiency of each well of the 96-well plate as a function of GFP-expressing cells to DAPI-expressing cells. infection efficiency data is then entered into GraphPad analysis software, where a one-way ANOVA with Tukey post-test is performed. For drug assays, EC_{50}'s are determined by fitting infection efficiency data to a sigmoidal dose-response curve (with variable slope) and nonlinear regression using the same software.

RT-PCR

For determining drug inhibition of viral replication, HeLa cells were plated at 70% confluence 4 h prior to the addition of drug. Cells were pre-incubated for 1 h in BSL2 with either 25 μM

imipramine, 30 μM manumycin A, 1 μM vacuolin-1, 25 μM U18666A, 25 μM desipramine, DMSO, or culture medium prior to inoculation with EBOV-GFP. Drug concentrations used were based on 3 to 5 times EC_{50} values, and were previously determined to be non-toxic using an Alamar Blue cytotoxicity assay. For inoculation in BSL4, concentrated EBOV-GFP stock was added to each well to generate an MOI of 0.3. Virus was incubated with cells for 24 h at 37^{o} C to allow for at least one round of viral replication and optimal EBOV NP expression. At termination, 1 mL per well of BioRad cell lysis buffer was added per well. Samples were then transferred to a 96-deep well plate and stored for 24 h at 4^{o} C in BSL4. Once in BSL2, cells were placed in -80^{o} C until mRNA purification. RNA purification was done using the BioRad Aurum Total RNA 96 kit as per the published protocol. qRT-PCR was done using a iScript One-Step RT-PCR Kit with SYBR Green, and the primers listed in Table 3. An annealing temperature of 59^{o} C was used. Changes in cycle thresholds, or ΔCt, were determined by comparing the Ct for treated and untreated samples using virus and GAPDH or actin specific primer sets. ΔΔCt values were calculated by normalizing ΔCt values for the virus probe signal to that of GAPDH or actin probe signal. This compensates for differences in mRNA recovery or changes in cellular mRNA levels due to each treatment. ΔΔCt and fold change in expression values were determined using BioRad CFX software (version 1.6). Expression and SEM expression values were further analyzed by GraphPad analytical software to assess statistical significance ($p<0.05$).

For determining fold changes in ASM or NSM2 mRNA expression, HeLa cells were reverse-transfected in 6-well plates using Lipofectamine 2000 and Qiagen Flexitube siRNA (target sequences listed in Table 2). At 48h post-transfection, cells were rinsed once with PBS, then lysed with 1mL per well of BioRad cell lysis buffer. mRNA was purified via the BioRad

Aurum Total RNA kit. qRT-PCR was conducted using an iScript One-Step RT-PCR Kit with SYBR Green and the primer sequences shown in Table 3. Changes in cycle thresholds, or ΔCt, were determined by comparing the Ct for treated and untreated samples using virus and GAPDH or actin specific primer sets. ΔΔCt values were calculated by normalizing ΔCt values for either SMPD1 (ASM), SMPD3 (NSM2), or NPC1 probe signal to that of GAPDH or actin probe signal. This compensates for differences in mRNA recovery or changes in cellular mRNA levels due to each treatment. ΔΔCt and fold change in expression values were determined using BioRad CFX software (version 1.6). Expression and SEM expression values were further analyzed by GraphPad analytical software to assess statistical significance ($p<0.05$).

Table 3. Primer pairs used for qRT-PCR analysis of gene expression, and virus genome replication.

GENE	GENE ID#	PRIMER SEQUENCE FORWARD (5' → 3')	PRIMER SEQUENCE REVERSE (5' → 3')	SOURCE
SMPD1 (ASM)	**NM_000543**	GCTGGCTCTATGAAGCGATGGC	AGAGCCAGAAGTTCTCACGGGA	OriGene, HP200515
SMPD3 (NSM2)	**NM_018667**	AGGACTGGCTGGCTGATTTC	TGTCGTCAGAGGAGCAGTTATC	Dr. Hannun, MUSC, SC
NPC1	**NM_000271**	TCTCTTTGCGGGATTGGCAGTC	CGCTTGTTCCATCTTCAGCACC	OriGene, HP200253
EBOV Zaire Mayinga NP	**911830**	AGCGTGATGGAGTGAAGCGCC	TCCGGCATGGCAGCAAGTGT	IDT

IMMUNOFLUORESCENCE ASSAY

For immunofluorescence assays, one antibody was applied per sample to avoid possible cross-reactivity with additional antibodies, and to prevent bleed through from far red channels into Texas red channels. For staining with anti-LAMP1 and anti-ASM, separate wells of fixed, unpermeabilized HeLa cells were incubated with 10% rabbit serum for 1 h, prior to overnight (at 4^{o} C) incubation with either 1:50 goat anti-Lamp1 or 1:50 goat anti-ASM in 2% serum. Cells were rinsed 3 times with PBS, and then incubated with 1:200 rabbit anti-goat Alexa Fluor 594 for 1 h in 2% serum. Cells were again rinsed 3 times before being stained with 200 μl of 20 mg/mL DAPI diluted 1:50,000. For staining with mouse anti-NPC1, separate wells of fixed HeLa cells were treated identically as anti-Lamp1 and anti-ASM antibodies, except goat serum and goat anti-mouse Alexa Fluor 594 were used. For sphingomyelin staining, separate wells of fixed, unpermeabilized HeLa cells were incubated with 2% BSA for 15min, and then incubated with 1:50 lysenin (toxin which specifically binds clustered sphingomyelin) for 2 h. Cells were rinsed 3 times in PBS, before being incubated with 1:1000 anti-lysenin for 1 h. Cells were again rinsed 3 times with PBS, and then incubated with 1:200 goat anti-rabbit Alexa Fluor 594 for 1 h. Cells were then rinsed 3 times before being stained with 200 μl of 20 mg/mL DAPI diluted 1:50,000. Cells were imaged using a T7 Nikon immunofluorescence microscope, NIS Elements (Nikon Instruments, Inc., Melville, NY) imaging software, and a 16-bit camera. Using an oil 100x objective lens, z-stacks were taken at 0.300 μm slices for each fluorophore. NIS Elements ND2 images were then processed using Autoquant deconvolution software (version 2.2.0) (Media Cybernetics, Bethesda, MD). The deconvolution software removes light dispersion artifacts due to convolution of fluorescence emissions. It works by identifying the most intense

pixels as the primary object, and then removing areas of decreasing fluorescence which radiate from it.

CELL PROFILER IMAGE ANALYSIS

For determining infection efficiency for 96-well drug and siRNA infection assays, plates were imaged using an automated Nikon T7 immunofluorescence microscope, NIS Elements imaging software (Nikon Instruments, Inc., Melville, NY), and 16-bit camera. The objective lens was set at 10x. Prior to automated imaging, the system was manually calibrated to ensure DAPI and GFP exposure times were set to minimize background and to prevent saturation of the detector. For each well of a 96-well plate, 9 images of DAPI-expressing cells were taken to determine the number of cells per well. Next, 9 images of the same cell population were taken using a GFP filter, to determine the number of cells infected with GFP-expressing EBOV. The NIS Elements ND2 image files were then converted to .tif files, and analyzed using Cell Profiler image analysis software (Broad Institute, MIT, Boston, MA). We developed an algorithm to identify and count all cell nuclei and associated GFP fluorescence (Figure 47). For optimization, Cell Profiler software was previously set to identify DAPI or GFP fluorescence intensity which is 18% above background. This threshold allows optimal differentiation between infected and non-infected cells. The DAPI and GFP images for each well of the 96-well plate were imaged as a pair. First, cell nuclei (DAPI-expressing cells), were identified as primary objects only if their fluorescence intensity was 18% or greater than background, and they were 4 to 20 pixels in diameter. Next, infected cells (GFP-expressing cells) were identified as secondary objects only if they were within 2 pixels of a previously identified nucleus, and had a fluorescence intensity of at least 18% higher than background. After setting the selection criteria for primary and secondary

objects, a "pipeline" was generated to allow these same parameters to be re-applied or adapted to other cells samples (Figure 48). Once the Cell Profiler image software counted all DAPI and GFP-expressing cells per well of a 96-well plate, % infectivity per well was calculated by dividing the number of GFP-expressing cells by the number of DAPI-expressing cells. Percent infection was further analyzed via a one-way ANOVA with Tukey post-test using GraphPad Prism analytical software (version 5.00 for Windows, GraphPad Software, San Diego, CA, www.graphpad.com). P values < 0.05 compared to negative controls were considered significant.

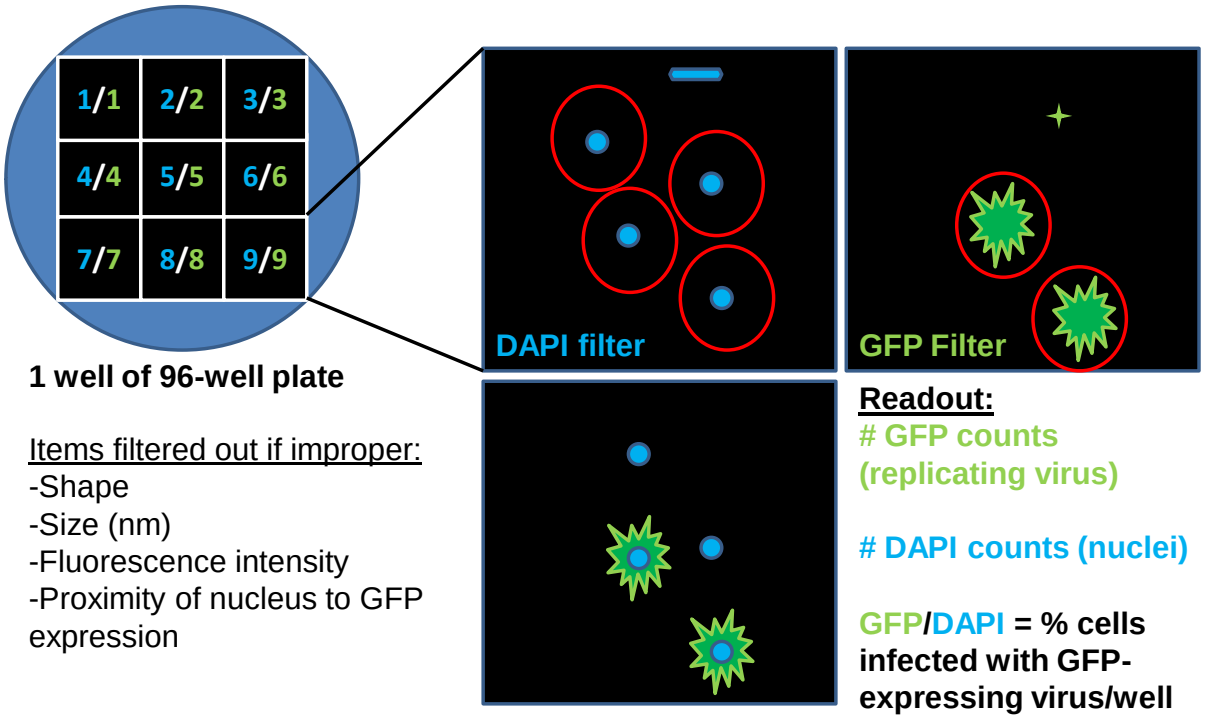

Figure 47. Determination of infection efficiency using Cell Profiler image analysis software. 96-well plates with either drug or siRNA treatment were incubated with EBOV-GFP for 24 h,

and then fixed. Cells were then stained with 100 µl per well of 20 mg/mL DAPI diluted 1:50,000. For each well of a 96-well, 9 DAPI images and 9 GFP images were taken, using a T7 Nikon immunofluorescent microscope with 10x objective lens, NIS Elements software, and 16-bit camera. To identify cell nuclei, objects must meet specific shape, size and fluorescence intensity thresholds. To identify EBOV-GFP infected cells, objects must fall within set shape, size, and fluorescence intensity thresholds, in addition to being associated with a cell nucleus. NIS Elements ND2 images were converted to tif images, and processed using Cell Profiler image analysis software. To determine the infection efficiency per well, the number of DAPI-expressing cells with associated GFP-expression were compared to cells only expressing DAPI.

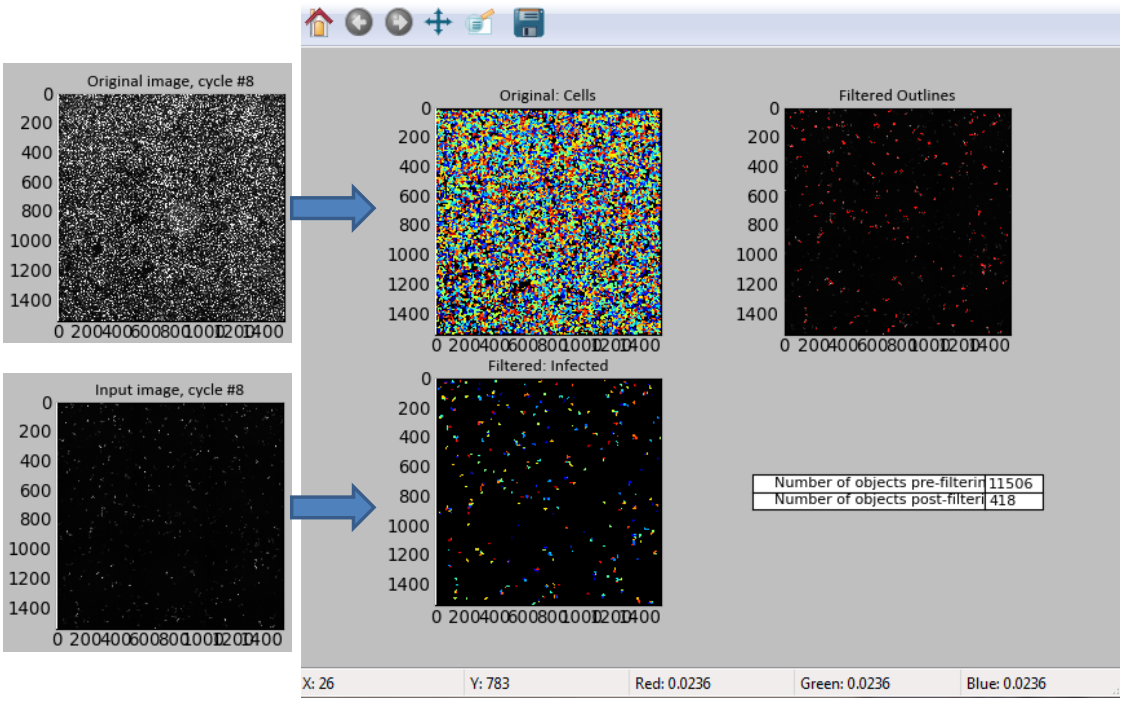

Figure 48. Screen view of Cell Profiler image software identifying cell nuclei and GFP-expressing cells. (Left) Software counting nuclei based on shape, size, and fluorescence intensity. (Center Top) Software showing nuclei, or "Cells," meeting criteria. (Left) Software identifying EBOV-GFP infected cells based on shape, size, fluorescence intensity, and proximity to nuclei. (Center Bottom) Objects meeting the "Infected" criteria are highlighted. (Right Bottom) The table shows the number of cell nuclei as "11,506" and number of EBOV-GFP-infected cells as "418." By dividing 11,506 by 418, the percent infection for this well is 3.6%.

REFERENCES

WHO. (1992). Viral haemorrhagic fever in imported monkeys. Wkly Epidemiol Rec *67*, 142-143.

WHO. (2007a). Outbreak news. Ebola virus haemorrhagic fever, Democratic Republic of the Congo. Wkly Epidemiol Rec *82*, 329.

WHO. (2007b). Outbreak news. Ebola virus haemorrhagic fever, Democratic Republic of the Congo--update. Wkly Epidemiol Rec *82*, 345-346.

Alvarez, C.P., Lasala, F., Carrillo, J., Muniz, O., Corbi, A.L., and Delgado, R. (2002). C-type lectins DC-SIGN and L-SIGN mediate cellular entry by Ebola virus in cis and in trans. J Virol *76*, 6841-6844.

Andrei, G., and De Clercq, E. (1993). Molecular approaches for the treatment of hemorrhagic fever virus infections. Antiviral Res *22*, 45-75.

Arenz, C. (2010). Small molecule inhibitors of acid sphingomyelinase. Cell Physiol Biochem *26*, 1-8.

Arenz, C., Thutewohl, M., Block, O., Waldmann, H., Altenbach, H.J., and Giannis, A. (2001). Manumycin A and its analogues are irreversible inhibitors of neutral sphingomyelinase. Chembiochem *2*, 141-143.

Avota, E., Gassert, E., and Schneider-Schaulies, S. (2010). Measles virus-induced immunosuppression: from effectors to mechanisms. Med Microbiol Immunol *199*, 227-237.

Avota, E., Gulbins, E., and Schneider-Schaulies, S. (2011). DC-SIGN mediated sphingomyelinase-activation and ceramide generation is essential for enhancement of viral uptake in dendritic cells. PLoS Pathog *7*, e1001290.

Avota, E., Muller, N., Klett, M., and Schneider-Schaulies, S. (2004). Measles virus interacts with and alters signal transduction in T-cell lipid rafts. J Virol *78*, 9552-9559.

Ayala, B.P., Vasquez, B., Clary, S., Tainer, J.A., Rodland, K., and So, M. (2001). The pilus-induced Ca2+ flux triggers lysosome exocytosis and increases the amount of Lamp1 accessible to Neisseria IgA1 protease. Cell Microbiol *3*, 265-275.

Ayala, P., Vasquez, B., Wetzler, L., and So, M. (2002). Neisseria gonorrhoeae porin P1.B induces endosome exocytosis and a redistribution of Lamp1 to the plasma membrane. Infect Immun *70*, 5965-5971.

Babiychuk, E.B., Monastyrskaya, K., Potez, S., and Draeger, A. (2011). Blebbing confers resistance against cell lysis. Cell death and differentiation *18*, 80-89.

Baize, S., Leroy, E.M., Georges-Courbot, M.C., Capron, M., Lansoud-Soukate, J., Debre, P., Fisher-Hoch, S.P., McCormick, J.B., and Georges, A.J. (1999). Defective humoral responses and extensive intravascular apoptosis are associated with fatal outcome in Ebola virus-infected patients. Nat Med *5*, 423-426.

Bao, J.X., Jin, S., Zhang, F., Wang, Z.C., Li, N., and Li, P.L. (2010a). Activation of membrane NADPH oxidase associated with lysosome-targeted acid sphingomyelinase in coronary endothelial cells. Antioxid Redox Signal *12*, 703-712.

Bao, J.X., Xia, M., Poklis, J.L., Han, W.Q., Brimson, C., and Li, P.L. (2010b). Triggering role of acid sphingomyelinase in endothelial lysosome-membrane fusion and dysfunction in coronary arteries. Am J Physiol Heart Circ Physiol *298*, H992-H1002.

Barenholz, Y. (2004). Sphingomyelin and cholesterol: from membrane biophysics and rafts to potential medical applications. Subcell Biochem *37*, 167-215.

Baron, R.C., McCormick, J.B., and Zubeir, O.A. (1983). Ebola virus disease in southern Sudan: hospital dissemination and intrafamilial spread. Bull World Health Organ *61*, 997-1003.

Barrette, R.W., Metwally, S.A., Rowland, J.M., Xu, L., Zaki, S.R., Nichol, S.T., Rollin, P.E., Towner, J.S., Shieh, W.J., Batten, B., *et al.* (2009). Discovery of swine as a host for the Reston ebolavirus. Science *325*, 204-206.

Bartke, N., and Hannun, Y.A. (2009). Bioactive sphingolipids: metabolism and function. J Lipid Res *50 Suppl*, S91-96.

Bausch, D.G., Towner, J.S., Dowell, S.F., Kaducu, F., Lukwiya, M., Sanchez, A., Nichol, S.T., Ksiazek, T.G., and Rollin, P.E. (2007). Assessment of the risk of Ebola virus transmission from bodily fluids and fomites. J Infect Dis *196 Suppl 2*, S142-147.

Bavari, S., Bosio, C.M., Wiegand, E., Ruthel, G., Will, A.B., Geisbert, T.W., Hevey, M., Schmaljohn, C., Schmaljohn, A., and Aman, M.J. (2002). Lipid raft microdomains: a gateway for compartmentalized trafficking of Ebola and Marburg viruses. J Exp Med *195*, 593-602.

Becker, S., Spiess, M., and Klenk, H.D. (1995). The asialoglycoprotein receptor is a potential liver-specific receptor for Marburg virus. J Gen Virol *76 (Pt 2)*, 393-399.

Bhattacharyya, S., Warfield, K.L., Ruthel, G., Bavari, S., Aman, M.J., and Hope, T.J. (2010). Ebola virus uses clathrin-mediated endocytosis as an entry pathway. Virology *401*, 18-28.

Bollinger, C.R., Teichgraber, V., and Gulbins, E. (2005). Ceramide-enriched membrane domains. Biochim Biophys Acta *1746*, 284-294.

Bosio, C.M., Aman, M.J., Grogan, C., Hogan, R., Ruthel, G., Negley, D., Mohamadzadeh, M., Bavari, S., and Schmaljohn, A. (2003). Ebola and Marburg viruses replicate in monocyte-derived dendritic cells without inducing the production of cytokines and full maturation. J Infect Dis *188*, 1630-1638.

Bosio, C.M., Moore, B.D., Warfield, K.L., Ruthel, G., Mohamadzadeh, M., Aman, M.J., and Bavari, S. (2004). Ebola and Marburg virus-like particles activate human myeloid dendritic cells. Virology *326*, 280-287.

Bowen, E.T., Lloyd, G., Harris, W.J., Platt, G.S., Baskerville, A., and Vella, E.E. (1977). Viral haemorrhagic fever in southern Sudan and northern Zaire. Preliminary studies on the aetiological agent. Lancet *1*, 571-573.

Bowen, E.T., Platt, G.S., Lloyd, G., Raymond, R.T., and Simpson, D.I. (1980). A comparative study of strains of Ebola virus isolated from southern Sudan and northern Zaire in 1976. J Med Virol *6*, 129-138.

Bradfute, S.B., Warfield, K.L., and Bavari, S. (2008). Functional CD8+ T cell responses in lethal Ebola virus infection. J Immunol *180*, 4058-4066.

Bray, M., and Geisbert, T.W. (2005). Ebola virus: the role of macrophages and dendritic cells in the pathogenesis of Ebola hemorrhagic fever. Int J Biochem Cell Biol *37*, 1560-1566.

Brindley, M.A., Hughes, L., Ruiz, A., McCray, P.B., Jr., Sanchez, A., Sanders, D.A., and Maury, W. (2007). Ebola virus glycoprotein 1: identification of residues important for binding and postbinding events. J Virol *81*, 7702-7709.

Bukreyev, A.A., Dinapoli, J.M., Yang, L., Murphy, B.R., and Collins, P.L. (2010). Mucosal parainfluenza virus-vectored vaccine against Ebola virus replicates in the respiratory tract of vector-immune monkeys and is immunogenic. Virology *399*, 290-298.

Burow, M.E., Weldon, C.B., Collins-Burow, B.M., Ramsey, N., McKee, A., Klippel, A., McLachlan, J.A., Clejan, S., and Beckman, B.S. (2000). Cross-talk between phosphatidylinositol 3-kinase and sphingomyelinase pathways as a mechanism for cell survival/death decisions. J Biol Chem *275*, 9628-9635.

Bwaka, M.A., Bonnet, M.J., Calain, P., Colebunders, R., De Roo, A., Guimard, Y., Katwiki, K.R., Kibadi, K., Kipasa, M.A., Kuvula, K.J., *et al.* (1999). Ebola hemorrhagic fever in Kikwit, Democratic Republic of the Congo: clinical observations in 103 patients. J Infect Dis *179 Suppl 1*, S1-7.

Cameron, C.E., and Castro, C. (2001). The mechanism of action of ribavirin: lethal mutagenesis of RNA virus genomes mediated by the viral RNA-dependent RNA polymerase. Curr Opin Infect Dis *14*, 757-764.

Canonico, P.G., Kende, M., Luscri, B.J., and Huggins, J.W. (1984). In-vivo activity of antivirals against exotic RNA viral infections. J Antimicrob Chemother *14 Suppl A*, 27-41.

Cavallo-Medved, D., and Sloane, B.F. (2003). Cell-surface cathepsin B: understanding its functional significance. Curr Top Dev Biol *54*, 313-341.

Cerny, J., Feng, Y., Yu, A., Miyake, K., Borgonovo, B., Klumperman, J., Meldolesi, J., McNeil, P.L., and Kirchhausen, T. (2004). The small chemical vacuolin-1 inhibits Ca(2+)-dependent lysosomal exocytosis but not cell resealing. EMBO Rep *5*, 883-888.

Chan, S.Y., Empig, C.J., Welte, F.J., Speck, R.F., Schmaljohn, A., Kreisberg, J.F., and Goldsmith, M.A. (2001). Folate receptor-alpha is a cofactor for cellular entry by Marburg and Ebola viruses. Cell *106*, 117-126.

Chandran, K., Sullivan, N.J., Felbor, U., Whelan, S.P., and Cunningham, J.M. (2005). Endosomal proteolysis of the Ebola virus glycoprotein is necessary for infection. Science (New York, NY *308*, 1643-1645.

Clarke, C.J., and Hannun, Y.A. (2006). Neutral sphingomyelinases and nSMase2: bridging the gaps. Biochimica et biophysica acta *1758*, 1893-1901.

Claus, R.A., Dorer, M.J., Bunck, A.C., and Deigner, H.P. (2009). Inhibition of sphingomyelin hydrolysis: targeting the lipid mediator ceramide as a key regulator of cellular fate. Curr Med Chem *16*, 1978-2000.

Cox, N.J., McCormick, J.B., Johnson, K.M., and Kiley, M.P. (1983). Evidence for two subtypes of Ebola virus based on oligonucleotide mapping of RNA. J Infect Dis *147*, 272-275.

Cremesti, A.E., Goni, F.M., and Kolesnick, R. (2002). Role of sphingomyelinase and ceramide in modulating rafts: do biophysical properties determine biologic outcome? FEBS letters *531*, 47-53.

Crotty, S., and Andino, R. (2002). Implications of high RNA virus mutation rates: lethal mutagenesis and the antiviral drug ribavirin. Microbes Infect *4*, 1301-1307.

Czarny, M., Liu, J., Oh, P., and Schnitzer, J.E. (2003). Transient mechanoactivation of neutral sphingomyelinase in caveolae to generate ceramide. J Biol Chem *278*, 4424-4430.

de Witte, L., Abt, M., Schneider-Schaulies, S., van Kooyk, Y., and Geijtenbeek, T.B. (2006). Measles virus targets DC-SIGN to enhance dendritic cell infection. J Virol *80*, 3477-3486.

Divangahi, M., Chen, M., Gan, H., Desjardins, D., Hickman, T.T., Lee, D.M., Fortune, S., Behar, S.M., and Remold, H.G. (2009). Mycobacterium tuberculosis evades macrophage defenses by inhibiting plasma membrane repair. Nat Immunol *10*, 899-906.

Dolnik, O., Kolesnikova, L., and Becker, S. (2008). Filoviruses: Interactions with the host cell. Cell Mol Life Sci *65*, 756-776.

Dowell, S.F., Mukunu, R., Ksiazek, T.G., Khan, A.S., Rollin, P.E., and Peters, C.J. (1999). Transmission of Ebola hemorrhagic fever: a study of risk factors in family members, Kikwit, Democratic Republic of the Congo, 1995. Commission de Lutte contre les Epidemies a Kikwit. J Infect Dis *179 Suppl 1*, S87-91.

Dreschers, S., Franz, P., Dumitru, C., Wilker, B., Jahnke, K., and Gulbins, E. (2007). Infections with human rhinovirus induce the formation of distinct functional membrane domains. Cell Physiol Biochem *20*, 241-254.

Dube, D., Schornberg, K.L., Shoemaker, C.J., Delos, S.E., Stantchev, T.S., Clouse, K.A., Broder, C.C., and White, J.M. (2010). Cell adhesion-dependent membrane trafficking of a binding partner for the ebolavirus glycoprotein is a determinant of viral entry. Proc Natl Acad Sci U S A *107*, 16637-16642.

Ebihara, H., Theriault, S., Neumann, G., Alimonti, J.B., Geisbert, J.B., Hensley, L.E., Groseth, A., Jones, S.M., Geisbert, T.W., Kawaoka, Y., *et al.* (2007). In vitro and in vivo characterization of recombinant Ebola viruses expressing enhanced green fluorescent protein. J Infect Dis *196 Suppl 2*, S313-322.

Empig, C.J., and Goldsmith, M.A. (2002). Association of the caveola vesicular system with cellular entry by filoviruses. J Virol *76*, 5266-5270.

Falcone, S., Cocucci, E., Podini, P., Kirchhausen, T., Clementi, E., and Meldolesi, J. (2006). Macropinocytosis: regulated coordination of endocytic and exocytic membrane traffic events. J Cell Sci *119*, 4758-4769.

Falcone, S., Perrotta, C., De Palma, C., Pisconti, A., Sciorati, C., Capobianco, A., Rovere-Querini, P., Manfredi, A.A., and Clementi, E. (2004). Activation of acid sphingomyelinase and its inhibition by the nitric oxide/cyclic guanosine 3',5'-monophosphate pathway: key events in Escherichia coli-elicited apoptosis of dendritic cells. J Immunol *173*, 4452-4463.

Falzarano, D., Krokhin, O., Wahl-Jensen, V., Seebach, J., Wolf, K., Schnittler, H.J., and Feldmann, H. (2006). Structure-function analysis of the soluble glycoprotein, sGP, of Ebola virus. Chembiochem *7*, 1605-1611.

Feldmann, H., and Geisbert, T.W. (2010). Ebola haemorrhagic fever. Lancet *377*, 849-862

Ferlinz, K., Hurwitz, R., Vielhaber, G., Suzuki, K., and Sandhoff, K. (1994). Occurrence of two molecular forms of human acid sphingomyelinase. Biochem J *301 (Pt 3)*, 855-862.

Fernandes, M.C., Cortez, M., Flannery, A.R., Tam, C., Mortara, R.A., and Andrews, N.W. (2011). Trypanosoma cruzi subverts the sphingomyelinase-mediated plasma membrane repair pathway for cell invasion. J Exp Med *208*, 909-921.

Filosto, S., Fry, W., Knowlton, A.A., and Goldkorn, T. (2010). Neutral sphingomyelinase 2 (nSMase2) is a phosphoprotein regulated by calcineurin (PP2B). J Biol Chem *285*, 10213-10222.

Frecha, C., Levy, C., Costa, C., Negre, D., Amirache, F., Buckland, R., Russell, S.J., Cosset, F.L., and Verhoeyen, E. (2011). Measles Virus Glycoprotein-Pseudotyped Lentiviral Vector-Mediated Gene Transfer into Quiescent Lymphocytes Requires Binding to both SLAM and CD46 Entry Receptors. J Virol *85*, 5975-5985.

Ganley, I.G., and Pfeffer, S.R. (2006). Cholesterol accumulation sequesters Rab9 and disrupts late endosome function in NPC1-deficient cells. J Biol Chem *281*, 17890-17899.

Gaspar, E.B., Mortara, R.A., Andrade, L.O., and da Silva, C.V. (2009). Lysosomal exocytosis: an important event during invasion of lamp deficient cells by extracellular amastigotes of Trypanosoma cruzi. Biochem Biophys Res Commun *384*, 265-269.

Gassert, E., Avota, E., Harms, H., Krohne, G., Gulbins, E., and Schneider-Schaulies, S. (2009). Induction of membrane ceramides: a novel strategy to interfere with T lymphocyte cytoskeletal reorganisation in viral immunosuppression. PLoS Pathog *5*, e1000623.

Gear, J.S., Cassel, G.A., Gear, A.J., Trappler, B., Clausen, L., Meyers, A.M., Kew, M.C., Bothwell, T.H., Sher, R., Miller, G.B., *et al.* (1975). Outbreake of Marburg virus disease in Johannesburg. Br Med J *4*, 489-493.

Geisbert, T.W., Hensley, L.E., Jahrling, P.B., Larsen, T., Geisbert, J.B., Paragas, J., Young, H.A., Fredeking, T.M., Rote, W.E., and Vlasuk, G.P. (2003a). Treatment of Ebola virus infection with a recombinant inhibitor of factor VIIa/tissue factor: a study in rhesus monkeys. Lancet *362*, 1953-1958.

Geisbert, T.W., Hensley, L.E., Larsen, T., Young, H.A., Reed, D.S., Geisbert, J.B., Scott, D.P., Kagan, E., Jahrling, P.B., and Davis, K.J. (2003b). Pathogenesis of Ebola hemorrhagic fever in cynomolgus macaques: evidence that dendritic cells are early and sustained targets of infection. Am J Pathol *163*, 2347-2370.

Geisbert, T.W., Young, H.A., Jahrling, P.B., Davis, K.J., Larsen, T., Kagan, E., and Hensley, L.E. (2003c). Pathogenesis of Ebola hemorrhagic fever in primate models: evidence that hemorrhage is not a direct effect of virus-induced cytolysis of endothelial cells. Am J Pathol *163*, 2371-2382.

Gene, O.G., Julia, B.E., Vanessa, M.R., Victoria, W.J., Thomas, G.W., and Lisa, H.E. (2009). Drug targets in infections with Ebola and Marburg viruses. Infect Disord Drug Targets *9*, 191-200.

Georges-Courbot, M.C., Lu, C.Y., Lansoud-Soukate, J., Leroy, E., and Baize, S. (1997a). Isolation and partial molecular characterisation of a strain of Ebola virus during a recent epidemic of viral haemorrhagic fever in Gabon. Lancet *349*, 181.

Georges-Courbot, M.C., Sanchez, A., Lu, C.Y., Baize, S., Leroy, E., Lansout-Soukate, J., Tevi-Benissan, C., Georges, A.J., Trappier, S.G., Zaki, S.R., *et al.* (1997b). Isolation and phylogenetic characterization of Ebola viruses causing different outbreaks in Gabon. Emerg Infect Dis *3*, 59-62.

Giocondi, M.C., Milhiet, P.E., Dosset, P., and Le Grimellec, C. (2004). Use of cyclodextrin for AFM monitoring of model raft formation. Biophys J *86*, 861-869.

Gitlin, L., Stone, J.K., and Andino, R. (2005). Poliovirus escape from RNA interference: short interfering RNA-target recognition and implications for therapeutic approaches. J Virol *79*, 1027-1035.

Gong, Y., Duvvuri, M., Duncan, M.B., Liu, J., and Krise, J.P. (2006). Niemann-Pick C1 protein facilitates the efflux of the anticancer drug daunorubicin from cells according to a novel vesicle-mediated pathway. J Pharmacol Exp Ther *316*, 242-247.

Grassme, H., Gulbins, E., Brenner, B., Ferlinz, K., Sandhoff, K., Harzer, K., Lang, F., and Meyer, T.F. (1997). Acidic sphingomyelinase mediates entry of N. gonorrhoeae into nonphagocytic cells. Cell *91*, 605-615.

Grassme, H., Jendrossek, V., Riehle, A., von Kurthy, G., Berger, J., Schwarz, H., Weller, M., Kolesnick, R., and Gulbins, E. (2003). Host defense against Pseudomonas aeruginosa requires ceramide-rich membrane rafts. Nat Med *9*, 322-330.

Grassme, H., Riehle, A., Wilker, B., and Gulbins, E. (2005). Rhinoviruses infect human epithelial cells via ceramide-enriched membrane platforms. J Biol Chem *280*, 26256-26262.

Groseth, A., Feldmann, H., and Strong, J.E. (2007). The ecology of Ebola virus. Trends Microbiol *15*, 408-416.

Gulbins, E., Dreschers, S., Wilker, B., and Grassme, H. (2004). Ceramide, membrane rafts and infections. J Mol Med *82*, 357-363.

Gulbins, E., and Li, P.L. (2006). Physiological and pathophysiological aspects of ceramide. Am J Physiol Regul Integr Comp Physiol *290*, R11-26.

Gupta, M., Greer, P., Mahanty, S., Shieh, W.J., Zaki, S.R., Ahmed, R., and Rollin, P.E. (2005). CD8-mediated protection against Ebola virus infection is perforin dependent. J Immunol *174*, 4198-4202.

Haka, A.S., Grosheva, I., Chiang, E., Buxbaum, A.R., Baird, B.A., Pierini, L.M., and Maxfield, F.R. (2009). Macrophages create an acidic extracellular hydrolytic compartment to digest aggregated lipoproteins. Mol Biol Cell *20*, 4932-4940.

Hanna, A.N., Chan, E.Y., Xu, J., Stone, J.C., and Brindley, D.N. (1999). A novel pathway for tumor necrosis factor-alpha and ceramide signaling involving sequential activation of tyrosine kinase, p21(ras), and phosphatidylinositol 3-kinase. J Biol Chem *274*, 12722-12729.

Harmala, A.S., Porn, M.I., Mattjus, P., and Slotte, J.P. (1994). Cholesterol transport from plasma membranes to intracellular membranes is inhibited by 3 beta-[2-(diethylamino)ethoxy]androst-5-en-17-one. Biochim Biophys Acta *1211*, 317-325.

Hartman, A.L., Towner, J.S., and Nichol, S.T. (2010). Ebola and marburg hemorrhagic fever. Clin Lab Med *30*, 161-177.

Hauck, C.R., Grassme, H., Bock, J., Jendrossek, V., Ferlinz, K., Meyer, T.F., and Gulbins, E. (2000). Acid sphingomyelinase is involved in CEACAM receptor-mediated phagocytosis of Neisseria gonorrhoeae. FEBS letters *478*, 260-266.

Hayman, D.T., Emmerich, P., Yu, M., Wang, L.F., Suu-Ire, R., Fooks, A.R., Cunningham, A.A., and Wood, J.L. (2010). Long-term survival of an urban fruit bat seropositive for Ebola and Lagos bat viruses. PLoS One *5*, e11978.

Herz, J., Pardo, J., Kashkar, H., Schramm, M., Kuzmenkina, E., Bos, E., Wiegmann, K., Wallich, R., Peters, P.J., Herzig, S., *et al.* (2009). Acid sphingomyelinase is a key regulator of cytotoxic granule secretion by primary T lymphocytes. Nat Immunol *10*, 761-768.

Heymann, D.L., Weisfeld, J.S., Webb, P.A., Johnson, K.M., Cairns, T., and Berquist, H. (1980). Ebola hemorrhagic fever: Tandala, Zaire, 1977-1978. J Infect Dis *142*, 372-376.

Hoenen, T., Groseth, A., Falzarano, D., and Feldmann, H. (2006). Ebola virus: unravelling pathogenesis to combat a deadly disease. Trends Mol Med *12*, 206-215.

Hood, C.L., Abraham, J., Boyington, J.C., Leung, K., Kwong, P.D., and Nabel, G.J. (2010). Biochemical and structural characterization of cathepsin L-processed Ebola virus glycoprotein: implications for viral entry and immunogenicity. J Virol *84*, 2972-2982.

Hurwitz, R., Ferlinz, K., and Sandhoff, K. (1994). The tricyclic antidepressant desipramine causes proteolytic degradation of lysosomal sphingomyelinase in human fibroblasts. Biol Chem Hoppe Seyler *375*, 447-450.

Huynh, C., and Andrews, N.W. (2005). The small chemical vacuolin-1 alters the morphology of lysosomes without inhibiting Ca2+-regulated exocytosis. EMBO Rep *6*, 843-847.

Ishitsuka, R., and Kobayashi, T. (2004). Lysenin: a new tool for investigating membrane lipid organization. Anat Sci Int *79*, 184-190.

Ito, H., Watanabe, S., Sanchez, A., Whitt, M.A., and Kawaoka, Y. (1999). Mutational analysis of the putative fusion domain of Ebola virus glycoprotein. J Virol *73*, 8907-8912.

Ivanov, A.I. (2008). Pharmacological inhibition of endocytic pathways: is it specific enough to be useful? Methods Mol Biol *440*, 15-33.

Jahrling, P.B., Geisbert, T.W., Dalgard, D.W., Johnson, E.D., Ksiazek, T.G., Hall, W.C., and Peters, C.J. (1990). Preliminary report: isolation of Ebola virus from monkeys imported to USA. Lancet *335*, 502-505.

Jan, J.T., Chatterjee, S., and Griffin, D.E. (2000). Sindbis virus entry into cells triggers apoptosis by activating sphingomyelinase, leading to the release of ceramide. J Virol *74*, 6425-6432.

Jasenosky, L.D., and Kawaoka, Y. (2004). Filovirus budding. Virus Res *106*, 181-188.

Jasenosky, L.D., Neumann, G., Lukashevich, I., and Kawaoka, Y. (2001). Ebola virus VP40-induced particle formation and association with the lipid bilayer. J Virol *75*, 5205-5214.

Jenkins, R.W., Canals, D., Idkowiak-Baldys, J., Simbari, F., Roddy, P., Perry, D.M., Kitatani, K., Luberto, C., and Hannun, Y.A. (2010). Regulated secretion of acid sphingomyelinase: implications for selectivity of ceramide formation. J Biol Chem *285*, 35706-35718.

Jenkins, R.W., Idkowiak-Baldys, J., Simbari, F., Canals, D., Roddy, P., Riner, C.D., Clarke, C.J., and Hannun, Y.A. (2011). A novel mechanism of lysosomal acid sphingomyelinase maturation - requirement for carboxyl-terminal processing. J Biol Chem *286*, 3777-3788.

Jenne, N., Rauchenberger, R., Hacker, U., Kast, T., and Maniak, M. (1998). Targeted gene disruption reveals a role for vacuolin B in the late endocytic pathway and exocytosis. J Cell Sci *111 (Pt 1)*, 61-70.

Johansen, K.A., Gill, R.E., and Vasil, M.L. (1996). Biochemical and molecular analysis of phospholipase C and phospholipase D activity in mycobacteria. Infect Immun *64*, 3259-3266.

Johnson, R.F., Bell, P., and Harty, R.N. (2006). Effect of Ebola virus proteins GP, NP and VP35 on VP40 VLP morphology. Virol J *3*, 31.

Jones, S.M., Feldmann, H., Stroher, U., Geisbert, J.B., Fernando, L., Grolla, A., Klenk, H.D., Sullivan, N.J., Volchkov, V.E., Fritz, E.A., *et al.* (2005). Live attenuated recombinant vaccine protects nonhuman primates against Ebola and Marburg viruses. Nat Med *11*, 786-790.

Kaletsky, R.L., Simmons, G., and Bates, P. (2007). Proteolysis of the Ebola virus glycoproteins enhances virus binding and infectivity. J Virol *81*, 13378-13384.

Kalongi, Y., Mwanza, K., Tshisuaka, M., Lusiama, N., Ntando, E., Kanzake, L., Shieh, W.J., Zaki, S.R., Lloyd, E.S., Ksiazek, T.G., *et al.* (1999). Isolated case of Ebola hemorrhagic fever with mucormycosis complications, Kinshasa, Democratic Republic of the Congo. J Infect Dis *179 Suppl 1*, S15-17.

Khan, A.S., Tshioko, F.K., Heymann, D.L., Le Guenno, B., Nabeth, P., Kerstiens, B., Fleerackers, Y., Kilmarx, P.H., Rodier, G.R., Nkuku, O., *et al.* (1999). The reemergence of Ebola hemorrhagic fever, Democratic Republic of the Congo, 1995. Commission de Lutte contre les Epidemies a Kikwit. J Infect Dis *179 Suppl 1*, S76-86.

Kiley, M.P., Bowen, E.T., Eddy, G.A., Isaacson, M., Johnson, K.M., McCormick, J.B., Murphy, F.A., Pattyn, S.R., Peters, D., Prozesky, O.W., *et al.* (1982). Filoviridae: a taxonomic home for Marburg and Ebola viruses? Intervirology *18*, 24-32.

Kim, S.K., Ahn, K.H., Jeon, H.J., Lee, D.H., Jung, S.Y., Jung, K.M., and Kim, D.K. (2010). Purification of neutral sphingomyelinase 2 from bovine brain and its calcium-dependent activation. J Neurochem *112*, 1088-1097.

Kima, P.E., Burleigh, B., and Andrews, N.W. (2000). Surface-targeted lysosomal membrane glycoprotein-1 (Lamp-1) enhances lysosome exocytosis and cell invasion by Trypanosoma cruzi. Cell Microbiol *2*, 477-486.

Kiyokawa, E., Baba, T., Otsuka, N., Makino, A., Ohno, S., and Kobayashi, T. (2005). Spatial and functional heterogeneity of sphingolipid-rich membrane domains. J Biol Chem *280*, 24072-24084.

Klingenstein, R., Lober, S., Kujala, P., Godsave, S., Leliveld, S.R., Gmeiner, P., Peters, P.J., and Korth, C. (2006). Tricyclic antidepressants, quinacrine and a novel, synthetic chimera thereof clear prions by destabilizing detergent-resistant membrane compartments. J Neurochem *98*, 748-759.

Ko, D.C., Gordon, M.D., Jin, J.Y., and Scott, M.P. (2001). Dynamic movements of organelles containing Niemann-Pick C1 protein: NPC1 involvement in late endocytic events. Mol Biol Cell *12*, 601-614.

Koivusalo, M., Jansen, M., Somerharju, P., and Ikonen, E. (2007). Endocytic trafficking of sphingomyelin depends on its acyl chain length. Mol Biol Cell *18*, 5113-5123.

Kolokoltsov, A.A., and Davey, R.A. (2004). Rapid and sensitive detection of retrovirus entry by using a novel luciferase-based content-mixing assay. J Virol *78*, 5124-5132.

Kolokoltsov, A.A., Fleming, E.H., and Davey, R.A. (2006a). Venezuelan equine encephalitis virus entry mechanism requires late endosome formation and resists cell membrane cholesterol depletion. Virology *347*, 333-342.

Kolokoltsov, A.A., Saeed, M.F., Freiberg, A.N., Holbrook, M.R., and Davey, R.A. (2009). Identification of novel cellular targets for therapeutic intervention against Ebola virus infection by siRNA screening. Drug Dev Res *70*, 255-265.

Kolokoltsov, A.A., Wang, E., Colpitts, T.M., Weaver, S.C., and Davey, R.A. (2006b). Pseudotyped viruses permit rapid detection of neutralizing antibodies in human and equine serum against Venezuelan equine encephalitis virus. The American journal of tropical medicine and hygiene *75*, 702-709.

Kolokoltsov, A.A., Weaver, S.C., and Davey, R.A. (2005). Efficient functional pseudotyping of oncoretroviral and lentiviral vectors by Venezuelan equine encephalitis virus envelope proteins. J Virol *79*, 756-763.

Kolzer, M., Werth, N., and Sandhoff, K. (2004). Interactions of acid sphingomyelinase and lipid bilayers in the presence of the tricyclic antidepressant desipramine. FEBS letters *559*, 96-98.

Kornhuber, J., Tripal, P., Reichel, M., Muhle, C., Rhein, C., Muehlbacher, M., Groemer, T.W., and Gulbins, E. (2010). Functional Inhibitors of Acid Sphingomyelinase (FIASMAs): a novel pharmacological group of drugs with broad clinical applications. Cell Physiol Biochem *26*, 9-20.

Kornhuber, J., Tripal, P., Reichel, M., Terfloth, L., Bleich, S., Wiltfang, J., and Gulbins, E. (2008). Identification of new functional inhibitors of acid sphingomyelinase using a structure-property-activity relation model. J Med Chem *51*, 219-237.

Kumari, S., Mg, S., and Mayor, S. (2010). Endocytosis unplugged: multiple ways to enter the cell. Cell Res *20*, 256-275.

Lange, Y., Ye, J., and Steck, T.L. (1998). Circulation of cholesterol between lysosomes and the plasma membrane. J Biol Chem *273*, 18915-18922.

Le Guenno, B., Formenty, P., Wyers, M., Gounon, P., Walker, F., and Boesch, C. (1995). Isolation and partial characterisation of a new strain of Ebola virus. Lancet *345*, 1271-1274.

Ledgerwood, J.E., Costner, P., Desai, N., Holman, L., Enama, M.E., Yamshchikov, G., Mulangu, S., Hu, Z., Andrews, C.A., Sheets, R.A., *et al.* (2010). A replication defective recombinant Ad5

vaccine expressing Ebola virus GP is safe and immunogenic in healthy adults. Vaccine *29*, 304-313.

Leroy, E.M., Baize, S., Mavoungou, E., and Apetrei, C. (2002). Sequence analysis of the GP, NP, VP40 and VP24 genes of Ebola virus isolated from deceased, surviving and asymptomatically infected individuals during the 1996 outbreak in Gabon: comparative studies and phylogenetic characterization. J Gen Virol *83*, 67-73.

Leroy, E.M., Kumulungui, B., Pourrut, X., Rouquet, P., Hassanin, A., Yaba, P., Delicat, A., Paweska, J.T., Gonzalez, J.P., and Swanepoel, R. (2005). Fruit bats as reservoirs of Ebola virus. Nature *438*, 575-576.

Liscum, L. (1990). Pharmacological inhibition of the intracellular transport of low-density lipoprotein-derived cholesterol in Chinese hamster ovary cells. Biochim Biophys Acta *1045*, 40-48.

Liscum, L., and Faust, J.R. (1989). The intracellular transport of low density lipoprotein-derived cholesterol is inhibited in Chinese hamster ovary cells cultured with 3-beta-[2-(diethylamino)ethoxy]androst-5-en-17-one. J Biol Chem *264*, 11796-11806.

Liscum, L., Ruggiero, R.M., and Faust, J.R. (1989). The intracellular transport of low density lipoprotein-derived cholesterol is defective in Niemann-Pick type C fibroblasts. J Cell Biol *108*, 1625-1636.

Luberto, C., Hassler, D.F., Signorelli, P., Okamoto, Y., Sawai, H., Boros, E., Hazen-Martin, D.J., Obeid, L.M., Hannun, Y.A., and Smith, G.K. (2002). Inhibition of tumor necrosis factor-induced cell death in MCF7 by a novel inhibitor of neutral sphingomyelinase. J Biol Chem *277*, 41128-41139.

Lusa, S., Blom, T.S., Eskelinen, E.L., Kuismanen, E., Mansson, J.E., Simons, K., and Ikonen, E. (2001). Depletion of rafts in late endocytic membranes is controlled by NPC1-dependent recycling of cholesterol to the plasma membrane. J Cell Sci *114*, 1893-1900.

Marathe, S., Schissel, S.L., Yellin, M.J., Beatini, N., Mintzer, R., Williams, K.J., and Tabas, I. (1998). Human vascular endothelial cells are a rich and regulatable source of secretory

sphingomyelinase. Implications for early atherogenesis and ceramide-mediated cell signaling. J Biol Chem *273*, 4081-4088.

Marchesini, N., and Hannun, Y.A. (2004). Acid and neutral sphingomyelinases: roles and mechanisms of regulation. Biochem Cell Biol *82*, 27-44.

Marchesini, N., Luberto, C., and Hannun, Y.A. (2003). Biochemical properties of mammalian neutral sphingomyelinase 2 and its role in sphingolipid metabolism. J Biol Chem *278*, 13775-13783.

Marsh, M., and van Meer, G. (2008). Cell biology. No ESCRTs for exosomes. Science (New York, NY *319*, 1191-1192.

Martinez, O., Johnson, J., Manicassamy, B., Rong, L., Olinger, G.G., Hensley, L.E., and Basler, C.F. (2010). Zaire Ebola virus entry into human dendritic cells is insensitive to cathepsin L inhibition. Cell Microbiol *12*, 148-157.

Martinez, O., Valmas, C., and Basler, C.F. (2007). Ebola virus-like particle-induced activation of NF-kappaB and Erk signaling in human dendritic cells requires the glycoprotein mucin domain. Virology *364*, 342-354.

Marzi, A., Moller, P., Hanna, S.L., Harrer, T., Eisemann, J., Steinkasserer, A., Becker, S., Baribaud, F., and Pohlmann, S. (2007). Analysis of the interaction of Ebola virus glycoprotein with DC-SIGN (dendritic cell-specific intercellular adhesion molecule 3-grabbing nonintegrin) and its homologue DC-SIGNR. J Infect Dis *196 Suppl 2*, S237-246.

Masson, M., Albouz, S., Boutry, J.M., Spezzatti, B., Castagna, M., and Baumann, N. (1989). Calmodulin antagonist W-7 inhibits lysosomal sphingomyelinase activity in C6 glioma cells. J Neurochem *52*, 1645-1647.

Masson, M., Spezzatti, B., Chapman, J., Battisti, C., and Baumann, N. (1992). Calmodulin antagonists chlorpromazine and W-7 inhibit exogenous cholesterol esterification and sphingomyelinase activity in human skin fibroblast cultures. Similarities between drug-induced and Niemann-Pick type C lipidoses. J Neurosci Res *31*, 84-88.

McIntosh, T.J., Simon, S.A., Needham, D., and Huang, C.H. (1992a). Interbilayer interactions between sphingomyelin and sphingomyelin/cholesterol bilayers. Biochemistry *31*, 2020-2024.

McIntosh, T.J., Simon, S.A., Needham, D., and Huang, C.H. (1992b). Structure and cohesive properties of sphingomyelin/cholesterol bilayers. Biochemistry *31*, 2012-2020.

Mercer, J., and Helenius, A. (2009). Virus entry by macropinocytosis. Nat Cell Biol *11*, 510-520.

Mercer, J., Schelhaas, M., and Helenius, A. (2010). Virus entry by endocytosis. Annu Rev Biochem *79*, 803-833.

Morrow, I.C., and Parton, R.G. (2005). Flotillins and the PHB domain protein family: rafts, worms and anaesthetics. Traffic *6*, 725-740.

Nanbo, A., Imai, M., Watanabe, S., Noda, T., Takahashi, K., Neumann, G., Halfmann, P., and Kawaoka, Y. (2010). Ebolavirus is internalized into host cells via macropinocytosis in a viral glycoprotein-dependent manner. PLoS Pathog *6*.

Nara, F., Tanaka, M., Hosoya, T., Suzuki-Konagai, K., and Ogita, T. (1999a). Scyphostatin, a neutral sphingomyelinase inhibitor from a discomycete, Trichopeziza mollissima: taxonomy of the producing organism, fermentation, isolation, and physico-chemical properties. J Antibiot (Tokyo) *52*, 525-530.

Nara, F., Tanaka, M., Masuda-Inoue, S., Yamasato, Y., Doi-Yoshioka, H., Suzuki-Konagai, K., Kumakura, S., and Ogita, T. (1999b). Biological activities of scyphostatin, a neutral sphingomyelinase inhibitor from a discomycete, Trichopeziza mollissima. J Antibiot (Tokyo) *52*, 531-535.

Ng, C.G., and Griffin, D.E. (2006). Acid sphingomyelinase deficiency increases susceptibility to fatal alphavirus encephalomyelitis. J Virol *80*, 10989-10999.

Nikiforov, V.V., Turovskii Iu, I., Kalinin, P.P., Akinfeeva, L.A., Katkova, L.R., Barmin, V.S., Riabchikova, E.I., Popkova, N.I., Shestopalov, A.M., Nazarov, V.P., *et al.* (1994). [A case of a laboratory infection with Marburg fever]. Zh Mikrobiol Epidemiol Immunobiol, 104-106.

Nkoghe, D., Nnegue, S., Mve, M.T., Formenty, P., Thompson, G., Iba Ba, J., Okome Nkoumou, M., and Leroy, E. (2005). [Isolated case of haemorrhagic fever observed in Gabon during the 2002 outbreak of Ebola but distant from epidemic zones]. Med Trop (Mars) *65*, 349-354.

Noda, T., Sagara, H., Suzuki, E., Takada, A., Kida, H., and Kawaoka, Y. (2002). Ebola virus VP40 drives the formation of virus-like filamentous particles along with GP. J Virol *76*, 4855-4865.

Ohanian, J., and Ohanian, V. (2001). Sphingolipids in mammalian cell signalling. Cell Mol Life Sci *58*, 2053-2068.

Okome-Nkoumou, M., and Kombila, M. (1999). [A case of Ebola virus hemorrhagic fever in Libreville (Gabon), fatal after evacuation to South Africa]. Med Trop (Mars) *59*, 411.

Onyango, C.O., Opoka, M.L., Ksiazek, T.G., Formenty, P., Ahmed, A., Tukei, P.M., Sang, R.C., Ofula, V.O., Konongoi, S.L., Coldren, R.L., *et al.* (2007). Laboratory diagnosis of Ebola hemorrhagic fever during an outbreak in Yambio, Sudan, 2004. J Infect Dis *196 Suppl 2*, S193-198.

Pakkanen, K., Kirjavainen, S., Makela, A.R., Rintanen, N., Oker-Blom, C., Jalonen, T.O., and Vuento, M. (2009a). Parvovirus capsid disorders cholesterol-rich membranes. Biochemical and biophysical research communications *379*, 562-566.

Pakkanen, K., Salonen, E., Makela, A.R., Oker-Blom, C., Vattulainen, I., and Vuento, M. (2009b). Desipramine induces disorder in cholesterol-rich membranes: implications for viral trafficking. Phys Biol *6*, 046004.

Pattyn, S., van der Groen, G., Courteille, G., Jacob, W., and Piot, P. (1977). Isolation of Marburg-like virus from a case of haemorrhagic fever in Zaire. Lancet *1*, 573-574.

Pourrut, X., Souris, M., Towner, J.S., Rollin, P.E., Nichol, S.T., Gonzalez, J.P., and Leroy, E. (2009). Large serological survey showing cocirculation of Ebola and Marburg viruses in Gabonese bat populations, and a high seroprevalence of both viruses in Rousettus aegyptiacus. BMC Infect Dis *9*, 159.

Rachman, H., Strong, M., Schaible, U., Schuchhardt, J., Hagens, K., Mollenkopf, H., Eisenberg, D., and Kaufmann, S.H. (2006). Mycobacterium tuberculosis gene expression profiling within the context of protein networks. Microbes Infect *8*, 747-757.

Rauchenberger, R., Hacker, U., Murphy, J., Niewohner, J., and Maniak, M. (1997). Coronin and vacuolin identify consecutive stages of a late, actin-coated endocytic compartment in Dictyostelium. Curr Biol *7*, 215-218.

Reed, D.S., Hensley, L.E., Geisbert, J.B., Jahrling, P.B., and Geisbert, T.W. (2004). Depletion of peripheral blood T lymphocytes and NK cells during the course of ebola hemorrhagic Fever in cynomolgus macaques. Viral Immunol *17*, 390-400.

Rogasevskaia, T., and Coorssen, J.R. (2006). Sphingomyelin-enriched microdomains define the efficiency of native Ca(2+)-triggered membrane fusion. J Cell Sci *119*, 2688-2694.

Ruigrok, R.W., Schoehn, G., Dessen, A., Forest, E., Volchkov, V., Dolnik, O., Klenk, H.D., and Weissenhorn, W. (2000). Structural characterization and membrane binding properties of the matrix protein VP40 of Ebola virus. J Mol Biol *300*, 103-112.

Ryabchikova, E.I., Kolesnikova, L.V., and Luchko, S.V. (1999). An analysis of features of pathogenesis in two animal models of Ebola virus infection. J Infect Dis *179 Suppl 1*, S199-202.

Saeed, M.F., Kolokoltsov, A.A., Albrecht, T., and Davey, R.A. (2010). Cellular entry of ebola virus involves uptake by a macropinocytosis-like mechanism and subsequent trafficking through early and late endosomes. PLoS Pathog *6*.

Saeed, M.F., Kolokoltsov, A.A., and Davey, R.A. (2006). Novel, rapid assay for measuring entry of diverse enveloped viruses, including HIV and rabies. J Virol Methods *135*, 143-150.

Saeed, M.F., Kolokoltsov, A.A., Freiberg, A.N., Holbrook, M.R., and Davey, R.A. (2008). Phosphoinositide-3 kinase-Akt pathway controls cellular entry of Ebola virus. PLoS Pathog *4*, e1000141.

Sanchez, A. (2007). Analysis of filovirus entry into vero e6 cells, using inhibitors of endocytosis, endosomal acidification, structural integrity, and cathepsin (B and L) activity. J Infect Dis *196 Suppl 2*, S251-258.

Sanchez, A., Lukwiya, M., Bausch, D., Mahanty, S., Sanchez, A.J., Wagoner, K.D., and Rollin, P.E. (2004). Analysis of human peripheral blood samples from fatal and nonfatal cases of Ebola (Sudan) hemorrhagic fever: cellular responses, virus load, and nitric oxide levels. J Virol *78*, 10370-10377.

Schissel, S.L., Jiang, X., Tweedie-Hardman, J., Jeong, T., Camejo, E.H., Najib, J., Rapp, J.H., Williams, K.J., and Tabas, I. (1998). Secretory sphingomyelinase, a product of the acid sphingomyelinase gene, can hydrolyze atherogenic lipoproteins at neutral pH. Implications for atherosclerotic lesion development. J Biol Chem *273*, 2738-2746.

Schissel, S.L., Schuchman, E.H., Williams, K.J., and Tabas, I. (1996). Zn2+-stimulated sphingomyelinase is secreted by many cell types and is a product of the acid sphingomyelinase gene. J Biol Chem *271*, 18431-18436.

Schornberg, K., Matsuyama, S., Kabsch, K., Delos, S., Bouton, A., and White, J. (2006). Role of endosomal cathepsins in entry mediated by the Ebola virus glycoprotein. J Virol *80*, 4174-4178.

Schornberg, K.L., Shoemaker, C.J., Dube, D., Abshire, M.Y., Delos, S.E., Bouton, A.H., and White, J.M. (2009). Alpha5beta1-integrin controls ebolavirus entry by regulating endosomal cathepsins. Proc Natl Acad Sci U S A *106*, 8003-8008.

Seto, M., Whitlow, M., McCarrick, M.A., Srinivasan, S., Zhu, Y., Pagila, R., Mintzer, R., Light, D., Johns, A., and Meurer-Ogden, J.A. (2004). A model of the acid sphingomyelinase phosphoesterase domain based on its remote structural homolog purple acid phosphatase. Protein Sci *13*, 3172-3186.

Shaik, G.M., Draberova, L., Heneberg, P., and Draber, P. (2009). Vacuolin-1-modulated exocytosis and cell resealing in mast cells. Cell Signal *21*, 1337-1345.

Shakor, A.B., Czurylo, E.A., and Sobota, A. (2003). Lysenin, a unique sphingomyelin-binding protein. FEBS Lett *542*, 1-6.

Shogomori, H., and Kobayashi, T. (2008). Lysenin: a sphingomyelin specific pore-forming toxin. Biochim Biophys Acta *1780*, 612-618.

Sidwell, R.W., Huffman, J.H., Khare, G.P., Allen, L.B., Witkowski, J.T., and Robins, R.K. (1972). Broad-spectrum antiviral activity of Virazole: 1-beta-D-ribofuranosyl-1,2,4-triazole-3-carboxamide. Science *177*, 705-706.

Simmons, G., Reeves, J.D., Grogan, C.C., Vandenberghe, L.H., Baribaud, F., Whitbeck, J.C., Burke, E., Buchmeier, M.J., Soilleux, E.J., Riley, J.L., *et al.* (2003a). DC-SIGN and DC-SIGNR bind ebola glycoproteins and enhance infection of macrophages and endothelial cells. Virology *305*, 115-123.

Simmons, G., Rennekamp, A.J., Chai, N., Vandenberghe, L.H., Riley, J.L., and Bates, P. (2003b). Folate receptor alpha and caveolae are not required for Ebola virus glycoprotein-mediated viral infection. J Virol *77*, 13433-13438.

Slotte, J.P., Hedstrom, G., and Bierman, E.L. (1989). Intracellular transport of cholesterol in type C Niemann-Pick fibroblasts. Biochimica et biophysica acta *1005*, 303-309.

Smit, J.M., Bittman, R., and Wilschut, J. (1999). Low-pH-dependent fusion of Sindbis virus with receptor-free cholesterol- and sphingolipid-containing liposomes. J Virol *73*, 8476-8484.

Smith, E.L., and Schuchman, E.H. (2008). The unexpected role of acid sphingomyelinase in cell death and the pathophysiology of common diseases. FASEB J *22*, 3419-3431.

Stroher, U., West, E., Bugany, H., Klenk, H.D., Schnittler, H.J., and Feldmann, H. (2001). Infection and activation of monocytes by Marburg and Ebola viruses. J Virol *75*, 11025-11033.

Sugimoto, Y., Ninomiya, H., Ohsaki, Y., Higaki, K., Davies, J.P., Ioannou, Y.A., and Ohno, K. (2001). Accumulation of cholera toxin and GM1 ganglioside in the early endosome of Niemann-Pick C1-deficient cells. Proc Natl Acad Sci U S A *98*, 12391-12396.

Takada, A., Robison, C., Goto, H., Sanchez, A., Murti, K.G., Whitt, M.A., and Kawaoka, Y. (1997). A system for functional analysis of Ebola virus glycoprotein. Proc Natl Acad Sci U S A *94*, 14764-14769.

Takada, A., Watanabe, S., Ito, H., Okazaki, K., Kida, H., and Kawaoka, Y. (2000). Downregulation of beta1 integrins by Ebola virus glycoprotein: implication for virus entry. Virology *278*, 20-26.

Takahashi, I., Takahashi, T., Abe, T., Watanabe, W., and Takada, G. (2000). Distribution of acid sphingomyelinase in human various body fluids. Tohoku J Exp Med *192*, 61-66.

Tam, C., Idone, V., Devlin, C., Fernandes, M.C., Flannery, A., He, X., Schuchman, E., Tabas, I., and Andrews, N.W. (2010). Exocytosis of acid sphingomyelinase by wounded cells promotes endocytosis and plasma membrane repair. The Journal of cell biology *189*, 1027-1038.

Tani, H., Shiokawa, M., Kaname, Y., Kambara, H., Mori, Y., Abe, T., Moriishi, K., and Matsuura, Y. (2010). Involvement of ceramide in the propagation of Japanese encephalitis virus. J Virol *84*, 2798-2807.

Tani, M., and Hannun, Y.A. (2007). Analysis of membrane topology of neutral sphingomyelinase 2. FEBS letters *581*, 1323-1328.

Tchernev, V.T., Mansfield, T.A., Giot, L., Kumar, A.M., Nandabalan, K., Li, Y., Mishra, V.S., Detter, J.C., Rothberg, J.M., Wallace, M.R., *et al.* (2002). The Chediak-Higashi protein interacts with SNARE complex and signal transduction proteins. Mol Med *8*, 56-64.

Teepe, R.G., Johnson, B.K., Ocheng, D., Gichogo, A., Langatt, A., Ngindu, A., Kiley, M., Johnson, K.M., and McCormick, J.B. (1983). A probable case of Ebola virus haemorrhagic fever in Kenya. East Afr Med J *60*, 718-722.

Teissier, E., Penin, F., and Pecheur, E.I. (2011). Targeting cell entry of enveloped viruses as an antiviral strategy. Molecules *16*, 221-250.

Tepper, A.D., Ruurs, P., Wiedmer, T., Sims, P.J., Borst, J., and van Blitterswijk, W.J. (2000). Sphingomyelin hydrolysis to ceramide during the execution phase of apoptosis results from phospholipid scrambling and alters cell-surface morphology. J Cell Biol *150*, 155-164.

Timmins, J., Scianimanico, S., Schoehn, G., and Weissenhorn, W. (2001). Vesicular release of ebola virus matrix protein VP40. Virology *283*, 1-6.

Towner, J.S., Paragas, J., Dover, J.E., Gupta, M., Goldsmith, C.S., Huggins, J.W., and Nichol, S.T. (2005). Generation of eGFP expressing recombinant Zaire ebolavirus for analysis of early pathogenesis events and high-throughput antiviral drug screening. Virology *332*, 20-27.

Towner, J.S., Sealy, T.K., Khristova, M.L., Albarino, C.G., Conlan, S., Reeder, S.A., Quan, P.L., Lipkin, W.I., Downing, R., Tappero, J.W., *et al.* (2008). Newly discovered ebola virus associated with hemorrhagic fever outbreak in Uganda. PLoS Pathog *4*, e1000212.

Trajkovic, K., Hsu, C., Chiantia, S., Rajendran, L., Wenzel, D., Wieland, F., Schwille, P., Brugger, B., and Simons, M. (2008). Ceramide triggers budding of exosome vesicles into multivesicular endosomes. Science (New York, NY *319*, 1244-1247.

van Blitterswijk, W.J., van der Luit, A.H., Veldman, R.J., Verheij, M., and Borst, J. (2003). Ceramide: second messenger or modulator of membrane structure and dynamics? Biochem J *369*, 199-211.

Veldman, R.J., Maestre, N., Aduib, O.M., Medin, J.A., Salvayre, R., and Levade, T. (2001). A neutral sphingomyelinase resides in sphingolipid-enriched microdomains and is inhibited by the caveolin-scaffolding domain: potential implications in tumour necrosis factor signalling. Biochem J *355*, 859-868.

Vignuzzi, M., Stone, J.K., and Andino, R. (2005). Ribavirin and lethal mutagenesis of poliovirus: molecular mechanisms, resistance and biological implications. Virus Res *107*, 173-181.

Warfield, K.L., Olinger, G., Deal, E.M., Swenson, D.L., Bailey, M., Negley, D.L., Hart, M.K., and Bavari, S. (2005). Induction of humoral and CD8+ T cell responses are required for protection against lethal Ebola virus infection. J Immunol *175*, 1184-1191.

Wascholowski, V., and Giannis, A. (2006). Sphingolactones: selective and irreversible inhibitors of neutral sphingomyelinase. Angew Chem Int Ed Engl *45*, 827-830.

Wienke, D., Drengk, A., Schmauch, C., Jenne, N., and Maniak, M. (2006). Vacuolin, a flotillin/reggie-related protein from Dictyostelium oligomerizes for endosome association. Eur J Cell Biol *85*, 991-1000.

Wilson, J.A., and Hart, M.K. (2001). Protection from Ebola virus mediated by cytotoxic T lymphocytes specific for the viral nucleoprotein. J Virol *75*, 2660-2664.

Wolf, M.C., Freiberg, A.N., Zhang, T., Akyol-Ataman, Z., Grock, A., Hong, P.W., Li, J., Watson, N.F., Fang, A.Q., Aguilar, H.C., *et al.* (2010). A broad-spectrum antiviral targeting entry of enveloped viruses. Proc Natl Acad Sci U S A *107*, 3157-3162.

Wool-Lewis, R.J., and Bates, P. (1998). Characterization of Ebola virus entry by using pseudotyped viruses: identification of receptor-deficient cell lines. J Virol *72*, 3155-3160.

Woolsey, A.M., Sunwoo, L., Petersen, C.A., Brachmann, S.M., Cantley, L.C., and Burleigh, B.A. (2003). Novel PI 3-kinase-dependent mechanisms of trypanosome invasion and vacuole maturation. J Cell Sci *116*, 3611-3622.

Wu, B.X., Clarke, C.J., and Hannun, Y.A. (2010). Mammalian neutral sphingomyelinases: regulation and roles in cell signaling responses. Neuromolecular Med *12*, 320-330.

Wymann, M.P., and Schneiter, R. (2008). Lipid signalling in disease. Nat Rev Mol Cell Biol *9*, 162-176.

Yamaji, A., Sekizawa, Y., Emoto, K., Sakuraba, H., Inoue, K., Kobayashi, H., and Umeda, M. (1998). Lysenin, a novel sphingomyelin-specific binding protein. J Biol Chem *273*, 5300-5306.

Yonezawa, A., Cavrois, M., and Greene, W.C. (2005). Studies of ebola virus glycoprotein-mediated entry and fusion by using pseudotyped human immunodeficiency virus type 1 virions: involvement of cytoskeletal proteins and enhancement by tumor necrosis factor alpha. J Virol *79*, 918-926.

Yoshida, Y., Arimoto, K., Sato, M., Sakuragawa, N., Arima, M., and Satoyoshi, E. (1985). Reduction of acid sphingomyelinase activity in human fibroblasts induced by AY-9944 and other cationic amphiphilic drugs. J Biochem *98*, 1669-1679.

Zampieri, C.A., Sullivan, N.J., and Nabel, G.J. (2007). Immunopathology of highly virulent pathogens: insights from Ebola virus. Nat Immunol *8*, 1159-1164.

Zeidan, Y.H., and Hannun, Y.A. (2010). The acid sphingomyelinase/ceramide pathway: biomedical significance and mechanisms of regulation. Curr Mol Med *10*, 454-466.

Zeidan, Y.H., Jenkins, R.W., and Hannun, Y.A. (2008). Remodeling of cellular cytoskeleton by the acid sphingomyelinase/ceramide pathway. The Journal of cell biology *181*, 335-350.

Zenni, M.K., Giardina, P.C., Harvey, H.A., Shao, J., Ketterer, M.R., Lubaroff, D.M., Williams, R.D., and Apicella, M.A. (2000). Macropinocytosis as a mechanism of entry into primary human urethral epithelial cells by Neisseria gonorrhoeae. Infect Immun *68*, 1696-1699.

Zha, X., Pierini, L.M., Leopold, P.L., Skiba, P.J., Tabas, I., and Maxfield, F.R. (1998). Sphingomyelinase treatment induces ATP-independent endocytosis. The Journal of cell biology *140*, 39-47.

VITA

Mary Miller was born July 13, 1974 in Fort Atkinson, WI, to Mr. Paul and Carol Miller. At age 17, Mary enlisted in the U.S. Army's military police corps. While earning her Bachelor's of Science degree in Biology at the University of Wisconsin-Whitewater, Mary joined the Reserve Officer Training Corps (ROTC). Upon graduation, she was commissioned as a Second Lieutenant in the Army's Medical Service Corps, and assigned to the Republic of Korea (ROK). There, Mary worked with the Korean National Institute of Health, ROK Army, and local public health to prevent the spread of malaria along the border by increasing mosquito surveillance, identifying and treating infected human populations, and increasing public awareness about disease prevention. A year later, Mary was assigned to the hospital at Fort Campbell, KY, where she conducted epidemiology surveys to identify important public health concerns – from lead poisoning to food borne illness. In 1999, First Lieutenant Miller was selected to attend the Army's helicopter flight training program at Fort Rucker, AL. After earning her wings, Captain Miller was assigned to Chunchon, Republic of Korea, where she served as both a MEDEVAC pilot and a flight platoon leader. A year later, she was assigned to the MEDEVAC company at Wheeler Army Airfield, HI, where she quickly advanced through the ranks of the MEDEVAC command. In 2004, Mary earned her Master's degree in Aeronautical Science from Embry-Aeronautical University. Additionally, she was awarded the Military's Outstanding Volunteer Service Award for serving over 500 hours as a volunteer researcher at the University of Hawaii, while studying bacteria from volcanic craters and sub-glacial lakes. In 2005, Captain Miller deployed in support of Operation Enduring Freedom, where she flew over 100 combat missions while commanding MEDEVAC operations in southern Afghanistan. For her service, she was awarded the Bronze Star and Air Medal. Within 9 months of returning to the U.S., Major Miller was deployed to Tikrit, Iraq. There, she worked alongside her Iraqi counterparts to re-establish the country's security forces, and emergency medical response system. There she was awarded the Senior Aviator badge for flying over 1,000 hours. While in Iraq, Major Miller was accepted to University of Texas Medical Branch, as part of the Army's highly competitive Long-Term Health Education and Training Program. In 2007, Mary returned from Iraq to begin her 4-year doctoral degree at the Graduate School of Biomedical Sciences. In 2008, she joined Dr. Robert Davey's lab where she studied the role of lysosomal exocytosis and sphingomyelinase in *Ebolavirus* entry. Upon graduation, Major Miller will be assigned to Armed Forces Research Institute of Medical Sciences (AFRIMS), Bangkok, Thailand, where she will work with local researchers to develop strategies against infectious diseases throughout Southeast Asia.

Education

B.S., May 1996, University of Wisconsin-Whitewater, Whitewater, Wisconsin
M.A., May 2004, Embry-Riddle Aeronautical University, Daytona Beach, Florida

Publications

Atasheva, A, Wang, E, Adams A, Plante, K, Ni, S, Taylor, K, Miller, M, Frolov, I, Weaver, S. 2009. Chimeric alphavirus vaccine candidates protect mice from intranasal challenge with western equine encephalitis virus. *Vaccine*. *27*, 4309-4319.

Gaidos, E, Marteinsson, V, Thorsteinsson, T, Johannesson, T, Runarsson, A, Stefansson, A, Glazer, B, Lanoil, B, Skidmore, M, Han, S, Miller, M, Rusch, A, Foo, W. 2008. An oligarchic microbial assemblage in the anoxic bottom waters of a volcanic sub-glacial lake. *ISME*. 1-12.

Gaidos E, Glazer B, Harris D, Heshiki Z, Jeppsson N, Miller M, Thorsteinsson T, Einarsson B, Kjartansson V, Stefansson, A, Johannesson T, Roberts M, Skidmore M & Lanoil B. 2007. A simple sampler for sub-glacial water bodies. *J. Glaciology*, *53*, 157-158.

Strickman, D., Miller, M., Lee, K., Kim, H., Wirtz, R., Perich, M., Novakowski, W., Feighner, B., Roh, C. (2001) Successful entomological intervention against *Anopheles sinensis*, limiting transmission of *Plasmodium vivax* to American soldiers in the Republic of Korea. *Korean J. Ento*. *31*, 189-195.

Strickman, D., Miller, M., Kim, H., Lee, K. (2000) Mosquito surveillance in the Demilitarized Zone, Republic of Korea, during an outbreak of *Plasmodium vivax* malaria in 1996 and 1997. *J. Am. Mosquito Control Assoc*. *16*, 100-113.

Strickman, D., Miller, M., Kelsey, L., Lee, W., Lee, H., Lee, K., Kim, H., Feighner, B. (1999) Evaluation of the malaria threat at the Multi-Purpose Range Complex, Yongp'yong, Republic of Korea. *Military Med*. *164*, 626-629.

Lee, K., Strickman, D., Miller, M., Kim, H. (1998) New record for the subspecies, *Aedes vexans vexans* in Korea (Diptera: Culicidae). *Korean J. Ento*. *28*, 65-67.